2013

Molecular-Level Investigations Combining Nanoscale Lithography and Atomic Force Microscopy

ChaMarra Karmelia Saner
Louisiana State University and Agricultural and Mechanical College, chamarras@gmail.com

Recommended Citation

Saner, ChaMarra Karmelia, "Molecular-Level Investigations Combining Nanoscale Lithography and Atomic Force Microscopy" (2013). *LSU Doctoral Dissertations*. 400.
https://digitalcommons.lsu.edu/gradschool_dissertations/400

MOLECULAR-LEVEL INVESTIGATIONS COMBINING NANOSCALE LITHOGRAPHY AND ATOMIC FORCE MICROSCOPY

A Dissertation

Submitted to the Graduate Faculty of the
Louisiana State University and
Agricultural and Mechanical College
in partial fulfillment of the
requirements for the degree of
Doctor of Philosophy

in

The Department of Chemistry

by
ChaMarra Karmelia Saner
M.S., North Carolina Agriculture and Technical State University, 2007
B.S., The University of North Carolina at Pembroke, 2004
December 2013

ACKNOWLEDGEMENTS

It is with the utmost respect and gratitude that I begin by thanking my heavenly father. Proverbs 1: 7 states “the fear of the lord is the beginning of knowledge; but only fools despise wisdom and knowledge.” I am grateful that these morals and values have been instilled in me at an early age, because at times, the only strength I had was from you Lord. “Faith is being sure of what we hope for and certain of what we do not see” (Hebrews 11:1) and this journey has allowed me to walk the lines of this verse on a daily basis. You have allowed me to accept the things I cannot change; courage to change the things I can; and the wisdom to know the difference.

I would like to express my deepest gratitude to my advisor Dr. Jayne C. Garno. Thank you for the opportunity to grow scientifically through the wealth of opportunities that you have provided. The training that you have created along this journey has helped shape me as a mature chemist and bring my scientific education full circle. You have provided me with a great skill set, needed to succeed. With your support you have truly made my experience at Louisiana State University memorable.

To members of my committee, past group members, present group members and the entering 2009 class of the LSU chemistry graduate program , I would like to thank you for your time, patience, reviews, comments and constructively critical discussions throughout my matriculation of LSU graduate chemistry milestones. The plethora of lunches, laughs, tears and walks have all been a necessary part of this experience. To my group members specifically, it has definitely been a ride!! The best and only way to describe the friendship, camaraderie and overall wealth of experiences that we have endured is through the following: 1) “Don’t stop believin,” Journey, 1982; 2) “Eye of the Tiger,” Survivor, 1982; 3) “We are the champions,” Queen, 1977. You guys will always have a special place in my heart, and I look forward to the friendships for years to come.

Finally, to my loving family, I can’t even begin to describe the support system that you guys have created for me throughout my years of schooling. There are not enough “thank-you’s” or expressions of gratitude that I can offer for your love, care and support. You all have been beside me, behind me, underneath me and all around me every step of the way. To my father Marvin Saner and my mother Wanda Bruner, I would like to say thank you, for ultimately without you two none of this would have been possible. You two have given me sound advice and words of wisdom. I would also like to give a special thanks to my motivator and biggest fan, my mother. Mom, it is through your strength that I have learned how to push through keep my head up and conquer. You have shown me how to be a successful woman through your journey and how to be diligent and persevere whenever things seem impossible. Words will never be able to express the adoration, admiration and respect that I have for you. To my sisters and brother-in-law, Alishia, Alonna and Marvin Clark, we have been there for each other no matter what. Through the good times, bad times, tough times and ridiculous times either of you have been there in some capacity or I can’t thank you enough for that. You all have blessed me with nephews (Jordan and Elijah), beautiful nieces (Gemiya and Paiton), a great niece (Zayla) and nephew (Xaiden) that keep me smiling and give me a reason to smile on a regular basis. Lastly, to my muse, thank you for being you. Your words, although sometimes rash, have been invaluable during the last half of this journey. You have a personality that is like no other and that combined with your sense of humor is unmatched to no one. You keep me grounded, sane and laughing when the time is right. You allow me to cry when I need to and work when I have to all selflessly. You are one of the most caring, loving and understanding individuals that I have ever met. I can’t wait to spend the rest of our lives together! Every one of you has played an integral role in my success in one way or another. Your constant support is just as necessary as my schooling, and I want to say thank you for that. I Love you all very much!!

TABLE OF CONTENTS

LIST OF TABLES

LIST OF FIGURES

LIST OF ABBREVIATIONS

Abbreviation	**Name**
°C	degree celsius
AFM	Atomic force microscopy
cm	centimeters
DETA	(3-trimethoxysilylpropyl) diethylenetriamine
EDC	1-ethyl-3-[dimethylaminopropyl]carbodiimide hydrochloride
F	force
g	grams
h	hours
Hz	hertz
IgG	Immunoglobulin G
ITO	indium tin oxide
k	force
kHz	kilohertz
mg/mL	milligrams/milliliters
min	minutes
mL	milliliters
NHS	N-hydroxysuccinimide
N/m	Newton’s per meter
nm	nanometers
NSOM	near-field scanning optical microscopy
OTS	octadecyltrichlorosilane

Abbreviation	**Name**
PDMS	polydimethylsiloxane
RGD	arginine-glycine-aspartic acid amino acid sequence
rpm	revolutions per minute
SAMs	self assembled monolayers
Si	silicon
Si_3N_4	silicon nitride
SPM	scanning probe microscopy
STM	scanning tunneling microscopy
TMMH	1,1,1-tris(mercaptomethyl)heptadecane
V	volume
v/v	volume to volume ratio
w/v	weight to volume ratio
x	vertical deflection
μL	microliter
μm	micrometer

ABSTRACT

In this dissertation, nanostructures of octadecyltrichlorosilane (OTS) and were prepared using particle lithography and evaluated using characterizations with atomic force microscopy (AFM). The nanostructures of OTS were used as a resist for patterning fibronectin, an extracellular matrix protein. Particle lithography provides a practical and reproducible approach to generate billions of nanostructures comprised of organic thin films or nanomaterials. A film of mesospheres can be applied as a surface mask to define the periodicity and size of nanopatterns using processes of self-assembly. A close-packed arrangement of mesospheres is produced spontaneously when monodisperse solutions of latex or silica are dried on a flat surface. Organosilanes attach to surfaces by successive steps of hydrolysis and condensation. Nanoscopic amounts of water are required to initiate the hydrolysis step of the reaction, if too much water is present the molecules cross-link to form polymer strands. The location of nanoscopic residues of water on the surface influence the geometry of the nanostructures produced with particle lithography. Three particle lithography approaches for preparing OTS nanostructures were evaluated using strategies for solution immersion, contact printing and vapor deposition. Surface platforms of organosilanes provided a foundation for building more complex molecular architectures by defining discrete surface sites for further steps of chemical patterning. Nanoscale patterning using organosilane chemistry was used to prepare test platforms to investigate protein binding and immunoassays at the molecular level. Studies with organosilanes provide groundwork for investigations with protein patterning to investigate the activity of fibronectin. The head groups of self-assembled monolayers (SAMs) were designed to selectively resist protein adsorption in areas surrounding small islands of protein-adhesive SAMs. A spatially selective platform for binding proteins was prepared to study protein binding at the molecular level using organosilane SAMs combined with particle lithography. Fibronectin attached selectively to the surface of (3-trimethoxysilylpropyl) diethylenetriamine SAMs to form nanopatterns over broad areas (microns). The periodicity and surface coverage of the nanostructures was determined by the diameter of the silica mesospheres. Studies with atomic force microscopy were used to evaluate the thickness and arrangement of SAMs, proteins and antibodies at each step of the fabrication procedure.

CHAPTER 1: INTRODUCTION

Nanolithography techniques are used to create nanometer scale structures that have at least one dimension within the 1-100 nm size regime. To accomplish surface fabrication at the nanoscale at such small scales, most protocols require expensive instrumentation and controlled environments such as clean rooms for processes with laser machining, electron or ion beam lithography, or photolithography. The protocols developed in this dissertation are based on chemical approaches using self-assembly processes. Fine control of the size, shape, surface chemistry and composition is critical for the fabrication of functional nanostructures.[1] Methods of particle lithography enable nanofabrication of organic thin films, proteins and nanomaterials using basic steps of chemistry such as immersion, heating, centrifugation and sonication. Changing the diameter of the mesosphere masks provides a way to control the periodicity and surface density of reactive sites or nanopores to simultaneously generate millions of organosilane nanostructures. The results of this dissertation encompass fundamental studies of organosilanes as platforms for building more complex molecular architectures. Characterizations with atomic force microscopy (AFM) reveal molecular-level details of the morphology, stability and surface chemistry of designed nanostructures. The experimental strategy was to develop methods for nanoscale patterning with organosilanes to prepare heterogeneous surface test platforms to enable spatial selectivity for binding proteins. In addition, protein binding and immunoassays have also been examined at the molecular level. Studies with scanning probe microscopy (SPM) provide advantages of achieving nanoscale resolution for detecting surface changes without requiring chemical modification of proteins or fluorescent labels. Surface platforms of protein nanopatterns have potential for applications with screening the selectivity of fluorescent markers and for investigating the binding of small molecules to proteins.

1.1 Atomic Force Microscopy

Molecular-level differences in the thickness and morphology of nanostructures can be investigated using atomic force microscopy (AFM). The background and history of new developments with AFM is summarized in Chapter 2. The history and basic operating principle of AFM is described. The operating principle of contact mode and tapping-mode AFM are described, which are the imaging modes used for scanning probe studies presented in this dissertation.

1.2 Particle Lithography Approaches for Patterning Nanomaterials and Proteins on Surfaces

Recent reports have disclosed protocols for fabricating functional nanostructures based on self-assembly strategies with particle lithography. Particle lithography provides capabilities for high throughput that enables nanoscale control of the surface organization of proteins and nanomaterials. Recent progress with approaches applying particle lithography to generate periodic nanostructures over broad areas of surfaces using proteins and nanomaterials is reviewed in Chapter 3.

1.3 Self-Assembly of Octadecytrichlorosilane: Surface Structures Formed Using Different Protocols of Particle Lithograph

Particle lithography offers generic capabilities for high-throughput fabrication of nanopatterns of organosilane self-assembled monolayers, which offers an opportunity for studies of surface chemical reactions at the molecular level. In Chapter 4, nanopatterns of octadecyltrichlorosilane (OTS) were prepared on surfaces of Si(111) using designed protocols of particle lithography combined with either vapor deposition, immersion, or contact printing. Changing the physical approaches for applying molecules to masked surfaces produced OTS nanostructures with different shapes and heights. Ring nanostructures, nanodots and uncovered nanopores within OTS were prepared using three protocols, with OTS surface coverage ranging from 10% to 85%. Thickness measurements from AFM cursor profiles were used to evaluate the orientation and density of OTS nanostructures. Differences in the thickness and morphology of OTS nanostructures were disclosed with atomic force microscopy (AFM) images. Images of OTS nanostructures prepared on Si(111) that were generated by the different approaches provide insight for the self-assembly mechanism of OTS, particularly for the role of water and solvents in hydrolysis and silanation.

1.4 Protocol Developed for Particle Lithography with Multidentate Thiol Adsorbates Using Vapor Deposition

Surface self-assembly of monothiolated *n*-alkylthiol SAMs have been studied extensively, however analogous studies with multidentate thiol adsorbates have not been as well investigated. A protocol for particle lithography with a tridentate adsorbate, 1,1,1-tris(mercaptomethyl)heptadecane (TMMH) was developed and is described in Chapter 5. Ring nanostructures of TMMH were prepared using the vapor deposition approach for particle lithography. Surface binding of TMMH molecules from a heated vapor was mediated by thiol-gold chemisorption. Characterizations using AFM were used to evaluate the thickness, periodicity and arrangement of TMMH nanostructures.

1.5 Spatially Selective Surface Platforms Prepared by Particle Lithography with Organosilanes for Attaching Fibronectin

By combining particle lithography with organosilane surface assembly, regularly arranged nanostructures can be prepared for immobilizing proteins. The organosilane nanopatterns furnish a robust surface platform that can sustain multiple successive measurements with scanning probe microscopy. Studies with atomic force microscopy (AFM) are presented in Chapter 6 demonstrating that fibronectin can selectively attach to organosilane nanopatterns. The particle lithography based approach for nanopatterning enabled fundamental investigations of protein-binding interactions.

1.6 Conclusions and Future Prospectus

Particle lithography provides high throughput capabilities for fabricating billions on nanostructures on surfaces. A brief summary of the key accomplishments of this dissertation are summarized in Chapter 6, with a prospectus on future directions for this research. Precisely designed and constructed surfaces prepared with particle lithography are useful for viewing antigen-antibody binding at the nanometer scale, to assess the specificity of selective binding, and to evaluate protein orientation and the accessibility of ligands for binding. To advance analytical chemistry approaches to the ultimate limits of sensitivity, miniaturization offers the rewards of reduced quantities of analytes and reagents, increased density of sensor and chip elements and faster reaction/response time. With rapid progress in development of large sets of characterized antibodies, protein and antibody arrays will provide significant advantages for diagnostics and medical science.

CHAPTER 2: ATOMIC FORCE MICROSCOPY

2.1 Overview of Scanning Probe Microscopy

Scanning probe microscopy (SPM) provides capabilities to visualize samples, as well as to characterize and manipulate surface structures. For SPM measurements, an ultra-sharp probe is scanned in a raster pattern across the surface to sensitively detect tip-sample forces. There are three main types of scanning probe instruments, scanning tunneling microscopy (STM), near-field scanning optical microscopy (NSOM) and atomic force microscopy (AFM). The first STM instrument was developed in 1981 at IBM research, Zurich by Gerd Binning and Heinrich Rohrer.[2] Advances with NSOM were introduced 1984, combining an AFM with optical microscopy.[3] The AFM was developed in 1986 by Gerd Binning, Calvin Quate and Christopher Gerber.[4] The main SPM technique used for this dissertation was AFM, which can be configured for multiple types of surface force measurements.

2.2 Atomic Force Microscopy (AFM) Background

Molecular level visualization of surfaces can be accomplished with AFM for characterizing magnetic and non-magnetic samples including polymers,[5,6] ceramics,[7,8] composites[9,10] and biomaterials.[11-14] Ultrasensitive measurements with AFM provide information of the surface properties of samples with nanoscale resolution. Improvements to the instrument design have increased the resolution of AFM to 0.01 nm vertically and 0.1 nm laterally a sharp tip.[15,16]

Probes for AFM measurements are usually made of silicon (Si) or silicon nitride (Si_3N_4) and typically have a diameter less than 30 nm.[17,18] Tips may be composed of diamond and other conducting or semi-conducting materials depending on the operating mode of AFM to be used. The tip is attached to a flexible cantilever.

A schematic of the AFM set-up is shown in Figure 2.1. The piezoelectric scanner directs the movement of the probe in the x, y and z direction to scan the tip across the surface in a raster pattern. The expansion and contraction of the piezoceramic elements of the scanner change dimension in response to voltages applied by an SPM controller. To obtain measurements light from a diode laser is deflected from the reflective coating of the cantilever to a position sensitive photodetector. Quadrant photodiodes detect small adjustments from the laser position as the tip moves up or down, or left and right during scans. The changes in deflection provide a digital map of the surface topography.

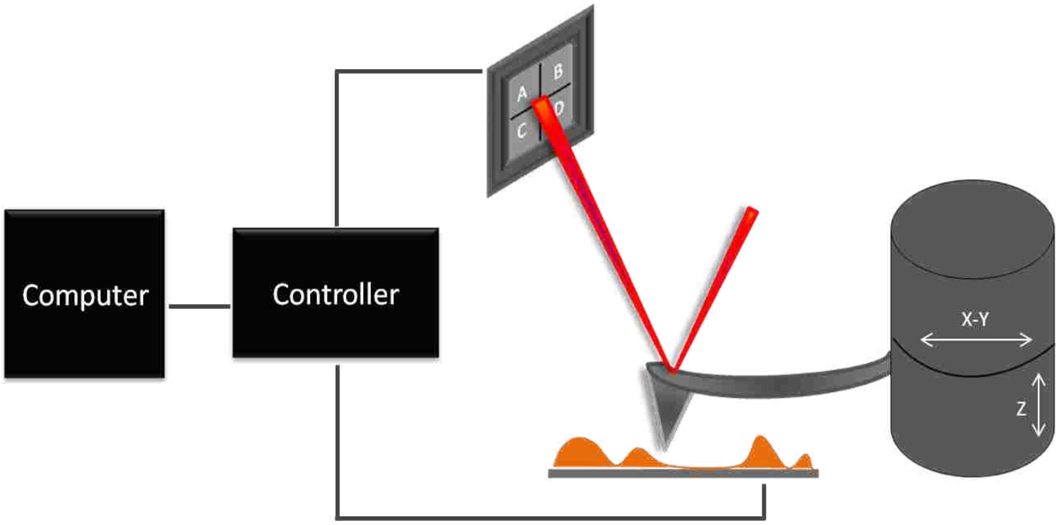

Figure 2.1 Operating principle of AFM.

2.3 Contact Mode and Lateral Force Imaging

In contact mode AFM the tip remains in continuous contact with the surface during a scan. The position of the cantilever is controlled by a feedback loop. A force setpoint is used to control the tip-sample distance by adjusting the magnitude of the cantilever deflection. The cantilever deflection is maintained by incremental adjustments of the voltages applied to the scanner in the z-direction.

Contact mode can achieve true atomic resolution at 0.01 nm vertically and 0.2 nm laterally.[19-22] Atomic corrugations on substrates such as graphite, molybdenum disulfide and pyrolytic boron nitride were imaged with a v-shaped silicon nitride dioxide to achieve less than three angstrom resolution by Albrecht et al.[19] Gold coated silicon dioxide cantilevers with rectangular shapes have been used to resolve individual carbon atoms of graphite to obtain lateral resolution of 2.5 Å.[20] When introducing liquid into the imaging environment, Marti et al. reported vertical resolution of 5 pm and lateral resolution of 0.15 nm using a cross of double wires attached to a diamond tip to scan the surfaces of highly oriented pyrolytic graphite (HOPG) and sodium chloride.[21] Pyrolytic graphite was imaged with a v-shaped silicon nitride tip to achieve atomic scale data in studies conducted by Ruan et al.[22]

Contact mode AFM provides sample information with topographic, deflection and lateral force channels. Topography images provide information of the height scales and lateral dimensions of the sample. As the tip is raster scanned across a surface the position of the laser spot deflected to the photodetector moves according to the up-and-down or left-to-right movement of the probe. Since AFM probes are not symmetric in shape, the left and right linesweeps are sorted into separate channels to generate trace and retrace images. The feedback loop of the instrument controller adjusts the voltages applied to the piezoscanner to correct the signal to the original setting. Topography images are generated by the difference in signal between the top and bottom half of the photodetector. With the four labeled quadrants shown in Figure 2.1, the signals for the topography image are generated by (A+B) - (C+D). The magnitude of the feedback corrects to the original setpoint value to provide information for the error signal, which generates a deflection image. The deflection images are often sensitive to the edges of surface features, but are not typically reported for experimental results. A lateral force image is generated simultaneously in contact mode, which is a map of the lateral twisting and turning of the cantilever. The digital signal for lateral force frames is calculated by the difference in the left and right signals from the quadrant photodiode (A+C) - (B+D). A frictional force image can be generated by subtracting the trace and retrace lateral force images. Nanoscale friction measurements are obtained with AFM by operating the tip in a left-to-right linescan and subtracting the trace and retrace signals.[23]

2.4 Force Spectroscopy with AFM

A force-distance or force curve can be acquired using AFM, an example is shown in Figure 2.2. The measurement was acquired using a v-shaped cantilever (Bruker model MSCT-AFM tip E), with a normal spring constant (k) of 0.10 N/m. Force curves can be obtained on any surface, in air or liquid, with high resolution.[24] Force-distance curves provide information of the long range attractive or repulsive forces between the tip and sample. Studies with AFM force spectroscopy have been reported for evaluating local chemical and mechanical properties such as adhesion,[25-27] and elasticity,[28-30] and bond rupture lengths.[31,32]

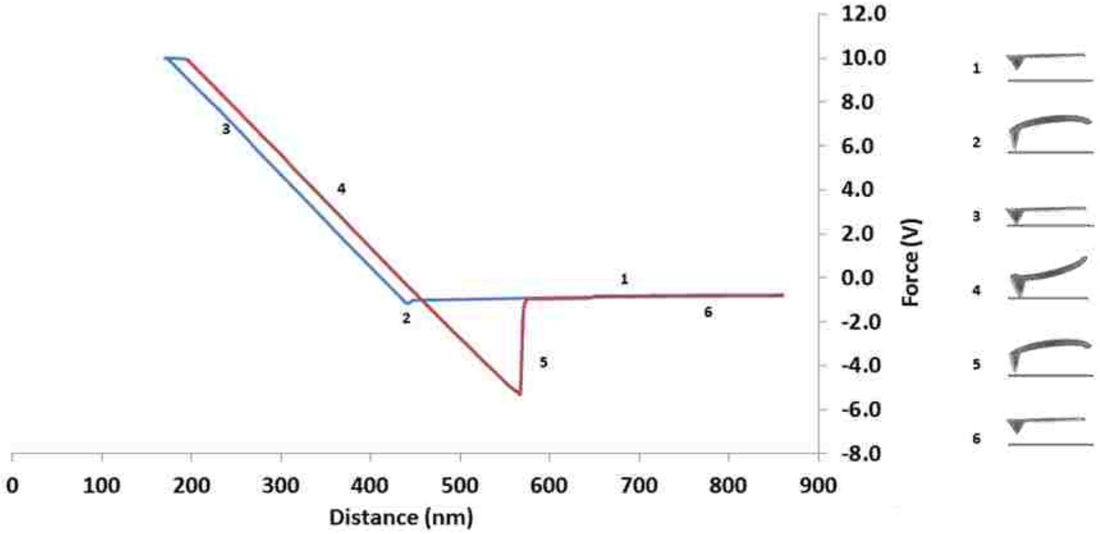

Figure 2.2 Force-distance curve obtained in air with a Si_3N_4 tip for a sample of OTS nanopatterns prepared on a Si(111) substrate.

To generate a force curve an incrementally ramped voltage is applied to the z-segment of the scanner in an approach-retract cycle. The tip is not translated in the x or y direction, rather it is brought into contact and then lifted from the surface at a fixed position. The attractive (red line) and repulsive (blue line) displacements are traced in the force curve of Figure 2.2. At the point where the tip approaches the surface no deflection is recorded, this corresponds to the region of the flat line labeled 1. As the tip snaps into contact with the surface there is an attractive force shown with the deflection of the curve at position 2. As the force is gradually increased while the tip remains in contact with the surface, long and short range repulsive forces cause the cantilever to deflect as shown with region 3 of the curve. As the force is decreased after the maximum deflection, the tip-surface interactions switch from an attractive regime to a repulsive regime, labeled region 4. Adhesive forces hold the probe in position, until the tip snaps off the surface at region 5 of Figure 2.2. Upon retraction, the tip is removed from the surface and no deflection is detected at region 6 of the approach-retract cycle.

A general mathematical description of force spectroscopy is described with Hooke's Law: F=kx; where F=force, k=tip spring constant and x=vertical deflection of the cantilever.[17,18] A plot of the force curve reveals the movement of the piezo versus the deflection of the cantilever. The cantilever deflection is directly proportional to the tip-sample interaction force and thus can be converted to quantitative values. Hysteresis can occur at three sections of the force distance curve: the zero force line (region 1), the contract portion (region 3) and adhesion area (region 4). Hysteresis can occur due to hydrodynamic lag, usually from a thin film of water that forms on the surface, also referred to as the contamination layer. Since the hysteresis is proportional to the velocity of the approach/retract cycle, it can be prevented by reducing the scan rate.

2.5 AFM Tapping-mode and Phase Imaging

Tapping-mode, also referred to as AC mode or intermittent contact mode AFM, was developed to achieve high resolution for soft or sticky samples without damaging the surface (Figure 2.3). For tapping-mode, the cantilever is driven to oscillate by a small piezoactuator located in the AFM tip holder. To control the height of the cantilever above the sample the instrument controller adjusts the height to maintain a certain oscillation amplitude as the probe is scanned over the sample. Tips used for tapping-mode typically are designed to have higher spring constants and longer aspect ratios for AFM operation in ambient air. In liquid media, standard soft probes are suitable for tapping-mode. The spring constant of soft levers is typically 0.1 N/m compared to that of tapping mode probes in air where the cantilever may be in the range

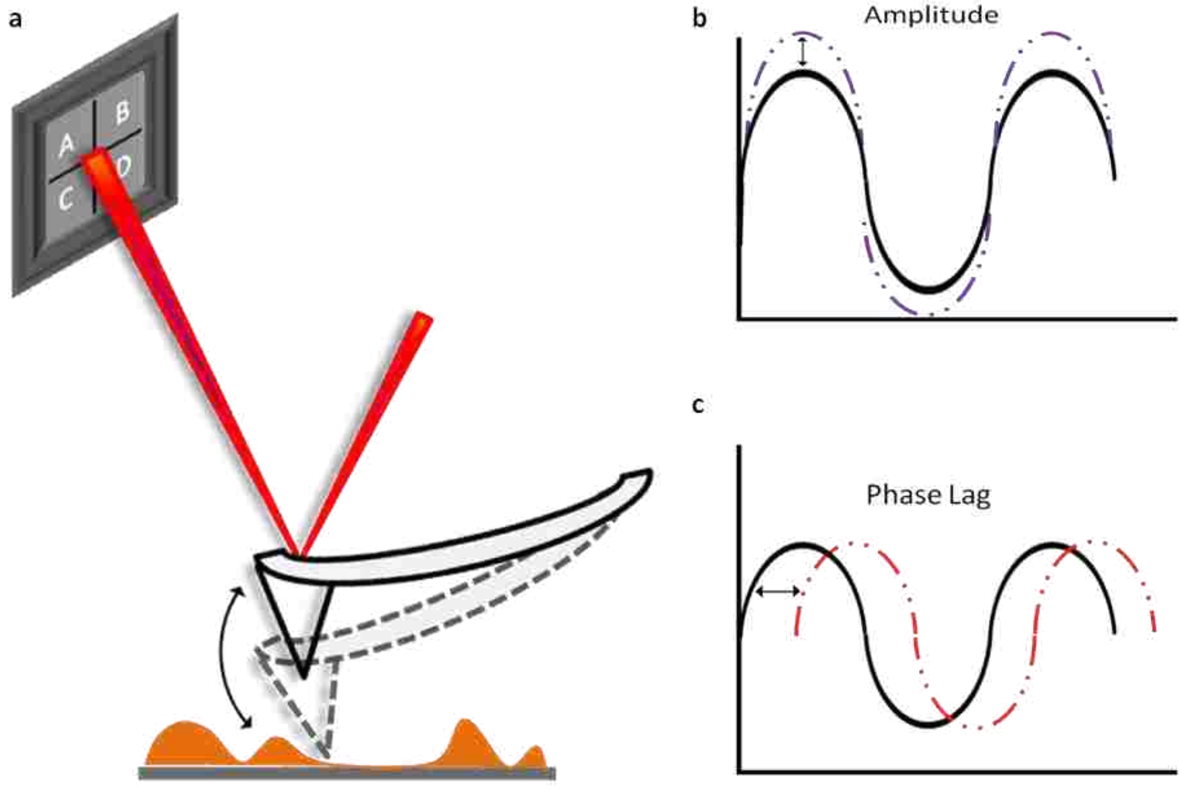

Figure 2.3 Operating principle for tapping-mode AFM.

of 1-100 N/m. Tapping-mode eliminates shear and frictional forces by intermittently tapping the surface, as shown in Figure 2.3a. The tip is driven to oscillate with sufficient amplitude to prevent adhesion to the surface. The oscillation amplitude is used for positional feedback to control the movement of the tip. Before imaging the natural frequency of the cantilever is identified; typically in the range of 200 to 400 kHz. Optimal imaging is achieved at frequencies near this value. As the tip is driven to tap the sample, changes in the surface composition will produce changes in the resonant frequency, oscillation and phase of the motion of the cantilever.

The types of information acquired with tapping-mode include topography, amplitude and phase images. Topography images obtained in tapping-mode are similar to contact mode and provide measurements of the height and lateral dimensions of surface features. Amplitude images in tapping-mode are not composed of actual amplitude measurements. The amplitude is recorded as the probe taps the surface and the net change in amplitude is recorded and compared to the driving amplitude to generate an amplitude image. Tapping the tip on areas of a sample with differences in composition also causes a change in the phase of the oscillation of the cantilever. Differences in phase signals between the measured oscillation of the cantilever and the driving oscillation correspond to surface composition, elasticity, adhesion and friction.

2.6 Artifacts in AFM Images

Image artifacts in AFM can occur from the probe geometry, the scanner, digital processing of images and environmental parameters. The uncertainty in topography measurements depend on the geometry of the tip. An AFM tip is typically less than 30 nm in diameter.[17] The shape of the AFM tip can cause a broadening of surface features known as tip-sample convolution. This occurs when the surface feature is sharper than the apex of the tip. In this case, the shape of the tip dominates the image to present a convolution of the tip and the surface geometry. This effect is illustrated in Figure 2.4. With a dull probe, protruding features appear wider as shown in Figure 2.4a. With a broad tip the probe may not be able to penetrate

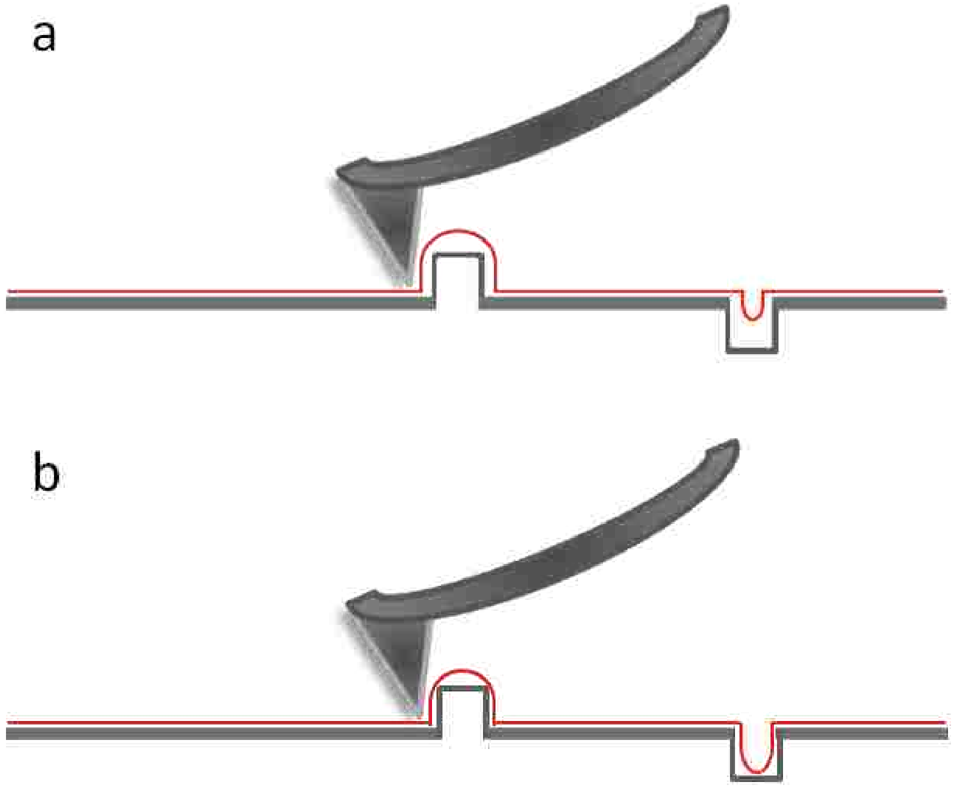

Figure 2.4 Effects of the shape of the AFM probe for representing the lateral dimensions of surface features. (a) The trace pattern of a dull tip scanned across the surface; (b) profile of the scan with a sharp tip.

to evaluate the depth of holes. Using a sharp probe can address the effects of tip-sample convolution, as illustrated in Figure 2.4b. With sharp probes, an accurate representation of the true morphology of the surface shape is traced to reveal finer structural features of the sample. Deconvolution algorithms to reconstruct the shape of surface features can be used if the actual size of the tip is known.

Replicate features are produced for AFM tips with multiple asperities, as shown in Figure 2.5, when the tip has two or more contact points with the sample. The topography images show double features of ring nanostructures of octadecyltrichlorosiloxane (Figure 2.5a). The nanorings were prepared on Si(111) with particle lithography combined with vapor deposition using a mask of 300 nm mesospheres. The true shape of the nanorings are shown in Figure 2.5b.

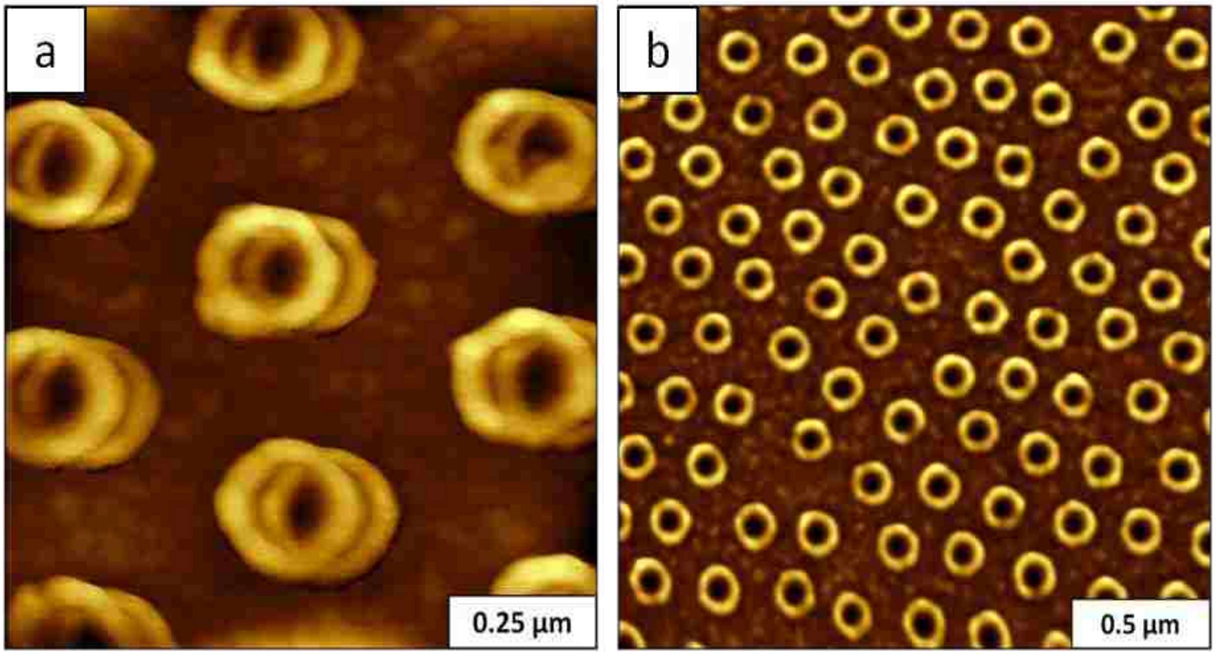

Figure 2.5 Ring nanostructures (a) imaged with a multiple tip and (b) imaged with a probe that did not have multiple asperities.

Artifacts such as line spikes, stretching or compression in AFM images can result from creep, drift and hysteresis of the scanner motion. Creep occurs when moving the probe over wider distances to a new location. If the piezo offsets continue to move the probe in the previous direction, stretching or a distortion may be observed at the edges of the image. To fix such problems, allow time for the scanner to stabilize and then restart the scan to acquire an image. An example of stretching is shown at the very top of the images in Figure 2.6. Nanorings of 2-[methoxy(polyethyleneoxy)propyl] (PEG) silane were prepared using particle lithography combined with vapor deposition. The geometry of the rings should be circular; however in the top two rows of the images the shapes appear to have an oval shape due to the stretching movement of the AFM probe.

Environmental artifacts also affect the quality of AFM images. Artifacts in images may be produced by acoustic or electronic noise from the environment surrounding an SPM instrument. The AFM topograph in Figure 2.7 shows a crisscross pattern of faint lines throughout the surface that were introduced by electronic noise. Electronic noise is readily identified by matching the periodicity to that of electrical outlets (60 Hz). The sample is a film of 1,1,1-tris(mercaptomethyl)heptadecanol (TMMH) prepared on template-stripped gold using particle lithography. Often electronic artifacts can be removed by changing the gain settings of the instrument controllers. Acoustic noise can also be detected by highly sensitive AFM instruments. Opening or closing a door or loud noises can generate linespikes where the probe scanning motion is interrupted. To remove the effects of acoustical noise, AFM scanners are placed within an insulated enclosure and suspended on a hanging platform with bungee cords. The enclosures provide a way to isolate the scanner from the noise and vibration of the environment.

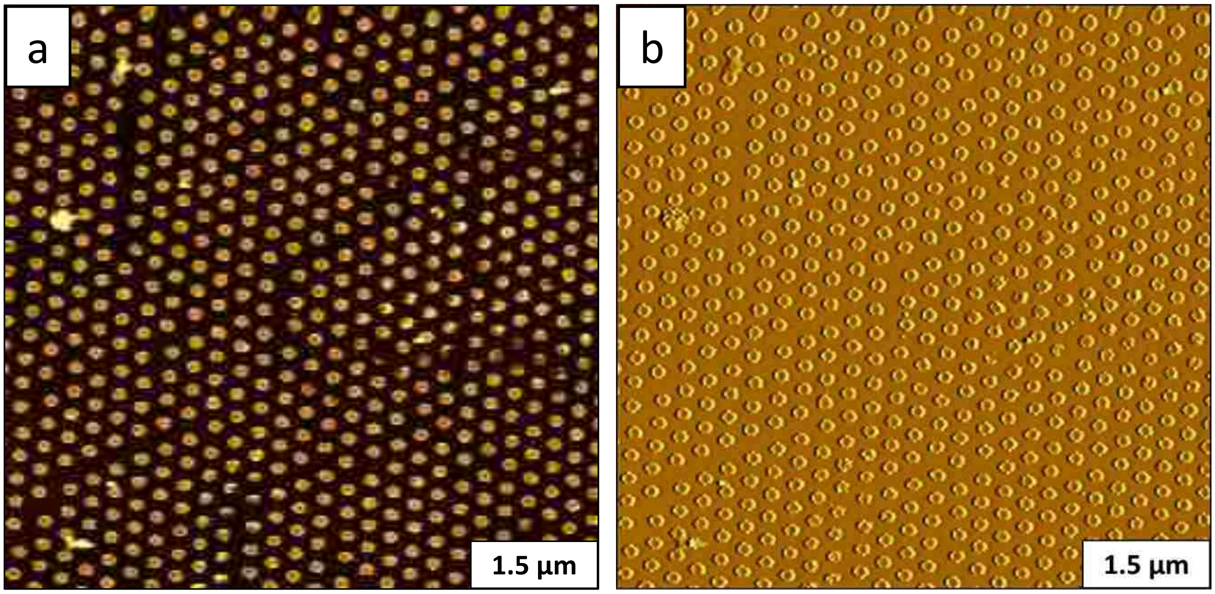

Figure 2.6 Ring nanostructures of 2-[methoxy(polyethyleneoxy)propyl] siloxane with 300 nm periodicity imaged with tapping-mode AFM. (a) Topography image; (b) simultaneously acquired phase image.

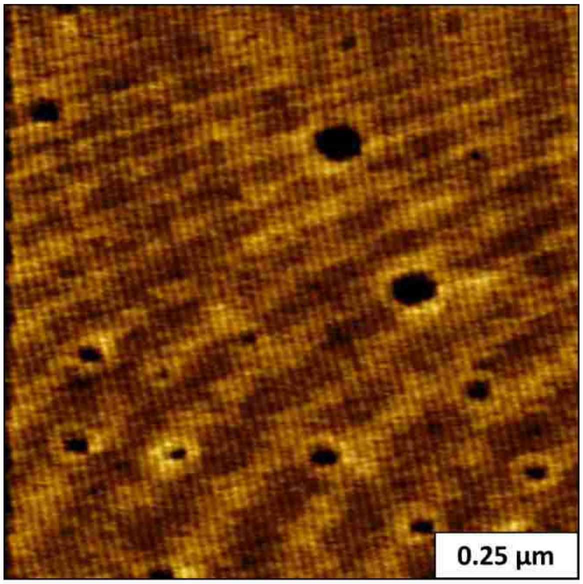

Figure 2.7 Noise artifacts produced in an AFM image.

CHAPTER 3: CHEMICAL APPROACHES FOR NANOSCALE PATTERNING BASED ON PARTICLE LITHOGRAPHY WITH SELF-ASSEMBLED MONOLAYERS

3.1 Introduction

Particle lithography approaches enable patterning of surfaces with nanoscale dimensions using processes of self-assembly. Strategies of particle lithography use latex or silica mesospheres as a surface mask to direct the deposition of molecular films, polymers, proteins, evaporated metals or nanoparticles. Particle lithography has also been referred to as colloidal lithography,[33] nanosphere lithography,[34,35] evaporative lithography[36] or natural lithography.[37] To generate surface patterns with particle lithography a surface mask or template is prepared with monodisperse mesospheres followed by steps of evaporation, etching or deposition. One of the first reports using ‘natural lithography’ was reported by Deckman and Dunsmuir in 1982 to prepare 80 nm silver posts using silica spheres as a deposition mask.[37] Considerable research has been reported for preparing arrays of metal nanostructures using nanosphere lithography for optical, photonic and SERS applications.[38,39] This report will describe developments with particle lithography that have recently emerged for patterning organic thin films as spatially selective surface templates to deposit polymers,[40,41] metals,[42-47] self-assembled monolayers (SAMs),[48-54] and proteins.[55-57]

Monodisperse spheres of latex and silica spontaneously assemble on flat surfaces to form periodic structures arranged in a hexagonal close-packed crystalline lattice. An example of the surface arrangement of polystyrene latex mesospheres prepared on a Si(111) substrate is shown in Figure 3.1, viewed with an atomic force microscopy (AFM) topography frame. Even with diameters as small as 300 nm the spheres assemble into a periodic arrangement. The upper surface viewed with the AFM image reveals a few missing particles, and does not disclose the organization of layers under the surface. It is likely that there are fewer defects in the bottom layer pressed against the substrate because the missing atoms are filled in. It has been reported that the bottom layer will have better packing than the top surface because rows of particles are filled in from upper layers of spheres.[58,59] The inset of Figure 3.1 displays the reciprocal space, Fast Fourier transform (FFT) analysis of the real space topography image to provide a quantitative picture of the long range order and periodicity. The interparticle spacing can be selected by choosing different sizes of spheres.

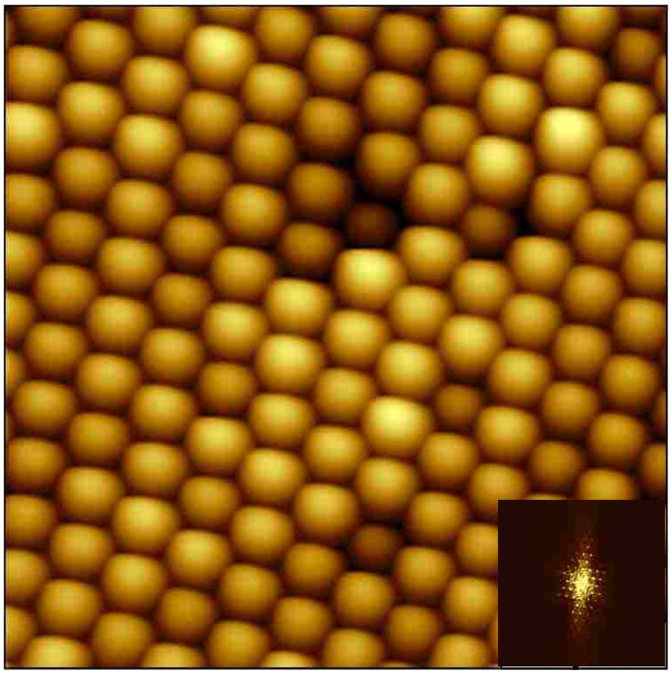

Figure 3.1 Close-packed layer of 300 nm polystyrene mesospheres prepared on Si(111). Contact-mode AFM topograph, 4 x 4 μm^2 with FFT analysis in the inset.

An advantage of approaches with particle lithography is the applicability for a broad range of substrates, including metal films, glass, mica or silicon wafers. The shapes, sizes, geometries and interpattern spacing are highly reproducible for wide areas of the surface. Representative examples of nanofabrication strategies with particle lithography are summarized in Table 3.1.

Table 3.1 Particle lithography examples.

Pattern type	**Surface mask**	**Patterning Method/Approach**	**Mask Removal**	**Pattern Size**	**Ref.**
Inorganic samples					
TiO_2 nanorods	PS, 350 nm- 1 µm	pulsed laser deposition	not removed	n/a	60
TiO_2 nanobowls	PS, 505 nm	atomic layer deposition, ion beam milling	toluene etching	~460 nm diameter	61
silicon nanopillars	PS, 280-440 nm	deposition of Cr nanoparticles via sputtering followed by reactive ion etching	sonication in CH_2Cl_2	9-60 nm diameter	62
Arrays of Ni, Co nanoparticles	PS, 100 nm- 1 µm	electron beam evaporation	dissolution in THF	65-180 nm diameter	63
Co, Fe rings, rods, and dots	PS, 540 nm	temperature treatment of mask, then electron beam evaporation	n/a	30-150 nm	47
rings or pores of cysteine coated CdS quantum dots	PS or silica 200-800 nm	drop deposition of a PS/QD solution with varying ratios, followed by drying	rinsing with ethanol or water		64
rings of CdSe quantum dots	PS, 200 nm- 2 µm	evaporation induced assembly	adhesive tape		36
Organic films					
concentric rings of alkanethiol SAMs	Silica 1.6 µm	printing with a planar PDMS stamp	sonication in water	ring widths of 30-340 nm	65
rings and porous membrane of hexadecanethiol	Silica 800 nm	vapor phase deposition	sonication in water	Avg width =110 nm	66

(Table 3.1 continued)

Pattern type	**Surface mask**	**Patterning Method/Approach**	**Mask Removal**	**Pattern Size**	**Ref.**
rings or pores of OTS, PEG-silane, 6-AAPTMS	PS, 100-500 nm	chemical vapor deposition	rinsing and sonicating in ethanol	~55-250 nm ring widths	51-54
porous OTS film	200-500 nm	solution immersion	sonication in aqueous medium	< 100 nm diameter	49
Biomolecules					
honeycomb rings of BSA, fibrinogen and antimouse IgG	PS, 0.56-5.43 μm	incubation in protein solution	ultrasound in HBSS-Ca^{2+} buffer solution		67
dot arrays of streptavidin and biotinylated antibody	PS, 400 nm	mixed SAMs of thiol-derivatives on gold dot arrays, then immersion in protein solution	sonication in THF		68
arrays of BSA and rabbit IgG	PS, 200-800 nm	solvent evaporation of mixed solutions of latex and protein	rinsing with water		56
ring arrays of BSA, ferritin, apoferritin and rabbit IgG	PS	Solvent evaporation of mixed solutions of latex and protein	rinsing with water		69

*PS, polystyrene; THF, tetrahydrofuran; PDMS, polydimethylsiloxane; ECT, eicosanethiol; SHA, sulfanylhexadecanoic acid; HDDT, 12 hydroxydodecanethiol; HDT, hexadecanethiol; OTS, octadecyltrichlorosilane; PEG-silane, 2-[methoxy-(polyethyleneoxy)propyl]trichlorosilane; 6-AAPTMS, N-(6-aminohexyl)-3-aminopropyltrimethoxysilane; BSA, bovine serum albumin; IgG, immunoglobin G

3.2 Patterning Self-Assembled Monolayers

Combining particle lithography with molecular self-assembly is a practical approach to pattern nanostructures of SAMs to enable nanoscale control of surface chemistry. Strategies with particle lithography have been developed for preparing surface patterns of SAMs, which are single layers of molecules that spontaneously self-assemble on surfaces. The properties of surfaces coated with SAMs can be tailored by the selection of molecular endgroups, i.e. adhesion, wettability and reactivity. Nanopatterns of SAMs can be used for attaching other molecules or nanomaterials to surfaces, and can potentially be used for sensor and electronic applications.[70]

3.2.1 Nanopatterns of Organothiol SAMs

The self-assembly of organothiols on surfaces was first reported in 1983 by Nuzzo and Allara, who discovered that alkanethiols spontaneously assemble on gold to form organized monolayers.[71] In assemblies of *n*-alkanethiol SAMs, thiol molecules form a close-packed, commensurate (√30 x √30)R30° lattice on the Au(111) surface.[72] The alkyl chains within the SAM tilt ~30° with respect to the surface normal. Due to the reproducible geometries and well-ordered surface structures, SAMs of organothiols have become a model platform for studying molecular, cellular and protein binding events.[73-75]

Several approaches based on particle lithography have been reported for patterning organothiols.[50,66] Surface of organothiol patterns with sub-100 nm dimensions were fabricated by a particle lithography based technique developed known as edge-spreading lithography (ESL) by McLellan et al.[50,65,76] With ESL, alkanethiol molecules are transferred from a planar polydimethysiloxane (PDMS) stamp through a particle mask to assemble on a gold substrate. The molecules form a ring-shaped SAM pattern around the circular base of each silica bead, as shown in Figure 3.2. With longer contact times between the PDMS stamp and masked substrate, the ring-shaped area of the SAM expands laterally by spreading.[50,76] The concentric ring patterns shown in Figure 3.2 were produced by successive printing of sulfanylhexadecanoic acid (SHA), 12-hydroxydodecanethiol (HDDT) and eicosanethiol (ECT) for different intervals of contact time. The widths of the rings were found to depend on the length of time for printing and the concentration of the organothiol ink.

3.2.2 Organosilane SAMs.

Organosilane SAMs form chemically robust films due to the covalent nature of surface binding and the cross-linked siloxane network that forms. Post-chemical modification of siloxane SAMs to tailor the surface properties can be accomplished with further chemical steps without destroying the original thin film. Organosilane SAMs have applicability to a wide range of substrates (e.g., silicon oxide, aluminum oxide, germanium oxide, quartz, glass, gold, mica).[77] Nanopatterns of organosilanes provide a molecular platform for integrating other molecules or nanomaterials into surface sites with designed geometries.[78,79] Applications of organosilane

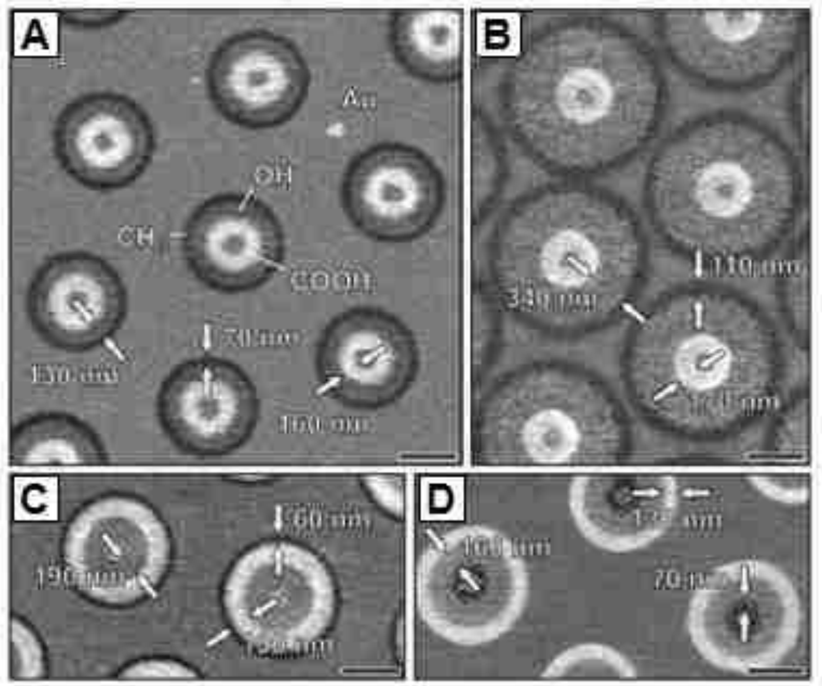

Figure 3.2 Concentric ring nanopatterns of alkanethiolate SAMs on gold prepared by ESL using 1.6 µm silica particles displayed with lateral force microscopy images: (a) ring patterns prepared by successive printing of SHA, HDDT, and ECT; (b) the ring width increased with longer printing times; (c) patterns prepared by changing the sequence of printing of HDDT, SHA and ECT; (d) concentric rings produced by first printing ECT, then HDDT and SHA. Scale bars are 500 nm. *Reproduced with permission from ref.* [65].

SAMs encompass functional films for surface sensors,[72,80] molecular electronic devices,[81] surface coatings[82] and lubricants.[83]

To form organosilane SAMs, trace amounts of water are required to initiate surface hydrolysis of triethoxy- or trichlorosilanes to form silanols, which then either form siloxane linkages to the surface or undergo condensation to effect polymerization of organosilanols.[84,85] The location of water residues on surfaces were found to influence the surface geometry of nanopatterns of organosilane SAMs prepared with particle lithography.[51,52,54] Changing the drying conditions of latex masks can be used to control the distribution of water residues on mica surfaces, as demonstrated in Figure 3.3 with nanopatterns of octadecyltrichlorosilane (OTS). During vapor deposition, the locations of water residues define the sites for deposition of organosilanes and influence the heights of nanostructures.[54]

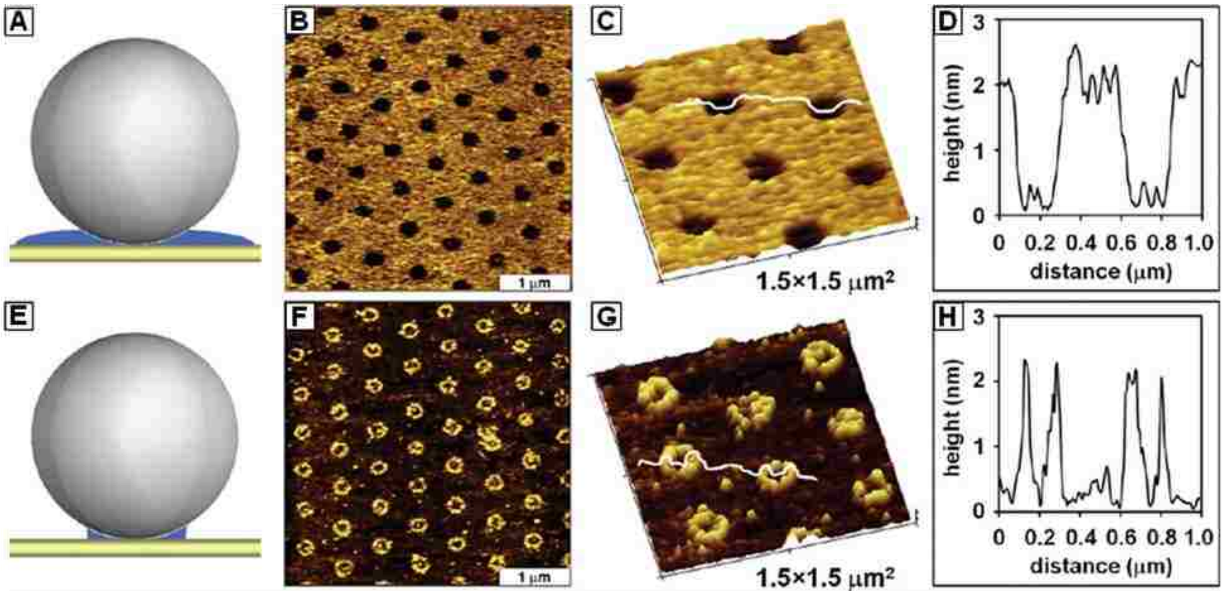

Figure 3.3 Nanopatterns prepared on mica(0001) with particle lithography masks (500 nm latex) exposed to OTS vapor. (a) A thin film of water covers the sites between spheres when the mask is dried briefly; (b) OTS film with periodic nanoholes of uncovered substrate shown with an AFM topograph; (c) zoom-in view of ***b***; (d) height profile for the line in ***c***. (e) A water meniscus forms around the base of mesospheres when masks are dried for several hours; (f) periodic ring patterns of OTS prepared with masks dried longer, viewed by a 4 x 4 μm^2 topography image; (g) close-up view of ***f***; (h) cursor profile for the line in ***g***. *Reproduced with permission from ref.* [52].

For particle lithography, areas where the spherical particles are in contact with the substrate remain protected from chemical modification during the vapor deposition process. Removal of the mask reveals arrays of the deposited molecules. The organosilane nanopatterns generated with particle lithography conform to the arrangement and periodicity of the mesospheres used for the mask. The distribution of water surrounding the mesosphere masks has also been found to influence the surface geometries, defining sites for organosilanes to bind (Figure 3.3). Particle lithography combined with vapor deposition has also been applied successfully for fabricating nanostructures of OTS on Au(111), Si(111) and glass substrates.[51,53] Nanopatterns of organosilanes with other functional groups have also been produced with particle lithography.[52,54]

3.3 Applications of SAM Nanopatterns Prepared with Particle Lithography

The chemical and physical properties of functionalized SAM nanopatterns can be applied as spatially selective sites for patterning proteins,[86-88] nanoparticles[89-91] and polymers.[13,92-94] Studies at the nanoscale are valuable for the development of robust bioconjugation chemistries, which are key for manufacturing surfaces for biochips and biosensors.[95,96]

3.3.1 Protein Nanopatterns Fabricated by Particle Lithography

Adsorption of proteins onto surfaces with preservation of function and activity for binding can be problematic. Proteins tend to self-aggregate, and often bind irreversibly to solids with denaturation caused by the loss of tertiary structure. Approaches for binding proteins to SAMs can improve the viability of protein films and consequently increase the sensitivity of biosensor surfaces. Protein nanopatterns provide a route to increase the surface density of sensor and chip elements as well as to significantly reduce the amount of analyte required for detection. High throughput fabrication methods for preparing protein nanopatterns offer promise for developing protein-based biosensors and biochips with efficiency and economy.[97-99]

A strategy for particle lithography using a mixture approach was developed for generating protein nanopatterns of bovine serum albumin (BSA) and immunoglobulin G (IgG).[56,69] Changing the ratio of mesospheres and protein provides a way to tune the surface coverage and geometries of protein nanostructures.[55] An example with BSA nanostructures produced using 500 nm latex mesospheres as a surface template is shown in Figure 3.4. To prepare nanopatterns of BSA, the protein and latex mesospheres were mixed in an aqueous buffer, deposited on a mica substrate and then dried under ambient conditions. During a brief drying step, the mesospheres assemble on the surface to produce crystalline assemblies, surrounded by protein. The surface template of latex spheres is removed by rinsing with deionized water. The proteins remain attached to the surface to form nanopatterns in areas surrounding and between the latex spheres. Local measurements with AFM cursor profiles reveal that the thickness of protein nanopatterns produced with particle lithography correspond to a monolayer of protein.

A strategy combining particle lithography and silane chemistry was developed for fabricating nanopatterns of lysozyme by Cai et al.[57] A monolayer of undecenyltrichlorosilane (UTS) was prepared on a silicon substrate, in which the vinyl groups were then oxidized to carboxylic groups. Polystyrene nanospheres were deposited on the oxidized UTS to form a mask for patterning. The surface mask was exposed to methyl-terminated OTS by vapor phase deposition and the mask was removed to generate periodic nanopatterns of oxidized UTS surrounded by an OTS resist. Lysozyme was deposited onto the surface where selective adsorption only occurred on the carboxylic acid terminated sites. To evaluate the selectivity of the surface nanopatterns, a drop of rabbit anti-hen white lysozyme antibody in 3 mM HEPES

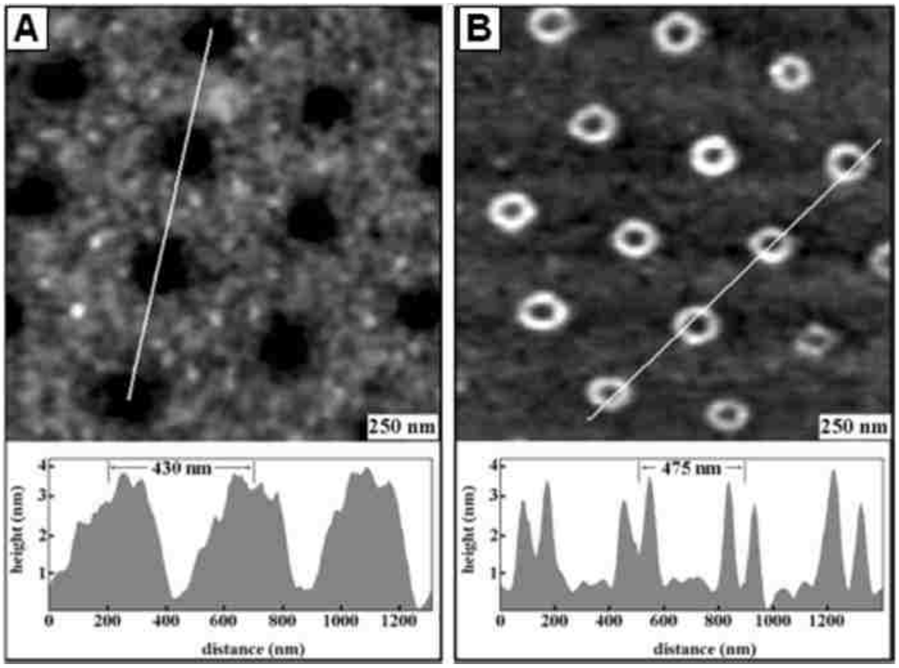

Figure 3.4 Periodic arrays of BSA nanostructures on mica(0001) produced with particle lithography using 500 nm latex spheres. (a) Nanoholes of uncovered substrate within a BSA film viewed with AFM topography image and corresponding cursor profile; (b) ring-shaped nanostructures of BSA formed at a low concentration of BSA, topography view and height profile. *Reproduced with permission from ref.* [55].

buffer was applied to the surface. Antibody adsorption was shown to occur selectively on the lysozyme nanopatterns, in Figure 3.5.

3.3.2 Periodic Arrays of Metal Nanoparticles Produced with Particle Lithography

Particle lithography is a practical route to fabricate nanopatterns of metal nanoparticles over large areas. Surface patterns of triangular metal nanostructures can be obtained by direct deposition of a heated metal vapor through 2D particle masks using techniques such as a magnetron sputtering, electron beam evaporation or thermal evaporation.[100] Most often metal evaporation through surface masks, produces nanostructures that are pyramidal,[101] triangular[94,102,103] or disk shapes.[47,101,104]

An approach using annealed latex masks was used to prepare periodic arrays of metal nanoparticles with pattern features as small as 30 nm, by Kosiorek et al (Figure 3.6).[47] For surface masks of polystyrene latex, the size of the apertures between nanospheres can be reduced by heating. The aperture between the 540 nm latex spheres was reduced from 200 to 30 nm by a heating step. Depositing a metal through the annealed latex mask was found to produce smaller nanostructures than when masks were not annealed.

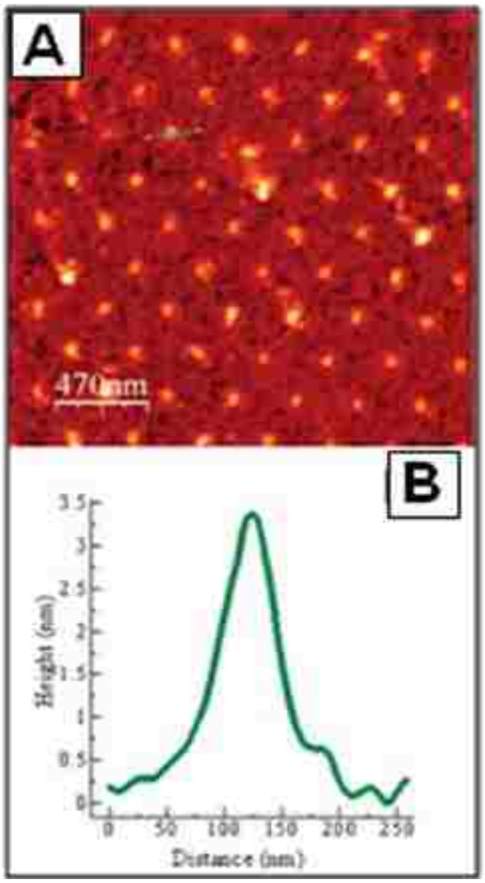

Figure 3.5 Adsorption of antibody on lysozyme nanopatterns prepared on silicon wafers using particle lithography combined with silane chemistry. (a) Lysozyme nanostructures after antibody adsorption viewed with an AFM topograph; (b) cursor profile for the green line in ***a***. *Reproduced with permission from ref.* [57].

Metal ring nanopatterns composed of Cu, Au and Pt nanoparticles were prepared on Si(100) and highly oriented pyrolytic graphite (HOPG) substrates using a particle lithography strategy developed by Bayati et al.[105] Nanorings were produced by exposing a surface template of 505 nm polystyrene spheres to a metal precursor solution (10 mM) for 2 h, followed by reduction of the metal salt with $NaBH_4$. Removal of the template was accomplished with chloroform rinses to produce arrays of metal nanorings. Examples with different metals are shown by AFM views in Figure 3.7.

Semiconducting nanoparticles or quantum dots exhibit unique size-dependent properties that can be useful for electronic, optical and sensing applications.[106-108] Arrays of semiconducting nanoparticles are potential candidates for solar cells and photovoltaic devices.[109] A particle lithography approach coined as "two-particle" lithography was reported by Lewandowski et al. for defining the arrangement of cysteine-coated CdS quantum dots.[64] For two-particle lithography, the larger latex spheres provide a structural template to define the arrangement of smaller nanoparticles. As the liquid mixture of two particles is dried, nanoparticles assemble surrounding the base of latex or silica spheres to generate patterns that conform to the arrangement of mesospheres. The arrangement of nanoparticles exhibit circular ring or pore morphologies according to the spherical shape of the meniscus sites at the base of

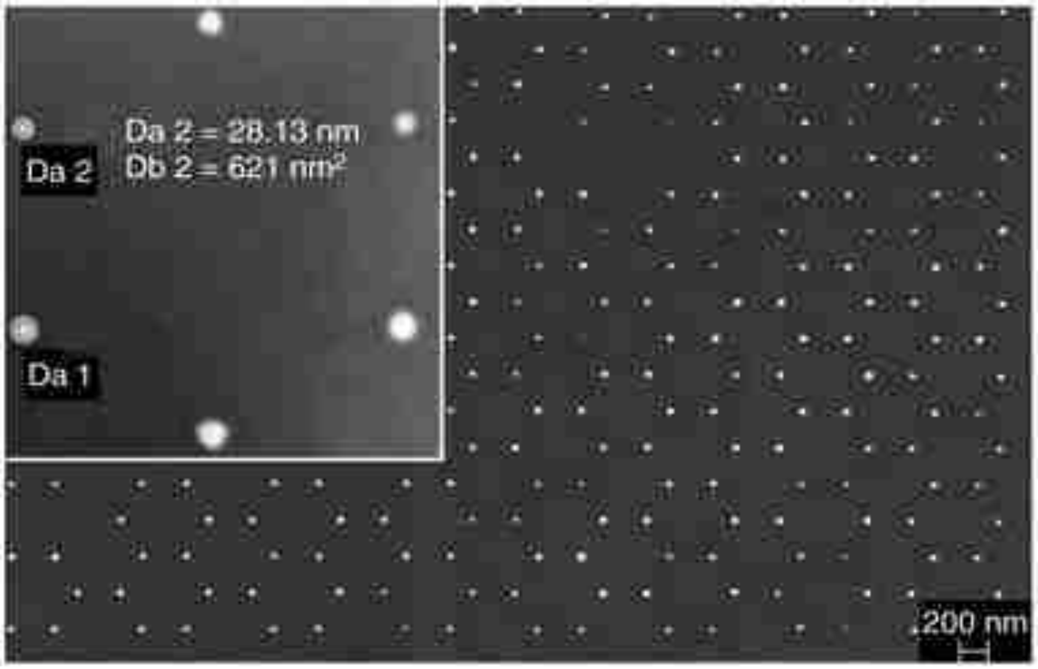

Figure 3.6**.** Arrays of Co nanoparticles on a silicon substrate prepared by evaporation of cobalt on annealed masks of 540 nm. Reproduced with permission from ref. [47].

mesospheres. Once the solution conditions are optimized, replicate samples prepared using a given ratio and particle diameter exhibit reproducible morphologies and periodicity.

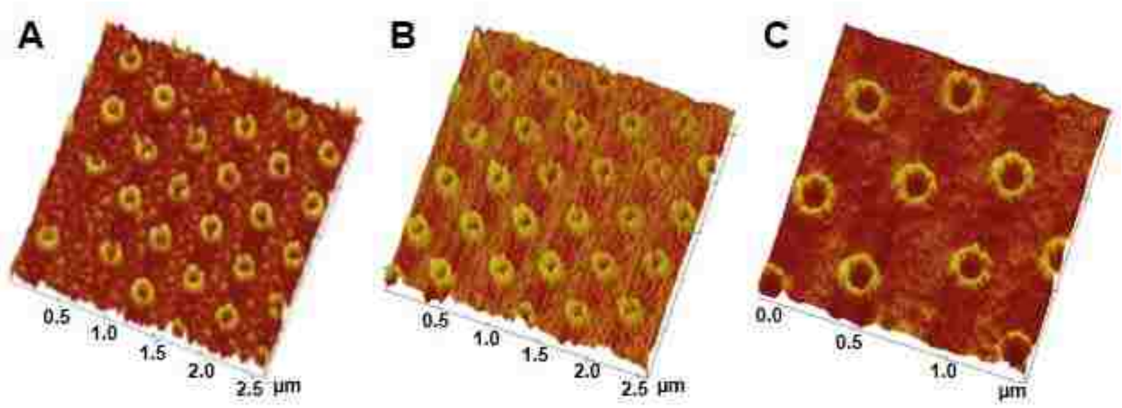

Figure 3.7 Arrays of metal rings produced by wicking metal precursor through the interstices between polystyrene nanospheres. Nanorings of (a) Cu, (b) Au, and (c) Pt prepared on Si(100) substrates viewed with AFM topographs; the vertical scale bars are 5 nm. *Reproduced with permission from ref.* [105].

A solution-based approach for patterning quantum dots was developed by Taylor et al.[110] A monolayer monodisperse polystyrene monolayer was applied to a glass substrate, then a protein repellant layer of methoxy-polyethylene glycol-silane was grafted onto the surface. The mask of mesospheres was removed to form spatially selective surface patterns for defining the sites for adsorption of quantum dots. An example of the nanopatterns of quantum dots is shown in Figure 3.8.

Patterns of organosilanes prepared by particle lithography furnish an excellent platform for binding metal nanoparticles, as demonstrated by Li et al.[52] Gold nanoparticles were selectively attached onto designed organosilane nanopatterns, which were prepared by particle lithography combined with vapor deposition.[52] To define the spatial selectivity for binding gold nanoparticles, arrays of OTS nanostructures were prepared by vapor deposition with 300 nm latex masks. When the mask was removed, a thin film of OTS with periodically arranged nanoholes of uncovered Si(111) substrate were exposed. The areas of bare substrate were

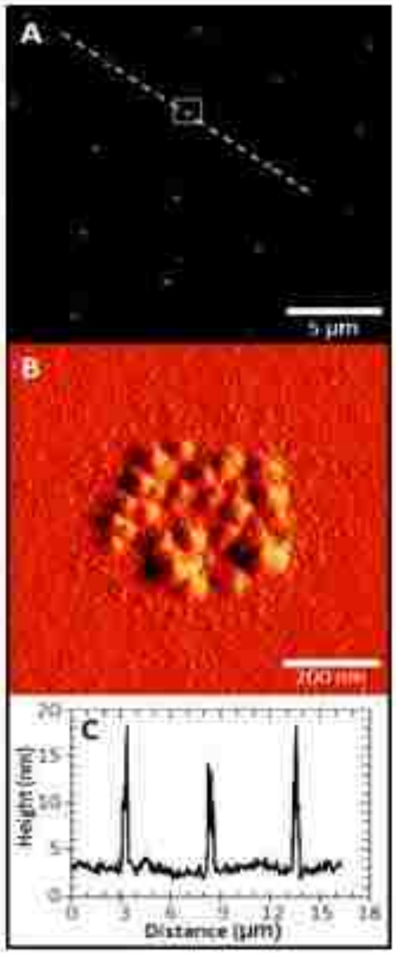

Figure 3.8 Dot nanostructures of quantum dots coated with IgG prepared by particle lithography with 500 nm latex spheres as a surface template. (a) AFM topography image; (b) close-up view of a single nanostructure within the box in ***a***; (c) cursor profile for the dotted line in ***a***. *Reproduced with permission from ref.* [110].

chemically modified with a second organosilane via solution immersion to define sites for binding gold nanoparticles. The nanoholes were backfilled with thiol-terminated 3-mercaptopropyltrimethoxysilane (MPTMS). The nanopatterns of MPTMS surrounded by an OTS matrix was immersed in a solution of gold nanoparticles for several hours. Gold nanoparticles were demonstrated to bind selectively on areas patterned with MPTMS, as shown in Figure 3.9.

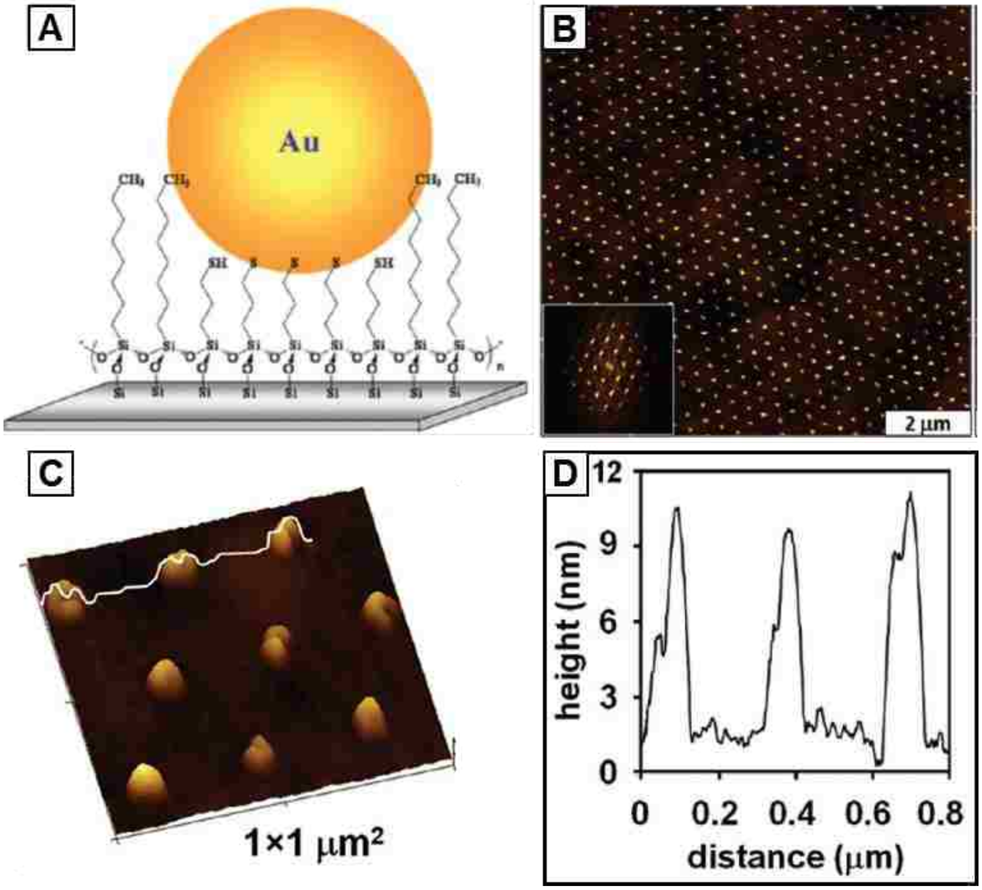

Figure 3.9 Nanopatterns of organosilanes were used to define the surface spatial selectivity to bind gold nanoparticles on Si(111). (a) Gold nanoparticles attached to areas with MPTMS; (b) Wide view of the arrangement of gold nanoparticles, 10 x 10 µm^2 topograph, inset is the corresponding FFT image; (c) zoom-in view of ***b***; (d) height profile for the line in ***c***. *Reproduced with permission from ref.* [52].

3.4 Approaches to Minimize Defect Density for High-Throughput Applications

Defects in the arrangement of close-packed lattices of the particle masks are introduced by variations in the sizes of the spheres; monodisperse sizes are a requirement for defect-free packing. Defects in the packing of spheres become an important consideration for developments of photonic crystals. When films of latex spheres are dried, a few cracks are formed over broader areas of microns, which are produced by shrinkage during the drying step. The roughness of the underlying substrate morphology can also contribute to shifts in registry and areas with vacancies. Surfaces which are atomically flat, such as mica(0001), generate a lower density of defects. Imperfections of the substrate, i.e. point defects, scratches, dislocations and grain boundaries can propagate into imperfections in the packing of the spheres. Multiple approaches have been developed to produce higher quality latex masks, and this topic has been reviewed in previous reports.[104,111-113] Surface arrays of mesospheres can be prepared by spin-coating,[114] drop-deposition, or Langmuir-Blodgett[115,116] protocols. Methods reported for producing defect-free arrays of spheres include driving the spheres to assemble using gravitational sedimentation,[117-119] surfactants[115] or with an electric field.[120,121] Controlling the evaporation of particles using convective assembly has also been proposed.[58]

3.5 Prospectus

When considering requirements for manufacturing surfaces with advancements in nanotechnology, self-assembly is emerging as an indispensable approach for organizing materials at the molecular scale for practical reasons. Particle lithography provides advantages of low cost, applicability to a wide range of substrates and nanomaterials, and capabilities for high-throughput construction of regularly-shaped surface patterns of defined dimensions and composition. Preparing chemically selective surface sites for selective adsorption of nanomaterials can be a problem, because of the potential issues of self-exchange, stability and self-reactive properties of organic thin films. Fundamental studies of surface changes in response to environmental parameters (heat, pH, solvents) will help to address the criteria for applications with designed nanostructures. Nanoscale test platforms prepared by particle lithography are particularly suited for developing surface-based assays with biomolecules, and will provide advancements for highly sensitive studies for screening fluorescent markers, evaluating protein-small molecule binding and testing the selectivity of protein binding.

CHAPTER 4: SELF-ASSEMBLY OF OCTADECYLTRICHLOROSILANE: SURFACE STRUCTURES FORMED USING DIFFERENT PROTOCOLS OF PARTICLE LITHOGRAPHY[122*]

4.1 Introduction

Self-assembled monolayers (SAMs) of organosilanes have become important as surface resists and functional coatings for micro and nanopatterning applications.[123-127] The surface self-assembly of organosilanes such as octadecyltrichlorosilane (OTS) is complicated, requiring mechanistic steps of hydrolysis, cross-linking and silanation.[128-131] To develop robust and reproducible lithography procedures with OTS, parameters such as temperature, humidity, solvents, physical deposition conditions and mask materials can be systematically changed to enable nanoscale studies of surface assembly.

For methods of particle lithography, a surface mask of polystyrene latex or silica mesospheres is used to direct the deposition of organic thin films and nanomaterials. Particle lithography with organosilanes provides a practical way to define spatial selectivity at the nanoscale for further steps of linking nanomaterials to surfaces. Billions of nanostructures can be prepared with relatively few defects and high reproducibility to enable patterning of large areas. Particle lithography has previously been applied to pattern metals,[132,133] nanoparticles,[134-137] proteins,[138-140] polymers[141-144] and self-assembled monolayers (SAMs).[145-149] Organosilane SAMs can be applied to substrates such as gold,[150,151] glass,[152] mica,[153-155] quartz,[156,157] indium-tin oxide (ITO),[158] or silicon (Si).[129,152,159-162] With particle lithography, organosilanes bind covalently to surface sites where trace amounts of water is to produce robust nanostructures.[158]

The morphology of SAMs or nanostructures of OTS reflect a balance of the interactions that occur between the silane precursor and the silanol groups, interactions between the end

---

*Reproduced with permission from the Beilstein Journal of Nanotechnology groups, interactions between the alkyl chains of the silane molecules, and the nature of the substrates.[163,164] These intramolecular interactions along with parameters such as temperature, solvent type and trace amounts of water present a challenge for reproducible fabrication with organosilanes such as OTS.[129,163-169] Preparation methods affect the growth rate, surface coverage and orientation of OTS.[170]

Molecular-level differences in the thickness and morphology of OTS nanostructures prepared by different lithography procedures can be investigated using atomic force microscopy (AFM). Particle lithography enables control of deposition parameters for tailoring the surface coverage, surface geometries and pattern dimensions. Close-packed arrays of latex or silica mesoparticles were used as surface masks to direct the deposition of OTS on surfaces to form nanopatterns. Essentially, the physical state of the molecule was changed for the three protocols. Molecules were applied either in a vapor phase, as a liquid film, or in dilute solvent conditions to enable nanoscale studies of the surface organization and self-assembly of OTS.

4.2 Results and Discussion

Comparing the geometries and thickness of nanostructures produced with particle lithography were used to systematically investigate parameters for surface self-assembly of octadecyltrichlorosilane (OTS). Three methods of particle lithography for preparing organosilane nanostructures are compared, as shown in Figure 4.1. Each approach uses a different strategy for applying organosilanes to the masked surface of Si(111), using either heated vapor deposition, contact printing, or immersion in a silane solution. For comparison of the different particle lithography strategies, the samples were prepared using masks of polystyrene latex (200 nm diameter); the mesospheres have a size variation of 1-2%. Organosilanes attach to surfaces by successive steps of hydrolysis and condensation, therefore nanoscopic amounts of water are needed to initiate the reaction. By controlling the drying parameters of the latex masks, different nanopattern geometries are produced.[148,158]

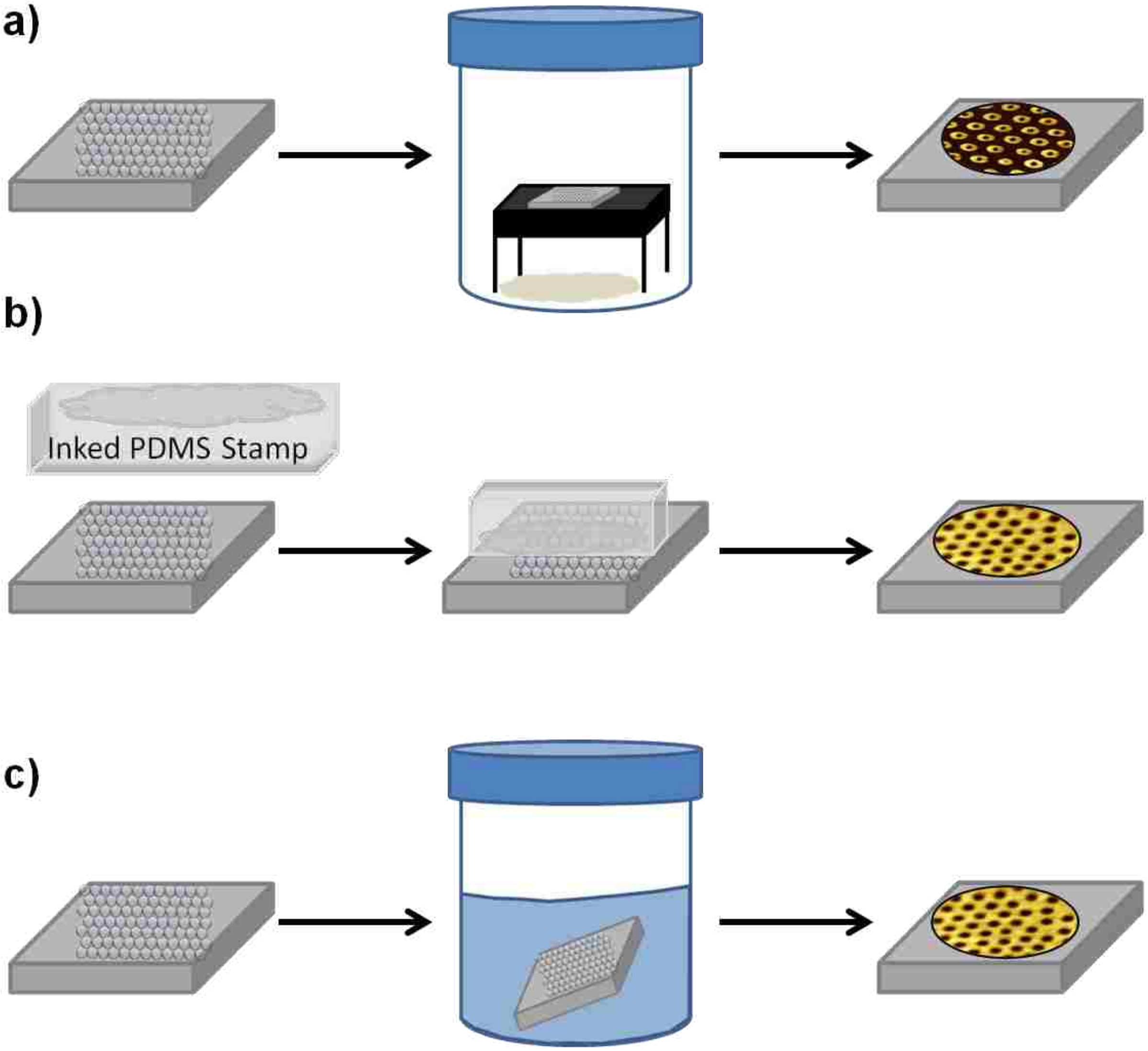

Figure 4.1 Strategies for preparing organosilane nanostructures using particle lithography. Basic steps are shown for (a) vapor deposition; (b) contact printing with PDMS; (c) solution immersion of Si(111) surfaces coated with mesoparticle masks.

4.2.1 Nanostructures Produced with Particle Lithography using Vapor Deposition of OTS

By combining particle lithography with vapor deposition of OTS, arrays of ring-shaped nanostructures were formed on Si(111), shown by the contact mode AFM images in Figure 4.2.

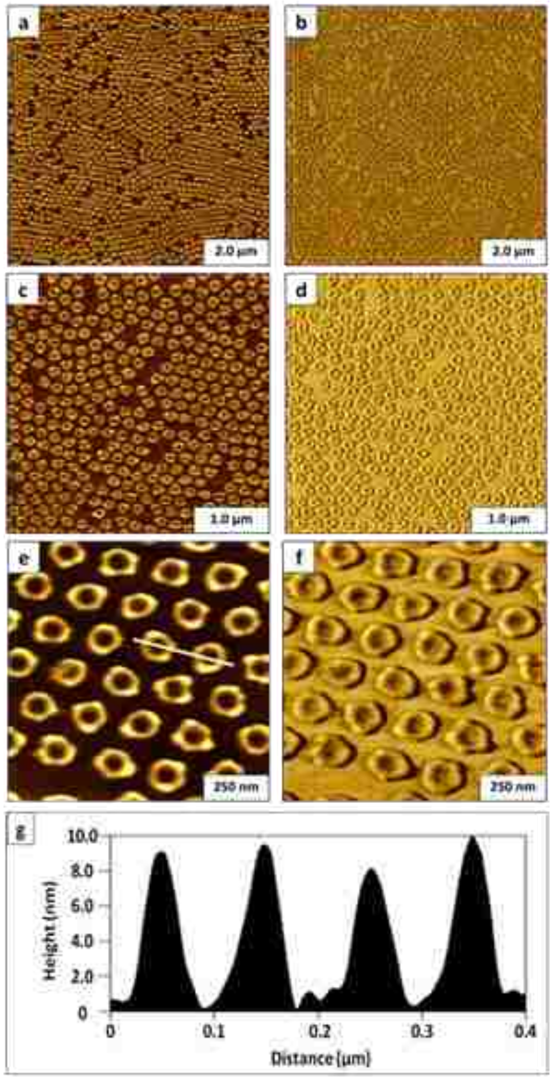

Figure 4.2 Combining particle lithography with vapor deposition of OTS produced ring-shaped nanostructures. (a) Contact-mode topograph, 8 × 8 μm^2; (b) simultaneously acquired lateral force image. (c) Higher magnification topograph (4 × 4 μm^2); (d) corresponding lateral force image. (e) zoom-in topography view of 1 × 1 μm^2 area; and (f) lateral force frame. (g) Height profile for the white line in ***e***.

A wide area frame (8 × 8 μm^2) in Figures 4.2a and 4.2b reveals the arrangement of hundreds of circular nanostructures, showing a few gaps of uncovered substrate. There are 336 ring nanostructures within the 4 × 4 μm^2 frame of Figures 4.2c and 4.2d. If the array were perfectly ordered and densely packed the frame would accommodate 360 nanostructures, indicating a defect density of ~ 7%. The dimensions and circular shapes of the nanostructures are highly regular circles of consistent heights. Within the 1 × 1 μm^2 close-up view, 29 patterns are packed closely together (Figures 4.2e and 4.2f). This scales to an overall surface density of 3×10^9 patterns/cm^2. The areas confined within the centers of the rings have the same color as the surrounding substrate for both topography and lateral force frames of Figures 4.2e and 4.2f. The central areas of the rings were masked by the latex mesospheres, and meniscus-shaped areas of OTS have formed surrounding the base of the latex particles to generate the nanopatterns.

The cursor line profile across two of the rings (Figure 4.2g) shows the baseline within the rings is the same height as the background areas of bare Si(111). A monolayer of OTS has a thickness ranging from 2.26 to 2.76 nm.[123,162,171-173] The height of the rings measures 10 ± 2 nm, which corresponds to 4-5 multiple layers of OTS. The center-to-center spacing between the ring structures is approximately 200 nm, which matches the diameter of the latex mask.

When the latex masks were dried, a water meniscus persists at the base of each latex sphere on the surface, which defines the reaction sites for hydrolysis and condensation of the organosilanes.[171] For the example of Figure 4.2, the interstitial areas between the OTS rings remain uncovered, and OTS was shown to bind only in the areas pinned beneath the base of latex spheres. The cursor profile shows the same height surrounding the rings and inside the rings, which references the baseline of uncoated subustrate. The location of water residues on the surface defines the sites for OTS binding; for example with the more hydrophilic substrate of mica(0001) attachment to the interstitial areas of the surface between spheres was observed for latex masks that were dried briefly.[174] If the masks formed on Si(111) are dried briefly more water persists on the surface, thus OTS also binds to the interstitial areas between the rings (Figure 4.3). An example is shown of OTS nanopatterns with different heights outside and within

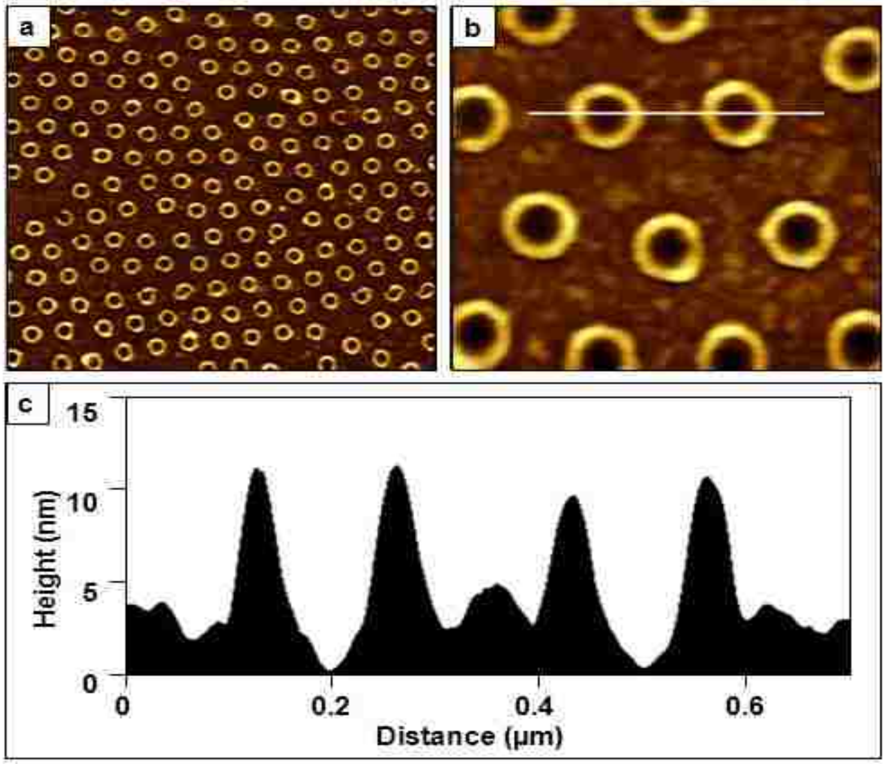

Figure 4.3 Particle lithography with vapor deposition of OTS produced multilayered ring nanostructures surrounded by an OTS monolayer. (a) Contact-mode topograph, 4 × 4 µm^2; (b) zoom-in view, 1 × 1 µm^2; (c) Corresponding cursor profile for ***b***.

the rings. The cursor profile across two of the ring patterns shows a height of 4±1 nm between the rings, the rings measure 12±2 nm in height, and the shallowest area inside the rings can be used as a reference baseline for the uncoated Si(111) substrate. Water residues persist throughout the surface; however there is a taller zone of water trapped in the meniscus areas surrounding the spheres. Interestingly, we have observed that the height of the meniscus is taller for larger diameter latex spheres, which correspondingly produces scalable heights for organosilane ring nanopatterns.[171]

4.2.2 Particle Lithography Combined with Contact Printing with PDMS Stamps

To produce monolayer nanostructures of OTS, particle lithography with contact printing and immersion were evaluated to optimize the deposition conditions for achieving a densely-packed SAM. Images of a nanostructured film of OTS prepared using particle lithography combined with contact printing are shown in Figure 4.4. A honeycomb arrangement of

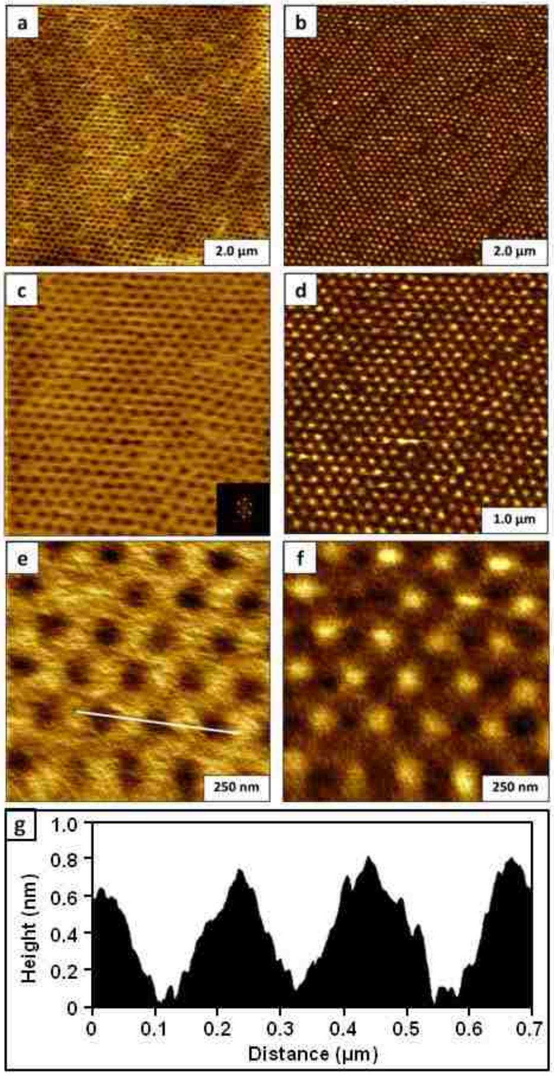

Figure 4.4 Nanopore structures of OTS were formed with particle lithography combined with contact printing. Contact mode AFM images are shown for a sample prepared with 200 nm latex mesospheres on Si(111). (a) 8 × 8 µm^2 topograph and (b) corresponding lateral force image. (c) Zoom-in topograph (4 × 4 µm^2) with FFT shown in the inset; (d) simultaneously-acquired lateral force frame. (e) Topography frame (1 × 1 µm^2) with (f) corresponding lateral force image. (g) Height profile for the white line in ***e***.

nanopores is shown in Figure 4.4a, with approximately 25 x 20 rows of dark holes within a film of OTS within the frame. The corresponding lateral force image of Figure 4.4b reveals the shapes of the holes as bright spots, for the bare areas of Si(111) where latex was displaced. At higher magnification, 438 nanopores are packed within the 4 × 4 μm^2 μm^2 images of Figures 4.4c and 4.4d which scales to an approximate surface density of 2.7×10^9 nanostructures/cm^2. This value is comparable to the pattern density for Figure 4.2, because the latex diameter of the surface masks determines the packing density. The inset of Figure 4.4c is an FFT of the topograph, and represents a mathematical average of the 2D lattice of the hexagonal array. A further magnified view is presented in Figures 4.4e and 4.4f showing ~ 27 nanopores. The lateral force image confirms that the holes are uncovered Si(111), because of the distinct change in chemical contrast between OTS and the nanopores. Referencing the uncovered areas of the substrate as a baseline the height of the OTS film measures 0.6 ± 0.1 nm (Figure 4.4g), which indicates that molecules have a side-on orientation with the hydrocarbon backbone oriented parallel to the substrate.

Multiple replicate samples were prepared using contact printing for different size masks, showing that the heights were consistent with the example of Figure 4.4. For OTS transfer by contact printing, a solution of solvent and silane at a 40% (v/v) concentration was placed on the surface of a PDMS block and dried. This process mostly likely forms a thin cross-linked film of OTS that does not bind to the polymeric surface of PDMS.

After the mask is placed in contact with the sample, the liquid film was transferred to the Si(111) substrate by liquid permeation through the latex mask. The side-on orientation of OTS could be attributable to the nature of the interface, with physisorption of the hydrocarbon backbones of OTS occurring on the highly charged surface of PDMS. The packing arrangement at the interface is transferred from the PDMS stamp to the Si(111) surface and retains the side-on orientation because of cross-linking between adjacent molecules. The evidence for a cross-linked film was acquired indirectly, by immersing the OTS nanostructures in a second silane solution. An incomplete or partial monolayer would likely be a poor quality resist for further chemical steps. However, this was not the case. Nanopores were backfilled with a second organosilane without evidence of non-specific binding on OTS coated areas (*data not shown*).

4.2.3 Particle Lithography by Immersion of Latex Masked Substrates in Silane Solutions

A completely different morphology than rings or nanopores was observed for OTS nanostructures produced by immersion of particle masks. Dot-shaped nanostructures were produced using latex particle lithography with immersion, as shown in Figure 4.5 with wide area and zoom-in topography views. The long range periodicity of the array of nanodots is shown with an FFT within the inset of Figure 4.5a. The surface density of the nanodots is approximately 3.3×10^9 nanostructures/cm^2, showing ~120 nanopatterns within the 2.5 × 2.5 μm^2 frame shown in Figure 4.5b. The heights of the nanodots measure 0.5 ± 0.3 nm.

Immersion of a masked substrate in a solvent is the most common approach for preparing films of OTS, and has produced the most consistent thickness of a monolayer. However, immersion in solvents causes rapid detachment of the latex masks. To enable an immersion process for particle lithography, a brief heating step was developed to solder the latex beads to the substrate (75°C for 30 min). Latex deforms when heated, leaving less area of the surface available for OTS deposition.[175] After the heating step, the only remaining areas that were not masked by latex are the triple hollow sites formed between spheres, and the geometries and periodicity of the nanodots shown in Figure 4.5 correspond to these sites.

4.2.4 Surface Masks of Colloidal Silica Mesospheres

Silica mesospheres do not deform as readily as polystyrene latex, and can sustain longer heating at higher temperatures.[146] Results for OTS nanostructures produced with silica masks are shown in Figure 4.6. Nanohole structures are shown in the wide area (Figure 4.6a; 2.75 × 2.75 μm^2) and high magnification (Figure 4.6d; 1.5 × 1.5 μm^2). The topography frames reveal periodic patterns within a monolayer film of OTS, with exquisitely small holes at the locations where silica mesospheres (250 nm diameter) were displaced. There are 38 nanopores in the zoom-in views of Figures 4.6d and 4.6e which would scale to a surface density of 1.7 billion patterns/cm^2. The depth of the OTS film measures 2.0 ± 0.2 nm (Figure 4.6c and 4.6f) referencing the uncovered area of Si(111) as the baseline. This value corresponds to a nearly upright configuration of an OTS monolayer. The diameters of the nanoholes measured 102 ± 11 nm. The center-to-center

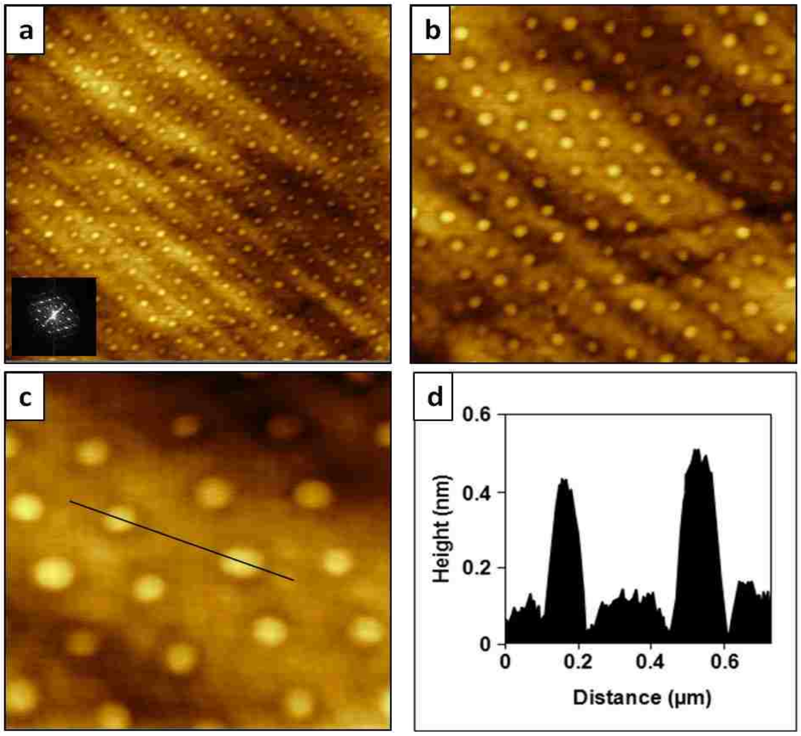

Figure 4.5 Nanodots of OTS produced with immersion of annealed latex masks. Contact mode AFM images are shown for OTS nanostructures formed on Si(111) with 200 nm latex. (a) Topography image, 4.5 × 4.5 μm^2 and FFT inset; (b) zoom-in, 2.5 × 2.5 μm^2; (c) close-up view, 1 × 1 μm^2; (d) height profile of the line in ***c***.

spacing between the holes corresponds to the diameters of the silica mesospheres (250 nm) used a structural template to pattern the OTS. The overall coverage of the OTS film was estimated to be ~85% of the surface.

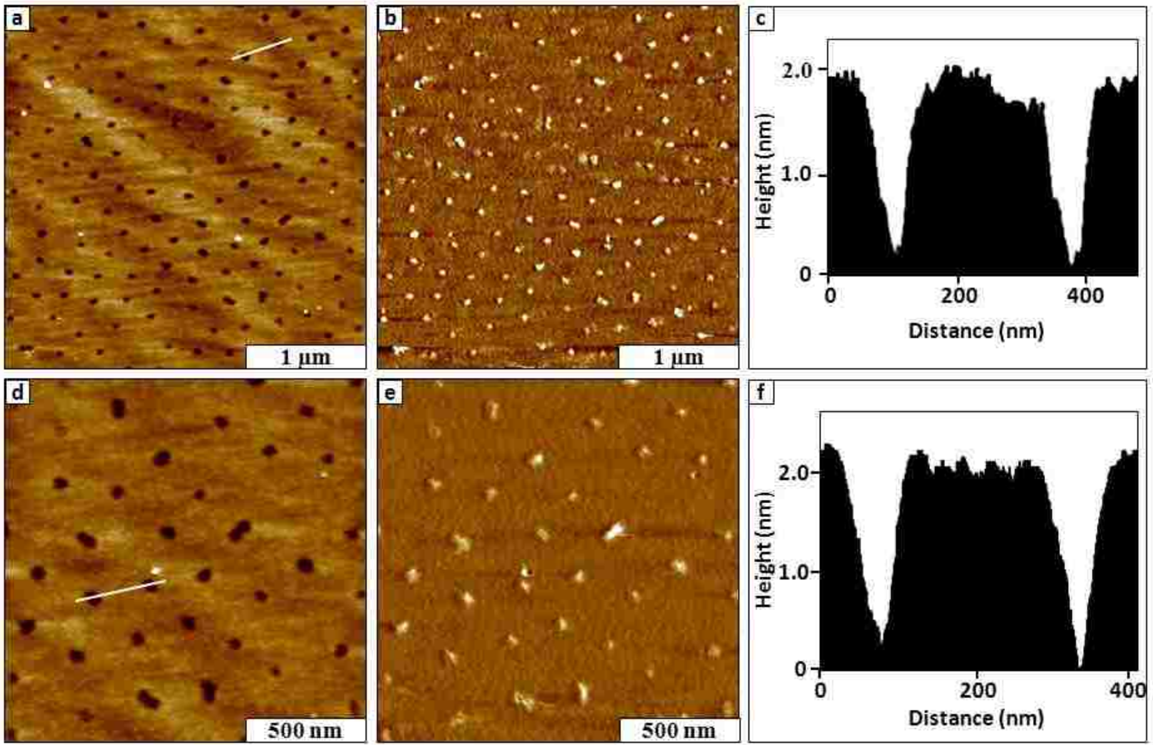

Figure 4.6 Nanostructured film of OTS produced by immersion of annealed silica masks in OTS solutions. Contact mode AFM images are shown for OTS nanostructures formed on Si(111) with 250 nm silica mesospheres: (a) 2.75 × 2.75 µm^2 topograph; (b) corresponding lateral force view; (c) height profile of the line in ***a***; (d) 1.5 × 1.5 µm^2 zoom-in view of the ***a***; (e) lateral force frame simultaneously acquired with ***d*;** (f) cursor plot for the line in ***d***.

4.2.5 Molecular Orientation of OTS within Nanopatterns

For the three approaches described, the procedures are highly reproducible. Multiple samples were prepared and form consistent shapes and thicknesses, summarized in Table 1. A cross-linked multilayer was formed for rings of OTS, with different thicknesses within the interstitial areas of the substrates between the rings (Figures 4.2, 4.3). Using the contact printing approach with PDMS stamps, the thickness of the OTS film corresponds to a side-on orientation of the molecules (Figure 4.4). Despite multiple tests and samples, a monolayer thickness was not achieved with latex masks and contact printing of OTS. A similar height was produced using immersion of annealed latex masks. The brief annealing step was effective for producing exquisitely small areas of the surface for preparing nanodot structures, however the heights do not correspond to an upright orientation of OTS (Figure 4.5). By changing to silica mesospheres for the immersion strategy, an ideal monolayer film was produced (Figure 4.6). This new result suggests that the nature of the surface of the mesosphere masks can affect the outcome for patterning with particle lithography. Polystyrene latex has been described as a “hairy” particle, with strands of polystyrene extending across the exterior surface areas of the beads. The strands provide surface sites for interacting with OTS to produce a cross-linked arrangement within the nanodot surface structures. However, silica mesospheres would be relatively inert to reacting with the molecules, resulting in an upright orientation of OTS molecules within the nanostructures. The consistent and reproducible geometries of the different OTS nanostructures are not necessarily a “failed” approach for particle lithography, rather a range of different surface shapes and thicknesses can be generated for selected applications. Overall, the highest quality monolayer of OTS was produced using immersion of annealed mesosphere masks of silica.

Table 4.1. Particle Lithography with OTS using different approaches for surface deposition.

Method	Mask	Nanostructure Shape	Surface Coverage (OTS)	OTS Thickness
vapor deposition	200 nm latex	ring nanostructures of OTS multilayers	40%	10 ± 2 nm
contact printing	200 nm latex	nanopores of uncovered substrate within an OTS film	26%	0.6 ± 0.1 nm
immersion of annealed latex masks	200 nm latex	Nanodots	10%	0.5 ± 0.3 nm
immersion of annealed silica masks	250 nm silica	nanopores of uncovered substrate within an OTS monolayer	85%	2.0 ± 0.2 nm

4.3 Conclusion

The surface self-assembly of OTS was studied using approaches of particle lithography combined with vapor deposition, contact printing and immersion. By changing the physical approaches for applying molecules to surfaces, the molecular arrangement and surface orientation can be controlled. For example, a cross-linked, side-on orientation of molecules was obtained using protocols with contact printing. Changing the material composition of the mesoparticle masks produced entirely different surface structures for annealed masks of latex and silica spheres. The meniscus sites of water residues at the base of latex spheres furnish local containers for self-polymerization reactions to generate multilayer surface structures. Optimized structures with monolayer thickness were achieved using annealed masks of colloidal silica mesospheres immersed in OTS solutions. Further experiments are in progress to directly compare the surface structures formed using immersion protocols with latex and silica masks.

4.4 Experimental

4.4.1 Atomic Force Microscopy (AFM)

Organosilane thin films were characterized using models 5420 and 5500 scanning probe microscopes operated in contact or tapping-mode AFM. (Agilent Technologies, Chandler, AZ). The tips were silicon nitride probes. Tips used with tapping-mode AFM were rectangular shaped ultra-sharp silicon tips that have an aluminum reflex coating, with a spring constant of 48 N/m (Nanoscience Instruments, Phoenix, AZ). For contact mode images, V-shaped tips (Veeco Probes, Santa Barbara, CA) with an average force constant of 0.5 N/m were used. Data files were processed using Gwyddion open source software, which is freely available on the internet and supported by the Czech Metrology Institute.[176] Estimates of surface coverage were obtained for individual topography frames by manually converting images to black and white using thresholding and pixel counting with UTHSCA Image Tool.[177]

4.4.2 Preparation of Latex Particle Masks

Polished silicon wafers doped with boron (Virginia Semiconductor, Fredericksburg, VA) were used as substrates. Pieces of Si(111) were cleaned by immersion in a 3:1 (v/v) piranha solution for 1 h. Piranha solution consists of sulfuric acid and hydrogen peroxide, which is highly corrosive, and should be handled carefully. After acid cleaning, the substrates were rinsed with copious amounts of deionized water and dried in air. Size-sorted, monodisperse polystyrene latex mesospheres (200 nm diameter) were used as surface masks for patterning (Thermo-Fisher Scientific, Waltman, MA). Aqueous solutions of latex were cleaned by centrifugation to remove surfactants or contaminants. Approximately 300 µl of the latex solution was placed into a microcentrifuge tube and centrifuged at 15,000 rpm for 15 min. A solid pellet was formed, and the supernatant was removed and replaced with deionized water. The latex pellet was re-suspended with 300 µl of deionized water by vortex mixing to prepare a 1% w/v solution. The washing process was repeated twice. A drop (10-15 µL) of the cleaned mesospheres was deposited onto clean Si(111) substrates and dried in ambient conditions (25 °C, ~ 50% relative humidity) for at least one hour, to form surface masks for nanolithography.

4.4.3 Particle Lithography Combined with Vapor Deposition

The masked substrates were placed into sealed glass vessels for vapor deposition of organosilane. The samples were placed on a raised platform in a jar containing 300 µL of neat octadecyltrichlorosilane (Gelest, Morrisville, PA). A vapor was generated by heating the vessel in an oven at 70 °C. After at least 6 h, the samples were removed and rinsed with ethanol and water to remove the latex masks.

4.4.4 Particle Lithography with Contact Printing

For contact printing, an inked block of polydimethylsiloxane (PDMS) (Sylgard 184, Dow Corning) was used to transfer OTS to the substrate through a physical mask of latex spheres. A drop (10-12 µL) of an OTS solution in bicyclohexyl was deposited onto a clean, dry block of PDMS (2 x 2 cm^2). A 30 µL volume of a 40% v/v solution of OTS in bicyclohexyl was deposited and spread evenly over the PDMS block, then quickly dried in a stream of ultrahigh purity argon. The PDMS block coated with OTS was placed on top of the masked substrate. The film of OTS was transferred from the PDMS block through the latex mask to the substrate by permeation. The areas of the Si(111) surface located directly underneath the latex particles were protected from silane deposition. After 1 h of physical contact, the PDMS block was removed. The sample was rinsed with copious amounts of deionized water. In the final step, the mask of latex particles was cleanly removed by sonication and rinsing with ethanol and deionized water. After removal of the mask, a nanostructured film of OTS was generated on the surface.

4.4.5 Particle Lithography with Immersion

For the immersion strategy of particle lithography, the masked substrates of latex were heated for 30 min at 75°c to anneal the beads to the surface. Masked substrates of colloidal silica mesospheres were heated for 12 h at 140°c. After heating, the samples were cooled for at least 20 min under ambient conditions. The mesosphere-coated substrates were then immersed into a 0.1% solution of OTS in bicyclohexyl or anhydrous toluene for 1 h. Next, the samples were removed and rinsed with ethanol and deionized water using sonication to remove the latex masks.

CHAPTER 5: PROTOCOL OF PARTICLE LITHOGRAPHY DEVELOPED WITH MULTIDENTATE THIOL ADSORBATES USING VAPOR DEPOSITION

5.1 Introduction

The synthesis of custom-designed multidentate thiol-based adsorbates offers opportunities for generating interfaces of well-defined structure and composition based on either bidentate or tridentate thiol groups, a crosslinked junction and tailgroups of tunable chemical composition.[178] The nature of the headgroup, junctions, hydrocarbon backbone, and tailgroups enable designs of complex architectures for preparing surface nanopatterns. The addition of multiple linker groups provides enhanced stability due to a chelate effect.[179] The oxidative and thermal stability of self-assembled monolayers (SAMs) is critical for potential applications such as chemical sensing or microfabrication devices. Multidentate molecules provide a model that will resist self-exchange and surface migration for completing further steps of chemical reactions. Recent studies with monolayer protected clusters, gold nanoparticles and a flat gold surface have demonstrated that films with multidentate S-Au linkages have increased stability attributed to the chelation of the sulfur atom and the increased steric bulk of the molecule.[178,180]

To investigate the surface structure and self-assembly for multidentate thiol adsorbates, protocols with particle lithography were developed with a tridentate molecule, 1,1,1-tris(mercaptomethyl)heptadecane (TMMH). The structure of TMMH is shown in Figure 5.1. Our goal was to apply particle lithography approaches to construct nanostructures as a model surface platform for evaluating the long term stability and self-exchange of designed architectures of multidentate SAMs using characterizations with atomic force microscopy (AFM).

5.2 Experimental Approach

Samples were prepared with a fresh solution of TMMH in ethanol (1 Mm). A glass cover slip and pieces of gold/mica were rinsed with deionized water and dried. The glass cover slip and gold film were cleaned in a UV/ozone generator for 30 min. A small drop of epoxy was placed onto the glass slide and positioned on the gold film. The sample was cured at 150 C for 2 h. After

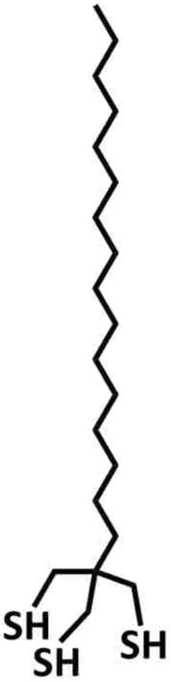

Figure 5.1 Structure of 1,1,1-tris(mercaptomethyl)heptadecane (TMMH).

cooling, the template-stripped gold (TSG) substrate was prepared by peeling the mica from the sample.[181,182] The TSG substrate was cleaned with UV/ozone for 30 minutes then coated with latex mesospheres that have a 500 nm diameter. The masked substrate was placed into a sealed glass vessel for vapor deposition of TMMH. The substrate was exposed to TMMH vapor generated at 70 C for 12 h. The sample was rinsed with ethanol using sonication to remove the mesospheres.

5.3 Results and Discussion

The arrangement and periodicity of the array of nanostructures correspond to the packing of the surface mask of mesospheres used for particle lithography (Figure 5.2a). The mask of latex mesospheres was cleanly removed; however TMMH adsorbates persisted on the surface to form nanorings in the meniscus sites of the latex beads. A close-up view of 15 nanostructures is shown in Figure 5.2b, revealing a regular circular geometry, with a few small islands of adsorbates in areas between the nanorings.

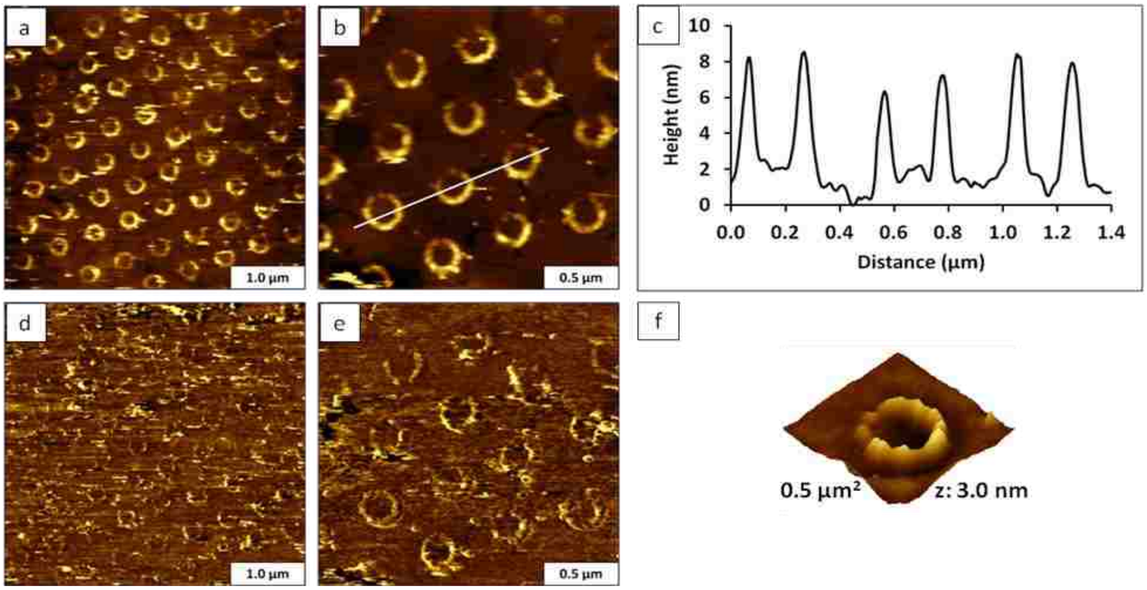

Figure 5.2 Ring nanostructures of 1,1,1-tris(mercaptomethyl)heptadecane prepared on Au(111) using particle lithography combined with vapor deposition. (a) Contact mode AFM topography image, 4 x 4 µm^2; (b) Zoom in view, 1 x 1 µm^2; (c) height profile for the white line in ***b***; (d) lateral force image corresponding to ***a***; (e) lateral force image for ***b***; (f) view of a single ring nanostructure of TMMH.

The nanorings measure approximately 8 nm in height, (Figure 5.2c) which indicates that multilayer nanostructures of TMMH were generated. A monolayer film of TMMH would measure 1.4 nm, which suggests that 4-6 layers were formed with disulfide bridges. Concurrently-acquired lateral force images (Figures 5.2d, 5.2e) distinguish the chemical differences of the areas of the nanorings and areas of the substrate. A single nanostructure is presented in Figure 5.2f, revealing that the edges of the nanorings vary in thickness around the circumference of the meniscus sites.

Binding of TMMH did not occur in central areas of the nanorings where the mesospheres protected the substrate, binding occurred primarily within the confined areas of water meniscus sites at the base of the mesospheres. A solvent or liquid interface may be necessary for binding TMMH. Essentially, the meniscus areas that surround the base of latex mesospheres provide a region of contained liquid which produces the interesting ring-shaped geometries of TMMH nanostructures.

5.4 Conclusions

Particle lithography offers generic capabilities for high-throughput fabrication of nanopatterns with organic thin films, which provides opportunities for studying surface-based chemical reactions at the molecular level with multidentate adsorbates. Organothiols have become increasingly important as surface resists and functional coatings for applications. To develop robust and reproducible lithography processes, parameters, such as temperature, humidity, solvents, physical deposition conditions and mask materials, can be systematically investigated to enable nanoscale studies of surface assembly. The studies here investigated the morphology and self assembly at the molecular level. The surface density of nanostructures can be designed by selecting the diameter of mesospheres used for particle lithography, to enable high-throughput patterning on the order of 10^9 nanostructures per square centimeter. Future experiments will be designed to investigate differences in the thickness and morphology of nanostructures with different molecule designs, and to particularly evaluate the role of liquid interfaces in chemisorptive binding to gold surfaces.

CHAPTER 6: SPATIALLY SELECTIVE ORGANOSILANE SURFACE PLATFORMS FOR ATTACHING FIBRONECTIN PREPARED WITH PARTICLE LITHOGRAPHY

6.1 Summary

Protein nanostructures are useful for viewing antigen-antibody binding at the nanometer scale with surface characterization techniques, to assess the specificity of selective binding, and to evaluate protein orientation and the accessibility of ligands for binding. With the commercial availability and development of large sets of characterized antibodies, protein and antibody arrays will provide significant advantages for diagnostics and medical science. Surface platforms prepared with particle lithography enable spatially selective binding of fibronectin on organosilane nanopatterns. By combining particle lithography with self-assembly of octadecyltrichlorosilane (OTS) and (3-trimethoxysilylpropyl)diethylenetriamine (DETA), regularly arranged nanostructures of organosilanes were prepared for binding fibronectin. Organosilane nanopatterns furnished a robust surface platform that was able to sustain multiple successive measurements with scanning probe microscopy. The high-throughput approach of particle lithography for nanopatterning enables molecular-level investigations of protein-binding interactions for potential applications in bioassays and biosensors.

6.2 Introduction

Development of surface platforms for biosensors and bioassays that are capable of achieving molecular-level detection will require protocols for nanolithography that are reproducible and enable spatial selectivity for binding proteins and biomolecules. Recent work has been reported for preparing nanopatterns of biological recognition elements on surfaces that enable biological activity and binding specificity to be preserved.[183-189] Several approaches for preparing nanopatterns with proteins have been developed. Glancing angle deposition uses a shadowing effect for physical vapor deposition of particles onto a substrate, by altering the angle of incidence to produce a range of nanoscale morphologies.[190-193] Molecular beam epitaxy has been applied in ultra-high vacuum to prepare an angular distribution of atoms or molecules onto a surface.[194] Methods such as reactive ion etching,[195] alkaline modifications[196] and controlled oxidative patterning[197,198] have been used to create nanoscale patterns for binding proteins.

Regions of fibronectin adhesion were investigated using AFM with regard to surface conductive properties as a consequence of electrostatic attraction between the protein and the surface by Gelmi et al.[199] Single cell force spectroscopy studies with AFM were used to evaluate adhesion of fibronectin on nanogrooved substrates after the introduction of an RGD peptide by Lamers et al.[200] Force spectroscopy with AFM was used to study fibronectin adsorption on grooved substrates by Elter et al.[201] A study using organothiol self-assembled monolayers (SAMs) to bind fibronectin was conducted by Dickerson et al.[202]

Particle lithography, also referred to as colloidal lithography, offers advantages of high-throughput, cost efficiency and parallel fabrication. Particle lithography was used to produce nanopillar arrays as stamps to pattern fibronectin by Kuo et al.[203] Polymer brushes were prepared as gradients to pattern fibronectin that remained bioactive by using colloidal lithography and fluorescence, by Li et al.[204] Scanning electron microscopy and fluorescence were used to study surface bound fibronectin for potential use in surface mediated cell signaling by Malmström et al.[205] Colloidal lithography combined with multiple and angled deposition was used by Kristensen et al. to demonstrate that the local distribution of fibronectin within a patch critically influences cell adhesion.[206]

Studies of protein interactions and surface binding reveal information about protein bonds and cellular responses. Organosilane SAMs furnish model surfaces for studies of protein adsorption. An advantage of organosilanes is that a range of different substrates that can be used for nanopatterning protocols, including glass, metal oxides, mica, and silicon wafers. Silane SAMs are robust and do not degrade with exposure to oxidation or heated conditions. Self-assembled monolayers (SAMs) of organosilanes form dense, ordered molecular films that bind covalently to hydroxyl groups of surfaces.

Fibronectin is an adhesive glycoprotein found in both plasma and the extracellular matrix, which has a role in physiological processes such as cell adhesion, migration and spreading. Fibronectin is a flexible molecule that can contract or expand based upon the local environment. In this report, a protocol for particle lithography with multiple steps of surface immersion was applied for studies of fibronectin characterized with atomic force microscopy (AFM). The arrangement and surface density of reactive sites was shown to affect the distribution and conformation of bound protein within an OTS resist film. Progressive changes in the morphology of nanopatterns were examined *ex situ* after each chemical step using AFM.

6.3 Experimental Approach

6.3.1 Preparations of Si(111) Substrates

Polished silicon wafers doped with boron (Virginia Semiconductor, Fredericksburg, VA) were used as substrates. Pieces of Si(111) were cleaned by immersion in a 3:1 (v/v) piranha solution for 1.5 h. Piranha solution consists of sulfuric acid and hydrogen peroxide (Sigma-Aldrich, St. Louis, PA) which is highly corrosive, and should be handled carefully. After acid cleaning, the substrates were rinsed with deionized water and dried in air. Size-sorted, monodisperse silica mesospheres, 500 and 250 nm in diameter (Fiber Optic Center Inc., New Bedford, MA) were used as surface masks for patterning. Silica powder was weighed (0.1 g) and added to 10 mL of ethanol (Pharmaco-Aaper, Brookfield, CT). The mesoparticles were dispersed by sonication. An aliquot of the silica solution was cleaned by centrifugation and resuspended in deionized water. A volume of 300 µL of the solution of silica mesospheres was placed into a microcentrifuge tube and spun at 15,000 rpm for 15 min. A solid pellet was formed, and the supernatant was removed and replaced with deionized water. The pellet was re-suspended with 300 µL of deionized water by vortex mixing to prepare a 1% w/v solution. The washing process was repeated twice.

6.3.2 Sample Preparations using Immersion Particle Lithography

An overview of the chemical steps for patterning fibronectin on organosilane nanostructures are shown in Figure 6.1. A drop (10 µL) of the Si mesospheres was deposited onto clean Si(111) substrates and dried in ambient conditions (25 C, ~ 50% relative humidity) for at least 1.5 h, to form surface masks. The sample was heated at 150 C for at least 12 h. The samples were immersed in a 0.1% (v/v) solution of octadecyltrichlorosilane (Gelest, Morrisville, PA) in bicyclohexyl (Sigma-Aldrich, St. Louis, MO). Samples were rinsed with ethanol to remove the mask of Si mesoparticles and dried. The areas protected with Si mesospheres formed nanoholes within a film of OTS (Figure 6.1a).

Next, a second organosilane for binding protein was backfilled into the uncovered areas of substrate within OTS (Figure 6.1b) using an immersion step. A heterobifuntional crosslinker (3-trimethoxysilylpropyl)diethylenetriamine (DETA) was inserted to the exposed sites of Si(111). The headgroups of DETA were activated by exposure to 1-ethyl-3-[dimethylaminopropyl]carbodiimide hydrochloride: N-hydroxysuccinimide (EDC-NHS) coupling (Figure 6.1c). The EDC-NHS coupling provides a covalent linkage from surface amine groups of DETA to bind to carboxyl groups of the protein. The crosslink targeted aspartic acid residues of the RGD sequence of the fibronectin molecule for surface binding.

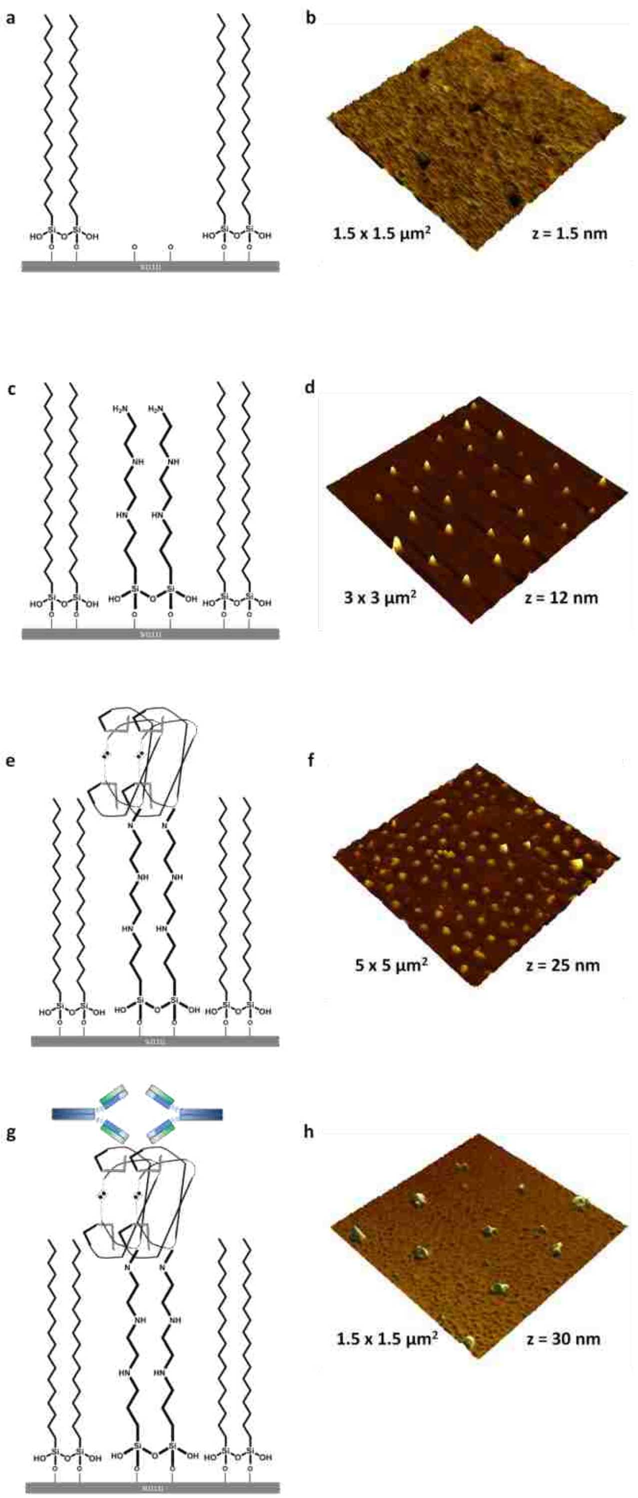

Figure 6.1 Steps for protein nanopatterning. (a) Nanopores were prepared within OTS using particle lithography combined with immersion; (b) the sample was immersed in a second solution of DETA; (c) the headgroups were activated with NHS/EDC; (d) the sample was immersed in fibronectin; (e) the immobilized protein was exposed to antibodies.

After the activation step, sample was immediately immersed in a 0.5 mg/mL fibronectin solution in Tris buffer (pH: 7.5) to selectively attach the protein to the DETA nanopatterns (Figure 6.1d). The final step of binding anti-fibronectin was used to test the activity for binding IgG after surface immobilization (Figure 6.1e). Both fibronectin and anti-fibronectin were purchased from Sigma-Aldrich, St. Louis, MO.

6.3.3 Atomic Force Microscopy

Surface characterizations with AFM were acquired using either a model 5420 or 5500 scanning probe microscope (Agilent Technologies, Chandler, AZ) using either contact or tapping-mode AFM in ambient air. The tips were fabricated from silicon nitride (Bruker Corporation, Billerica, MA). Probes used for tapping-mode AFM were rectangular shaped ultra-sharp silicon tips with an aluminum reflex coating, with a spring constant ranging from 13-77 N/m with frequencies in the range of 200-400 kHz. Cantilevers with an average force constant of 0.1 N/m were used for contact mode AFM. Data files were processed using Pico image analysis software provided by Agilent. Estimates of surface coverage were obtained for individual topography frames by manually converting images to black and white pixels using manual thresholding with UTHSCA Image Tool.[177]

6.4 Results and Discussion

The general strategy for surface patterning of fibronectin was to prepare a methyl-terminated resist coating on the substrate with a well-defined arrangement of isolated areas of exposed substrate available to be backfilled with protein. A film of OTS with a periodic arrangement of nanoholes is shown in Figure 6, which was prepared by rinsing away the Si mesospheres. A surface mask of 500 nm Si mesospheres was used to prepare the OTS nanoholes in Figure 6.2a and 6.2b. There are 27 nanopatterns viewed within the 3 × 3 μm^2 topograph, which would scale to a surface density of 3×10^8 nanopatterns/cm^2. A closer view (1×1 µm^2) is shown in Figure 6.2b of three nanopores. The thickness of the surrounding OTS measured 0.7 ± 0.1 nm, estimated from measurements of the depth of 50 nanopores. The width of the nanopores is approximately 100 nm, shown with a representative cursor line profile in Figure 6.2c. Changing the diameter of the Si mesospheres of the surface masks provides a reproducible approach for tuning the surface density of the nanopores. An example is shown in Figures 6.2d and 6.2e for a sample prepared prepared with 250 nm diameter mesospheres. There are ~160 nanopores visible in the topography frame which is more closely packed together within the 3×3 µm^2 area. The diameter of the nanoholes measures ~ 78 nm, shown with a representative cursor line measurement across four nanopores in Figure 6.2e. The average depth of the nanopores measured 0.9 ± 0.1 nm (n=50). The differences in surface density for 500 nm versus 250 nm mesospheres is evident by comparing the topography frames for a 1×1 µm^2 area; the surface mask with a larger diameter produced three nanoholes (Figure 6.2b) compared to 21 nanoholes in Figure 6.2e. The shapes of the nanoholes is circular for both examples, however the diameter of the holes is slightly larger with 500 nm mesospheres.

A dense monolayer of OTS has been reported to measure from 2.2-2.5 nm in thickness.[207] The nature of the substrate and conditions for sample preparation influence the surface packing of OTS. With particle lithography, the local thickness measurements with AFM indicate that the film is not densely packed, however the resist qualities of the methyl-terminated SAM were sufficient for further *ex situ* steps with backfilling and protein attachment.

The next step for preparing protein nanopatterns was to backfill the nanoholes with a reactive organosilane for binding fibronectin. This was accomplished by immersing the samples shown in Figure 6.2 in a solution of DETA. The surface changes were investigated with AFM after reaction with DETA, shown in Figure 6.3. Within the 3×3 μm^2 are of Figure 6.3a there are 30 nanostructures of DETA, it appears that all of the exposed sites of the nanopores have been backfilled. Closer examination of multiple areas did not reveal unfilled sites. The height of the nanodots of DETA measure 5 ±1 nm above the OTS layer; shown with an example line profile (Figures 6.3b and 6.3c). Topography images acquired with backfilling nanoholes prepared from 250 nm Si masks are presented in Figures 6.3d and 6.3e. The heights are shorter for the smaller nanopores, measuring 1.7 ± 0.3 nm, (*n*=50). There are 18 nanopatterns visible within the 1×1 μm^2 area of Figure 6.3d, compared to 4 nanodots in Figure 6.3b for the same size area.

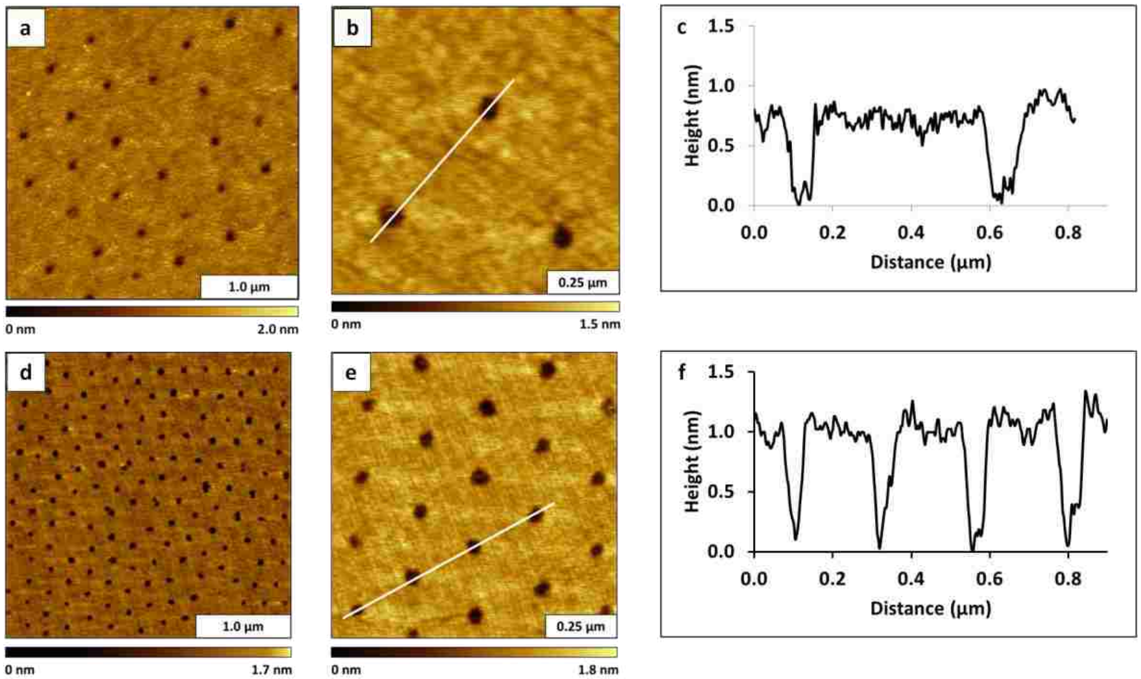

Figure 6.2 Nanoholes within OTS produced on Si(111) using immersion particle lithography. (a) Nanoholes prepared using 500 nm Si mesospheres viewed within a 3×3 μm^2 area with an AFM topograph; (b) Zoom-in topograph; (c) height profile for the line in ***b***. (d) Nanoholes prepared using 250 nm Si mesospheres; (e) zoom-in view; (f) cursor profile for ***e***.

The heights of the backfilled nanostructures of DETA correspond to a multilayer, and the larger nanoholes prepared with the 500 nm Si template have correspondingly taller nanodots. Crosslinking of the trimethoxy groups to form a polymer should leave one or more amine groups at the surface available for binding protein. The height of a fully upright DETA molecule measures 0.6 nm.[208-210] The widths of the nanodots correspond precisely to the diameters of the nanoholes shown in Figure 6.2, thus the backfilling step provided localization of the DETA to the exposed sites of Si(111) substrate.

Surface changes during the activation step with EDC-NHS were not captured with AFM, because the reaction is time restricted. The process of drying the sample and imaging with *ex situ* AFM would likely prevent protein coupling. Views of the surface changes with immobilization of fibronectin are shown in Figure 6.4. A periodic arrangement of bright dots pinpoints the sites of protein clusters in Figure 6.4a. In the close-up view of Figure 6.4b there are four protein nanopatterns within the 1×1 μm^2 area. The surface texture of the surrounding OTS film has changed from a smooth appearance to a rougher morphology. This is caused by incomplete steps of rinsing that did not completely remove all residues of reagents from the EDC-NHS treatment.

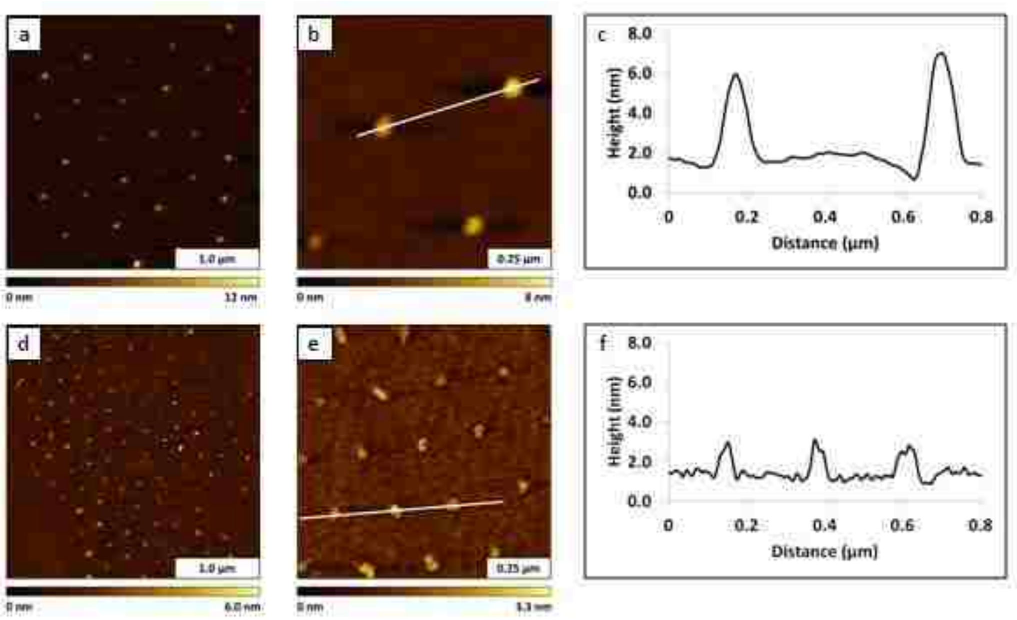

Figure 6.3 Nanostructures of DETA produced within an OTS resist. (a) Backfilled nanopores prepared with 500 nm mesospheres shown with an AFM topograph; (b) close-up view, 1×1 µm^2; (c) cursor profile for ***b***. (d) Nanostructures of DETA prepared with 250 nm Si mesospheres shown with an AFM topograph; (e) zoom-in topography view; (f) height profile for ***e***.

The distinct shapes and outline of larger protein residues are not detected between the taller nanodots, evidence that the surrounding OTS film was an adequate resist for preventing nonspecific binding of protein in between DETA nanodots. The white frame in Figure 6.4a pinpoints the magnified area presented in Figure 6.4b. The heights of the nanostructures increased to 8 ± 1 nm, shown with an example cursor profile in Figure 6.4c. Nanopatterns of fibronectin prepared with 250 nm mesospheres are shown in Figures 6.4d and 6.4e. In the magnified view there appears to be individual proteins attached at sites between the nanopatterns on areas of OTS. These results suggest that rinsing protocols need to be refined such as with using detergent solutions to fully isolate the protein sites. The heights of the protein nanopatterns are shorter with 250 nm mesosphere masks, after binding fibronectin the heights increased to 3.4 ± 1.0 nm. With 500 nm surface mask, approximately 3% of the surface is covered with fibronectin whereas the surface coverage for nanostructures prepared from 250 nm mesospheres was ~9%.

Fibronectin can attach to surfaces with either a globular conformation or an elongated form. It has been reported that fibronectin adopts a globular conformation on hydrophobic surfaces and an elongated conformation is detected with hydrophilic surfaces.[211-214] The heights and dimensions of fibronectin molecules depend on the conformation. The elongated form has dimensions measuring 70±20 nm × 25±5 nm × 3.5±1 nm, as determined by AFM.[3,215,216] The globular form has a length of 16-35 nm with a height measuring 7 nm as reported by Koteliansky et al., to have overall dimensions of 15.5 ±1.3 nm × 8.8 ±1.7 nm.[215,217-220] Both conformations have lengths ranging from 120-180 nm, measured using techniques of x-ray and neutron scattering and electron microscopy.[211,215,221,222]

The height increase of the nanopatterns after binding fibronectin measured thicknesses of 8 ± 1 nm for 500 nm periodicity and 3 ± 1 nm 250 nm templates. For protein patterns prepared with 500 nm mesosphere masks, the height increase after binding fibronectin corresponds approximately to the dimensions of the compact, globular form (7 nm). However, when the spacing between nanopattern sites was smaller, such as for the patterns prepared with 250 nm masks, the height of the pattern corresponds to the elongated, linear form of fibronectin (3.5 nm).

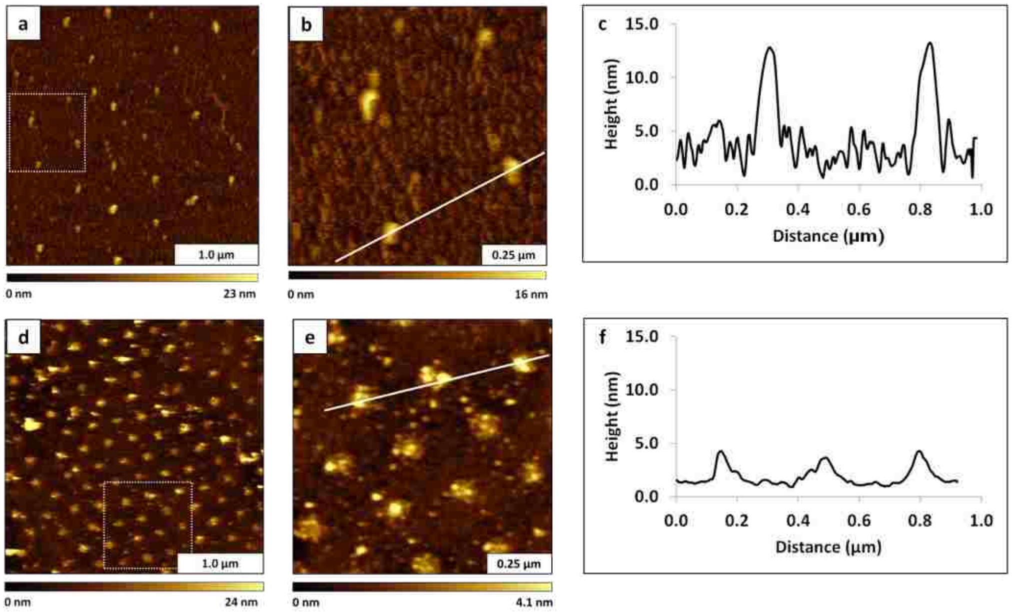

Figure 6.4 Surface changes after binding fibronectin to activated DETA nanodots. (a) Protein nanostructures from 500 nm masks viewed with an AFM topograph, 3×3 μm^2; (b) zoom-in view of the boxed area in ***a***; (c) height profile of the line in ***b***. (d) Fibronectin nanopatterns prepared with 250 nm Si mesospheres shown with an AFM topograph; (e) magnified view, 1×1 μm^2; (f) cursor line profile for ***e***.

A final step was developed to evaluate the activity of fibronectin nanopatterns for binding antibodies, shown in Figure 6.5. The samples shown in Figure 6.4 were immersed in a solution of anti-fibronectin in buffer, and then imaged *ex situ* with AFM. Most of the nanostructures grew in lateral and vertical dimensions (Figures 6.5a and 6.5b). The height increased from 8 ± 1 nm with fibronectin to 11 ± 2 nm after immersion in anti-fibronectin. An example height profile is presented in Figure 6.5c for two nanostructures. For the experiment with 500 nm mesospheres there is no evidence of non-specific binding between the nanodots and the protein binding is localized at the reactive sites of DETA.

When the spacing between nanopatterns was reduced to 250 nm, there is clear evidence of protein binding taking place on areas between the reactive sites, as shown in Figures 6.5d and 6.5e. However the bright spots of the protein nanostructures can still be resolved with AFM. A height profile across three protein nanostructures is shown in Figure 6.5f; the average height measured 8 ± 1 nm after binding anti-fibronectin.

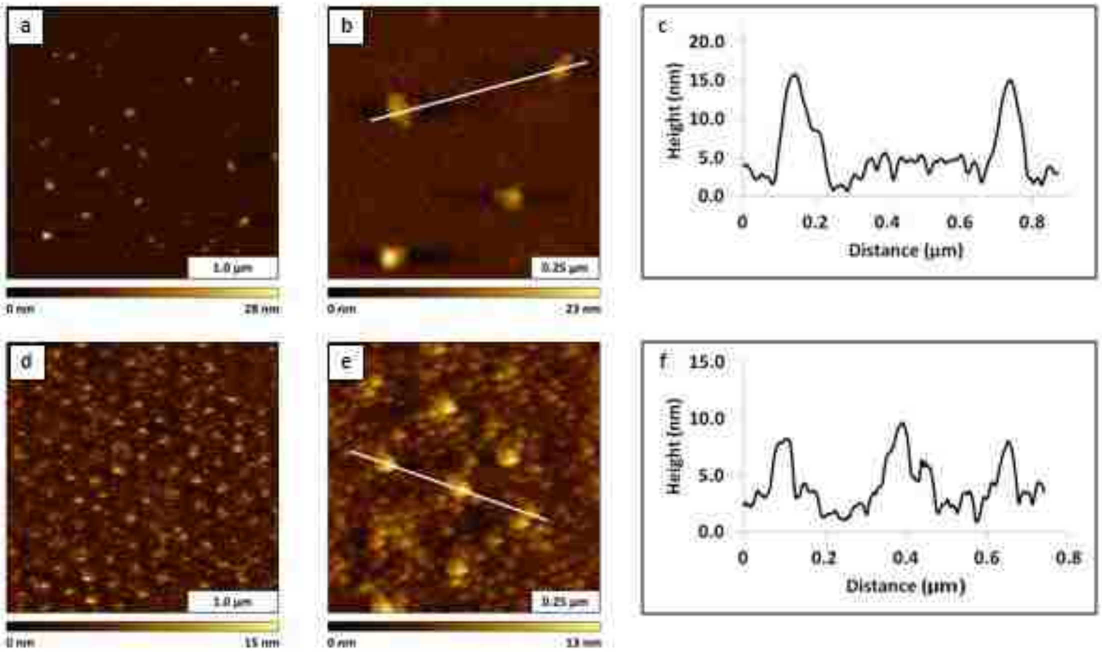

Figure 6.5 Surface views after binding anti-fibronectin acquired with tapping-mode AFM in air. (a) Nanostructures prepared with 500 nm periodicity viewed with topography frames acquired in air; (b) zoom-in topograph; (c) height profile for the line in ***b***. (d) Nanostructures prepared with 250 nm Si mesospheres viewed with a topography frame, 3×3 µm^2; (e) zoom-in view, 1×1 µm^2; (f) height profile for ***e***.

A significant advantage of local measurements with AFM for studies of surface reactions is that highly local views can be achieved for small clusters of proteins. It is readily apparent whether or not protein binding took place in AFM topography views, the actual heights of nanostructures can be measured at carefully selected locations rather than making approximations for a spatially averaged response from spectroscopy measurements across broad areas of the sample. Completing protocols with multiple steps for nanoscale studies with AFM can pose a challenge, since each reagent introduces potential contamination. Some examples of contamination may include, dust from the air or residual protein and anti-body. Potential errors from surface contamination are readily visible in topography frames.

For the studies with nanopatterns of fibronectin, the distance between nanopatterns influenced the localization of protein binding events. With 500 nm periodicity, the islands of reactive sites were well-isolated and the hydrophobic nature of the methyl-terminated OTS provided superb resist qualities for defining the deposition of proteins and antibodies. However, using the same OTS resist with 250 nm spacing between reaction sites was not as effective. The reported length of fibronectin ranges from 120-180 nm, so that overlap between nanopatterns could take place. Thus, future experiments with protocols of particle lithography need to match the dimensions of the protein with the design for spacing reactive sites, to ensure that the size of the protein does not overlap to adjacent reaction sites.

6.5 Conclusion

Particle lithography with steps of immersion was demonstrated to be an effective approach for isolating reactive surface sites for binding fibronectin. The periodicity of the surface masks of mesospheres can be selected to tailor the surface density of protein. Protein immobilization with EDC-NHS chemistry provided robust and specific binding of fibronectin within a resist film of OTS. The reproducibility of surface geometries and surface density of particle lithography offers new possibilities for making quantitative measurements of protein binding events on surfaces, with the high-throughput manufacture of well-defined surface arrays of defined surface coverage.

CHAPTER 7: CONCLUSIONS AND FUTURE PROSPECTUS

Particle lithography with organosilane and organothiol films uses a mask of monodisperse mesoparticles to guide the surface deposition of molecules. A crystalline arrangement of mesospheres is spontaneously produced when solutions of latex or silica beads are dried on flat surfaces. Particle lithography offers a practical and reproducible approach to produce nanopatterns of organic thin films. The close-packed arrangement of mesospheres provides surface masks for nanolithography which have well-defined dimensions and interparticle spacing.

Characterizations with atomic force microscopy (AFM) are suitable for investigation the geometries and arrangement of octadecyltrichlorosilane (OTS) nanostructures prepared with particle lithography. Differences in the thickness and morphology of OTS nanostructures can be evaluated with molecular-level resolution using AFM, providing insight of the self-assembly mechanism. The influence of temperature, water and experimental parameters were evaluated for OTS nanostructures prepared with strategies of particle lithography. The arrangement and surface orientation are affected by changing the physical approaches for applying organosilanes. For example, when combining particle lithography with vapor deposition nanorings were produced of cross-linked polymer nanostructures (Chapter 4).

Nanostructures of OTS were used as a resist film leaving exposed areas of the substrate available for further chemical steps of backfilling. The functional groups of organosilanes that were introduced were designed to selectively bind the protein, fibronectin (Chapter 6). Protocols developed with particle lithography provided a spatially selective foundation for depositing proteins. Changing the diameter of the mesosphere masks provided a way to control the surface density of reactive sites, with nanoscale precision. The protein nanopatterns furnished a robust surface platform that sustained multiple successive measurements with scanning probe microscopy. High resolution AFM imaging can be achieved with well-defined surface arrangements of proteins that persist despite the perturbation of a scanning probe. Proteins were found to attach to the surface as single layers in designated reactive sites. Direct detection of protein adsorption and surface changes with protein-antibody binding using AFM studies are an advancement for surface-based biochip and biosensor surface designs. The newly developed nanopatterning protocols offer an opportunity to use ultra small quantities of dilute protein solutions for surface studies of biomolecule reactions.

For continued studies with fibronectin, nanopatterns will be used to mediate surface-directed growth of cells. Cell adhesion to extracellular matrix proteins are mediated by the integrin family of cell surface receptors.[223] *In situ* studies of antibody-antigen binding can be accomplished with liquid AFM.[224] Liquid imaging with AFM offers advantages of improved resolution, provided that highly dilute solutions of reagents are introduced slowly to the sample environment. The resolution is improved by reducing or eliminating capillary and van der Waals forces between the tip and sample that cause the probe to adhere to the sample. With liquid AFM, aqueous buffers that simulate physiological conditions can be used to study biochemical reactions. New molecules can be introduced and time-lapse imaging of surface changes can be accomplished over time.

A significant advantage of the protocol for particle lithography developed in Chapter 6 using EDC/NHS chemistry to mediate covalent binding of protein is that a generic approach was developed; the protocol is not limited to studies of fibronectin. The headgroups of organosilane SAMs provide robust sites for linking proteins to glass, mica or silicon substrates so that future studies are not limited to AFM investigations. For example, transparent substrates of glass or thin pieces of mica would be suitable for studies with optical microscopy. Future goals are to apply measurements with scanning probe microscopy (SPM) for *in situ* studies of biochemical reactions at the molecular level. Protocols based on particle lithography offer advantages of high throughput, reproducibility and ease of preparation. By changing the diameter of the mesosphere masks, the periodicity and surface density of reactive sites (nanoholes) can be reproducibly controlled to simultaneously generate millions of organosilane nanostructures. For example, the number of protein binding sites can be adjusted to range from 3 to 80 nanopatterns per square micron. Surface platforms of proteins bound to organosilane nanopatterns are suitable for screening the selectivity of fluorescent markers or for investigating the binding of small molecules or DNA to surface-bound proteins.

REFERENCES

(1) Merkel, T. J.; Herlihy, K. P.; Nunes, J.; Orgel, R. M.; Rolland, J. P.; DeSimone, J. M. *Langmuir* 2010, *26*, 13086.

(2) Binnig, G.; Rohrer, H. *Helvetica Physica Acta* 1982, *55*, 726.

(3) Lewis, A.; Isaacson, M.; Muray, A.; Harootunian, A. *Biophys. J.* 1983, *41*, A405.

(4) Binnig, G.; Quate, C. F.; Gerber, C. *Physical Review Letters* 1986, *56*, 930.

(5) Dayyoub, E.; Hobler, C.; Nonnweiler, P.; Keusgen, M.; Bakowsky, U. *Materials science & engineering. C, Materials for biological applications* 2013, *33*.

(6) Gautam, D.; Ikram, S.; Gupta, B. *Journal of Applied Polymer Science* 2013, *128*, 3205.

(7) Kumar, A.; Arruda, T. M.; Tselev, A.; Ivanov, I. N.; Lawton, J. S.; Zawodzinski, T. A.; Butyaev, O.; Zayats, S.; Jesse, S.; Kalinin, S. V. *Scientific Reports* 2013, *3*.

(8) Zhong, Z. X.; Xing, W. H.; Zhang, B. B. *Ceramics International* 2013, *39*, 4355.

(9) Akhter, T.; Saeed, S.; Siddiqi, H. M.; Park, O. O. *Polymers for Advanced Technologies* 2013, *24*, 407.

(10) Grisedale, L. C.; Moffat, J. G.; Jamieson, M. J.; Belton, P. S.; Barker, S. A.; Craig, D. Q. M. *Molecular Pharmaceutics* 2013, *10*, 1815.

(11) Ngunjiri, J.; Garno, J. C. *Anal. Chem.* 2008, *80*, 1361.

(12) Ngunjiri, J. N.; Daniels, S. L.; Li, J. R.; Serem, W. K.; Garno, J. C. *Nanomedicine* 2008, *3*, 529.

(13) Park, S. C.; Na, J. H.; Lee, S. D. *J. Appl. Phys.* 2012, *112*.

(14) Romano, N. H.; Sengupta, D.; Chung, C.; Heilshorn, S. C. *Biochimica Et Biophysica Acta-General Subjects* 2011, *1810*, 339.

(15) Hansma, P. K.; Elings, V. B.; Marti, O.; Bracker, C. E. *Science* 1988, *242*, 209.

(16) Goksu, E. I.; Vanegas, J. M.; Blanchette, C. D.; Lin, W. C.; Longo, M. L. *Biochimica Et Biophysica Acta-Biomembranes* 2009, *1788*, 254.

(17) Bhushan *Springer Handbook of Nanotechnology* 2007.

(18) Peter Eaton, P. W. *Introduction to atomic force microscopy*; 'Oxford University Press', 2010.

(19) Albrecht, T. R.; Quate, C. F. *J. Appl. Phys.* 1987, *62*, 2599.

(20) Binnig, G.; Gerber, C.; Stoll, E.; Albrecht, T. R.; Quate, C. F. *Europhysics Letters* 1987, *3*, 1281.

(21) Marti, O.; Drake, B.; Hansma, P. K. *Applied Physics Letters* 1987, *51*, 484.

(22) Ruan, J. A.; Bhushan, B. *J. Appl. Phys.* 1994, *76*, 5022.

(23) Ogletree, D. F.; Carpick, R. W.; Salmeron, M. *Rev. Sci. Instrum.* 1996, *67*, 3298.

(24) Cappella, B.; Dietler, G. *Surface Science Reports* 1999, *34*, 1.

(25) Balzer, B. N.; Micciulla, S.; Dodoo, S.; Zerball, M.; Gallei, M.; Rehahn, M.; von Klitzing, R.; Hugel, T. *ACS Appl. Mater. Interfaces* 2013, *5*, 6300.

(26) Razvag, Y.; Gutkin, V.; Reches, M. *Langmuir* 2013, *29*, 10102.

(27) Ritzefeld, M.; Walhorn, V.; Anselmetti, D.; Sewald, N. *Amino Acids* 2013, *44*, 1457.

(28) Bujalowski, P. J.; Oberhauser, A. F. *Methods* 2013, *60*, 151.

(29) Reeves, K. J.; Hou, J.; Higham, S. E.; Sun, Z.; Trzeciakowski, J. P.; Meininger, G. A.; Brown, N. J. *Nanomedicine* 2013, *8*, 921.

(30) Zou, S.; Chisholm, R.; Tauskela, J. S.; Mealing, G. A.; Johnston, L. J.; Morris, C. E. *PLoS One* 2013, *8*, 13.

(31) Guo, S. L.; Li, N.; Lad, N.; Desai, S.; Akhremitchev, B. B. *J. Phys. Chem. C* 2010, *114*, 8755.

(32) Sekatskii, S. K.; Benedetti, F.; Dietler, G. *J. Appl. Phys.* 2013, *114*, 8.

(33) Denis, F. A.; Hanarp, P.; Sutherland, D. S.; Gold, J.; Mustin, C.; Rouxhet, P. G.; Dufrene, Y. F. *Langmuir* 2002, *18*, 819.

(34) Hulteen, J. C.; Van Duyne, R. P. *J. Vac. Sci. Technol. A* 1995, *13*, 1553.

(35) Lipson, A. L.; Comstock, D. J.; Hersam, M. C. *Small* 2009, *5*, 2807.

(36) Chen, J.; Liao, W.-S.; Chen, X.; Yang, T.; Wark, S. E.; Son, D. H.; Batteas, J. D.; Cremer, P. S. *ACS Nano* 2009, *3*, 173.

(37) Deckman, H. W.; Dunsmuir, J. H. *Appl. Phys. Lett.* 1982, *41*, 377.

(38) Tessier, P. M.; Velev, O. D.; Kalambur, A. T.; Rabolt, J. F.; Lenhoff, A. M.; Kaler, E. W. *J. Am. Chem. Soc.* 2000, *122*, 9554.

(39) Haynes, C. L.; Van Duyne, R. P. *J Phys. Chem. B* 2001, *105*, 5599.

(40) Mornet, S.; Bretagnol, F.; Mannelli, I.; Valsesia, A.; Sirghi, L.; Colpo, P.; Rossi, F. *Small* 2008, *4*, 1919.

(41) Trujillo, N. J.; Baxamusa, S. H.; Gleason, K. K. *Chem. Mater.* 2009, *21*, 742.

(42) Sun, Z.; Li, Y.; Zhang, J.; Li, Y.; Zhao, Z.; Zhang, K.; Zhang, G.; Guo, J.; Yang, B. *Adv. Funct. Mater.* 2008, *18*, 4036.

(43) Abdelsalam, M. E.; Bartlett, P. N.; Baumberg, J. J.; Coyle, S. *Adv. Mater.* 2004, *16*, 90.

(44) Wang, W.; Dai, Z.; Sun, Y.; Sun, Y. *Thin Solid Films* 2009, *517*, 6050.

(45) Zhou, C. M.; Gall, D. *Thin Solid Films* 2007, *516*, 433.

(46) Jeong, J.-R.; Kim, S.; Kim, S.-H.; Bland, J. A. C.; Shin, S.-C.; Yang, S.-M. *Small* 2007, *3*, 1529

(47) Kosiorek, A.; Kandulski, W.; Glaczynska, H.; Giersig, M. *Small* 2005, *1*, 439.

(48) Chen, X.; Chen, Z.; Fu, N.; Lu, G.; Yang, B. *Adv. Mater.* 2003, *15*, 1413.

(49) Bae, C.; Shin, H. *Chem. Mater.* 2006, *18*, 1085.

(50) McLellan, J. M.; Geissler, M.; Xia, Y. *J. Am. Chem. Soc.* 2004, *126*, 10830.

(51) Li, J. R.; Garno, J. C. *Nano Lett* 2008, *8*, 1916.

(52) Li, J. R.; Lusker, K. L.; Yu, J. J.; Garno, J. C. *ACS Nano* 2009, *3*, 2023.

(53) Li, J.-R.; Garno, J. C. *ACS Appl. Mater. Interfaces* 2009, *1*, 969.

(54) Lusker, K. L.; Yu, J.-J.; Garno, J. C. *Thin Solid Films* 2011, *519*, 5223.

(55) Li, J.-R.; Henry, G. C.; Garno, J. C. *Analyst* 2006, *131*, 244.

(56) Garno, J. C.; Amro, N. A.; Wadu-Mesthrige, K.; Liu, G.-Y. *Langmuir* 2002, *18*, 8186.

(57) Cai, Y.; Ocko, B. M. *Langmuir* 2005, *21*, 9274.

(58) Prevo, B. G.; Velev, O. D. *Langmuir* 2004, *20*, 2099.

(59) Denkov, N. D.; Velev, O. D.; Kralchevsky, P. A.; Ivanov, I. B.; Yoshimura, H.; Nagayama, K. *Langmuir* 1992, *8*, 3183.

(60) Li, Y.; Fang, X.; Koshizaki, N.; Sasaki, T.; Li, L.; Gao, S.; Shimizu, Y.; Bando, Y.; Golberg, D. *Adv. Funct. Mater.* 2009, *19*, 2467.

(61) Wang, X. D.; Graugnard, E.; King, J. S.; Wang, Z. L.; Summers, C. J. *Nano Lett.* 2004, *4*, 2223.

(62) Kuo, C.-W.; Shiu, J.-Y.; Chen, P.; Somorjai, G. A. *J. Phys. Chem. B* 2003, *107*, 9950.

(63) Rybczynski, J.; Ebels, U.; Giersig, M. *Colloids Surf., A* 2003, *219*, 1.

(64) Lewandowski, B. R.; Kelley, A. T.; Singleton, R.; Li, J.-R.; Lowry, M.; Warner, I. M.; Garno, J. C. *J. Phys. Chem. C* 2009, *113*, 5933.

(65) Geissler, M.; McLellan, J. M.; Chen, J.; Xia, Y. *Angew. Chem. Int. Ed.* 2005, *44*, 3596

(66) McLellan, J. M.; Geissler, M.; Xia, Y. *Chem. Phys. Lett.* 2005, *408*, 80.

(67) Marquez, M.; Patel, K.; Carswell, A. D. W.; Schmidtke, D. W.; Grady, B. P. *Langmuir* 2006, *22*, 8010.

(68) Kim, H.; Park, J. H.; Cho, I.-H.; Kim, S.-K.; Paek, S.-H.; Lee, H. *J. Colloid Interface Sci.* 2009, *334*, 161.

(69) Ngunjiri, J. N.; Daniels, S. L.; Li, J.-R.; Serem, W. K.; Garno, J. C. *Nanomedicine* 2008, *3*, 529.

(70) Kumar, A.; Biebuyck, H. A.; Whitesides, G. M. *Langmuir* 1994, *10*, 1498.

(71) Nuzzo, R. G.; Allara, D. L. *J. Am. Chem. Soc.* 1983, *105*, 4481.

(72) Schreiber, F. *Prog. Surf. Sci.* 2000, *65*, 151.

(73) Battaglini, N.; Qin, Z.; Campiglio, P.; Repain, V.; Chacon, C.; Rousset, S.; Lang, P. *Langmuir* 2012, *28*, 15095.

(74) Bi, X. Y.; Xu, H.; Lai, S. L.; Yang, K. L. *Biofouling* 2009, *25*, 435.

(75) Deng, Z.; Weng, I. C.; Li, J. R.; Chen, H. Y.; Liu, F. T.; Liu, G. Y. *ACS Nano* 2011, *5*, 8672.

(76) Geissler, M.; McLellan, J. M.; Xia, Y. *Nano Lett.* 2005, *5*, 31.

(77) Ulman, A. *Chem. Rev.* 1996, *96*, 1533.

(78) Lusker, K. L.; Li, J.-R.; Garno, J. C. *Langmuir* 2011, *27*, 13269.

(79) Englade-Franklin, L. E.; Saner, C. K.; Garno, J. C. *Interface Focus* 2013, *405*, 1985.

(80) Kim, J.-H.; Cotton, T. M.; Uphaus, R. A. *J. Phys. Chem.* 1988, *92*, 5575.

(81) Vuillaume, D.; Boulas, C.; Collet, J.; Allan, G.; Delerue, C. *Phys. Rev. B* 1998, *58*, 16491.

(82) Angst, D. L.; Simmons, G. W. *Langmuir* 1991, *7*, 2236.

(83) Xiao, X.; Hu, J.; Charych, D. H.; Salmeron, M. *Langmuir* 1996, *12*, 235.

(84) Sagiv, J. *J. Am. Chem. Soc.* 1980, *102*, 92.

(85) Allara, D. L.; Parikh, A. N.; Rondelez, F. *Langmuir* 1995, *11*, 2357.

(86) Ellinas, K.; Tserepi, A.; Gogolides, E. *Langmuir* 2011, *27*, 3960.

(87) Malmstrom, J.; Lovmand, J.; Kristensen, S.; Sundh, M.; Duch, M.; Sutherland, D. S. *Nano Lett.* 2011, *11*, 2264.

(88) Ogaki, R.; Bennetsen, D. T.; Bald, I.; Foss, M. *Langmuir* 2012, *28*, 8594.

(89) Chen, K.; He, J. J.; Li, M. Y.; LaPierre, R. *Chin. Phys. Lett.* 2012, *29*.

(90) Chen, Z.; Fu, J.; Xu, Q.; Guo, Y.; Zhang, H.; Chen, J.; Zhang, J.; Tian, G.; Yang, B. *J. Colloid Interface Sci.* 2013, *391*, 54.

(91) Yu, Y.; Gan, L.; Zhang, G.; Yang, B. *Colloids Surf. A* 2012, *405*, 51.

(92) Chen, T.; Chang, D. P.; Jordan, R.; Zauscher, S. *Beilstein J. Nanotech.* 2012, *3*, 397.

(93) Ding, T.; Song, K.; Yang, G. Q.; Tung, C. H. *Macromolecular Rapid Communications* 2012, *33*, 1562.

(94) Wang, B. Z.; Han, M. Y.; Chua, S. J. *J. Vacuum Sci. Technol. B* 2012, *30*.

(95) Gooding, J. J.; Ciampi, S. *Chem. Soc. Rev.* 2011, *40*, 2704.

(96) Lisboa, P.; Valsesia, A.; Colpo, P.; Rossi, F.; Mascini, M. *Anal. Lett.* 2010, *43*, 1556.

(97) Bergveld, P. *Sens. Actuators, A* 1996, *56*, 65.

(98) Templin, M. F.; Stoll, D.; Schwenk, J. M.; Potz, O.; Kramer, S.; Joos, T. O. *Proteomics* 2003, *3*, 2155.

(99) Walt, D. R. *Science* 2005, *308*, 217.

(100) Yang, S.-M.; Jang, S. G.; Choi, D.-G.; Kim, S.; Yu, H. K. *Small* 2006, *2*, 458.

(101) Wickman, B.; Fredriksson, H.; Gustafsson, S.; Olsson, E.; Kasemo, B. *Nanotechnology* 2011, *22*.

(102) Goncalves, M. R.; Makaryan, T.; Enderle, F.; Wiedemann, S.; Plettl, A.; Marti, O.; Ziemann, P. *Beilstein J. Nanotech.* 2011, *2*, 448.

(103) Taguchi, A.; Saito, Y.; Watanabe, K.; Yijian, S.; Kawata, S. *App. Phys. Lett.* 2012, *101*.

(104) Zhang, J. H.; Li, Y. F.; Zhang, X. M.; Yang, B. *Adv. Mater.* 2010, *22*, 4249.

(105) Bayati, M.; Patoka, P.; Giersig, M.; Savinova, E. R. *Langmuir* 2010, *26*, 3549.

(106) Shipway, A. N.; Katz, E.; Willner, I. *Chem. Phys. Chem.* 2000, *1*, 18.

(107) Lu, N.; Chen, X. D.; Molenda, D.; Naber, A.; Fuchs, H.; Talapin, D. V.; Weller, H.; Muller, J.; Lupton, J. M.; Feldmann, J.; Rogach, A. L.; Chi, L. F. *Nano Lett.* 2004, *4*, 885.

(108) Henzie, J.; Barton, J. E.; Stender, C. L.; Odom, T. W. *Acc. Chem. Res.* 2006, *39*, 249.

(109) Hillhouse, H. W.; Beard, M. C. *Current Opinion in Colloid & Interface Science* 2009, *14*, 245.

(110) Taylor, Z. R.; Sanchez, E. S.; Keay, J. C.; Johnson, M. B.; Schmidtke, D. W. *Langmuir* 2010, *26*, 18938.

(111) Hoa, M. L. K.; Lu, M.; Zhang, Y. *Adv. Colloid Interface Sci.* 2006, *121*, 9.

(112) Yang, S.-M.; Jang, S. G.; Choi, D.-G.; Kim, S.; Yu, H. Y. *Small* 2006, *2*, 458.

(113) Jiang, P.; Bertone, J. F.; Hwang, K. S.; Colvin, V. L. *Chem. Mater.* 1999, *11*, 2132.

(114) Ozin, G. A.; Yang, S. M. *Adv. Funct. Mater.* 2001, *11*, 95.

(115) Marquez, M.; Grady, B. P. *Langmuir* 2004, *20*, 10998.

(116) Tao, A. R.; Huang, J.; Yang, P. *Acc. Chem. Res.* 2008, *41*, 1662.

(117) Davis, K. E.; Russel, W. B.; Glantschnig, W. J. *Science* 1989, *245*, 507.

(118) Mayoral, R.; Requena, J.; Moya, J. S.; Lopez, C.; Cintas, A.; Miguez, H.; Meseguer, F.; Vazquez, L.; Holgado, M.; Blanco, A. *Adv. Mater.* 1997, *9*, 257.

(119) Salvarezza, R. C.; Vazquez, L.; Miguez, H.; Mayoral, R.; Lopez, C.; Meseguer, F. *Phys. Rev. Lett.* 1996, *77*, 4572.

(120) Hayward, R. C.; Saville, D. A.; Aksay, I. A. *Nature* 2000, *404*, 56.

(121) Trau, M.; Saville, D. A.; Aksay, I. A. *Science* 1996, *272*, 706.

(122) Saner, C. K.; Lusker, K. L.; LeJeune, Z. M.; Serem, W. K.; Garno, J. C. *Beilstein Journal of Nanotechnology* 2012, *3*, 114.

(123) Jeon, N. L.; Finnie, K.; Branshaw, K.; Nuzzo, R. G. *Langmuir* 1997, *13*, 3382.

(124) Maoz, R.; Frydman, E.; Cohen, S. R.; Sagiv, J. *Advanced Materials* 2000, *12*, 725.

(125) Dulcey, C. S.; Georger, J. H.; Krauthamer, V.; Stenger, D. A.; Fare, T. L.; Calvert, J. M. *Science* 1991, *252*, 551.

(126) Calvert, J. M. *J. Vac. Sci. Technol. B* 1993, *11*, 2155.

(127) Ingall, M. D. K.; Honeymand, C. H.; Mercure, J. V.; Bianconi, P. A.; Kunz, R. R. *Journal of the American Chemical Society* 1999, *121*, 3607.

(128) Wen, K.; Maoz, R.; Cohen, H.; Sagiv, J.; Gibaud, A.; Desert, A.; Ocko, B. M. *Acs Nano* 2008, *2*, 579.

(129) Sagiv, J. *Journal of the American Chemical Society* 1980, *102*, 92.

(130) Parikh, A. N.; Allara, D. L.; Azouz, I. B.; Rondelez, F. *Journal of Physical Chemistry* 1994, *98*, 7577.

(131) Carson, G. A.; Granick, S. *J. Mater. Res.* 1990, *5*, 1745.

(132) Jiang, P.; McFarland, M. J. *Journal of the American Chemical Society* 2004, *126*, 13778.

(133) Tessier, P.; Velev, O. D.; Kalambur, A. T.; Lenhoff, A. M.; Rabolt, J. F.; Kaler, E. W. *Advanced Materials* 2001, *13*, 396.

(134) Chen, J. X.; Liao, W. S.; Chen, X.; Yang, T. L.; Wark, S. E.; Son, D. H.; Batteas, J. D.; Cremer, P. S. *Acs Nano* 2009, *3*, 173.

(135) Hulteen, J. C.; Treichel, D. A.; Smith, M. T.; Duval, M. L.; Jensen, T. R.; Van Duyne, R. P. *J. Phys. Chem. B* 1999, *103*, 3854.

(136) Lewandowski, B. R.; Kelley, A. T.; Singleton, R.; Li, J. R.; Lowry, M.; Warner, I. M.; Garno, J. C. *J. Phys. Chem. C* 2009, *113*, 5933.

(137) Zrimsek, A. B.; Boman, F.; Van Duyne, R. P. *Abstr. Pap. Am. Chem. Soc.* 2011, *241*.

(138) Nonckreman, C. J.; Fleith, S.; Rouxhet, P. G.; Dupont-Gillain, C. C. *Colloid Surf. B-Biointerfaces* 2010, *77*, 139.

(139) Singh, G.; Gohri, V.; Pillai, S.; Arpanaei, A.; Foss, M.; Kingshott, P. *Acs Nano* 2011, *5*, 3542.

(140) Singh, G.; Griesser, H. J.; Bremmell, K.; Kingshott, P. *Adv. Funct. Mater.* 2011, *21*, 540.

(141) Briseno, A. L.; Han, S. B.; Rauda, I. E.; Zhou, F. M.; Toh, C. S.; Nemanick, E. J.; Lewis, N. S. *Langmuir* 2004, *20*, 219.

(142) Ellinas, K. E. K.; Tserepi, A.; Gogolides, E. *Langmuir* 2011, *27*, 3960.

(143) Jiang, P.; Hwang, K. S.; Mittleman, D. M.; Bertone, J. F.; Colvin, V. L. *Journal of the American Chemical Society* 1999, *121*, 11630.

(144) Singh, A.; Kulkarni, S. K.; Khan-Malek, C. *Microelectron. Eng.* 2011, *88*, 939.

(145) Bae, C.; Kim, H.; Shin, H. *Chem. Commun.* 2011, *47*, 5145.

(146) Bae, C.; Shin, H. J.; Moon, J.; Sung, M. M. *Chem. Mat.* 2006, *18*, 1085.

(147) Geissler, M.; McLellan, J. M.; Chen, J. Y.; Xia, Y. N. *Angew. Chem.-Int. Edit.* 2005, *44*, 3596.

(148) Li, J. R.; Garno, J. C. *Nano Lett.* 2008, *8*, 1916.

(149) McLellan, J. M.; Geissler, M.; Xia, Y. N. *Journal of the American Chemical Society* 2004, *126*, 10830.

(150) Finklea, H. O.; Robinson, L. R.; Blackburn, A.; Richter, B.; Allara, D.; Bright, T. *Langmuir* 1986, *2*, 239.

(151) Sabatani, E.; Rubinstein, I.; Maoz, R.; Sagiv, J. *J. Electroanal. Chem.* 1987, *219*, 365.

(152) Gun, J.; Sagiv, J. *J. Colloid Interface Sci.* 1986, *112*, 457.

(153) Carson, G.; Granick, S. *Journal of Applied Polymer Science* 1989, *37*, 2767.

(154) Kessel, C. R.; Granick, S. *Langmuir* 1991, *7*, 532.

(155) Schwartz, D. K.; Steinberg, S.; Israelachvili, J.; Zasadzinski, J. A. N. *Physical Review Letters* 1992, *69*, 3354.

(156) Brandriss, S.; Margel, S. *Langmuir* 1993, *9*, 1232.

(157) Mathauer, K.; Frank, C. W. *Langmuir* 1993, *9*, 3002.

(158) Li, J. R.; Lusker, K. L.; Yu, J. J.; Garno, J. C. *Acs Nano* 2009, *3*, 2023.

(159) Legrange, J. D.; Markham, J. L.; Kurkjian, C. R. *Langmuir* 1993, *9*, 1749.

(160) Maoz, R.; Sagiv, J. *J. Colloid Interface Sci.* 1984, *100*, 465.

(161) Silberzan, P.; Leger, L.; Ausserre, D.; Benattar, J. J. *Langmuir* 1991, *7*, 1647.

(162) Wasserman, S. R.; Tao, Y. T.; Whitesides, G. M. *Langmuir* 1989, *5*, 1074.

(163) Yang, S. R.; Kolbesen, B. O. *Appl. Surf. Sci.* 2008, *255*, 1726.

(164) Parikh, A. N.; Liedberg, B.; Atre, S. V.; Ho, M.; Allara, D. L. *Journal of Physical Chemistry* 1995, *99*, 9996.

(165) Allara, D. L.; Parikh, A. N.; Rondelez, F. *Langmuir* 1995, *11*, 2357.

(166) Brzoska, J. B.; Shahidzadeh, N.; Rondelez, F. *Nature* 1992, *360*, 719.

(167) McGovern, M. E.; Kallury, K. M. R.; Thompson, M. *Langmuir* 1994, *10*, 3607.

(168) Tripp, C. P.; Hair, M. L. *Langmuir* 1992, *8*, 1120.

(169) Wen, K.; Maoz, R.; Cohen, H.; Sagiv, J.; Gibaud, A.; Desert, A.; Ocko, B. M. *ACS Nano* 2008, *2*, 579.

(170) Bierbaum, K.; Grunze, M.; Baski, A. A.; Chi, L. F.; Schrepp, W.; Fuchs, H. *Langmuir* 1995, *11*, 2143.

(171) Lusker, K. L.; Yu, J. J.; Garno, J. C. *Thin Solid Films* 2011, *519*, 5223.

(172) Tillman, N.; Ulman, A.; Schildkraut, J. S.; Penner, T. L. *Journal of the American Chemical Society* 1988, *110*, 6136.

(173) Vallant, T.; Brunner, H.; Mayer, U.; Hoffmann, H.; Leitner, T.; Resch, R.; Friedbacher, G. *J. Phys. Chem. B* 1998, *102*, 7190.

(174) Li, J. R.; Garno, J. C. *ACS Appl. Mater. Interfaces* 2009, *1*, 969.

(175) Visschers, M.; Laven, J.; German, A. L. *Prog. Org. Coat.* 1997, *30*, 39.

(176) Nečas, D. K., P.; 2.25 ed.; Czech Metrology Institute: Brno, Czech Republic 2009, p A modular program for SPM (scanning probe microscopy) data visualization and analysis.

(177) Wilcox, C. D.; Dove, S. B.; McDavid, W. D.; Greer, D. B.; University of Texas Health Science Center (UTHSCSA): San Antonio, TX, 1996-2002.

(178) Srisombat, L. O.; Park, J. S.; Zhang, S.; Lee, T. R. *Langmuir* 2008, *24*, 7750.

(179) Purcell, K. F.; Yeh, S. M.; Eck, J. S. *Inorg. Chem.* 1977, *16*, 1708.

(180) Srisombat, L. O.; Zhang, S. S.; Lee, T. R. *Langmuir* 2010, *26*, 41.

(181) Hegner, M.; Wagner, P.; Semenza, G. *Surface Science* 1993, *291*, 39.

(182) Wagner, P.; Hegner, M.; Guntherodt, H. J.; Semenza, G. *Langmuir* 1995, *11*, 3867.

(183) Anand, G.; Sharma, S.; Dutta, A. K.; Kumar, S. K.; Belfort, G. *Langmuir* 2010, *26*, 10803.

(184) Andrade, J. D.; Hlady, V. *Advances in Polymer Science* 1986, *79*, 1.

(185) Awsiuk, K.; Bernasik, A.; Kitsara, M.; Budkowski, A.; Rysz, J.; Haberko, J.; Petrou, P.; Beltsios, K.; Raczkowska, J. *Colloids and Surfaces B-Biointerfaces* 2010, *80*, 63.

(186) Corum, L. E.; Eichinger, C. D.; Hsiao, T. W.; Hlady, V. *Langmuir* 2011, *27*, 8316.

(187) Malmsten, M.; Muller, D.; Lassen, B. *Journal of Colloid and Interface Science* 1997, *193*, 88.

(188) Park, T. J.; Lee, S. Y.; Lee, S. J.; Park, J. P.; Yang, K. S.; Lee, K. B.; Ko, S.; Park, J. B.; Kim, T.; Kim, S. K.; Shin, Y. B.; Chung, B. H.; Ku, S. J.; Kim, D. H.; Choi, I. S. *Analytical Chemistry* 2006, *78*, 7197.

(189) Valsesia, A.; Mannelli, I.; Colpo, P.; Bretagnol, F.; Rossi, F. *Analytical Chemistry* 2008, *80*, 7336.

(190) Buzea, C.; Beydaghyan, G.; Elliott, C.; Robbie, K. *Nanotechnology* 2005, *16*, 1986.

(191) Dolatshahi-Pirouz, A.; Hovgaard, M. B.; Rechendorff, K.; Chevallier, J.; Foss, M.; Besenbacher, F. *Physical Review B* 2008, *77*.

(192) Rechendorff, K.; Hovgaard, M. B.; Chevallier, J.; Foss, M.; Besenbacher, F. *Applied Physics Letters* 2005, *87*.

(193) Robbie, K.; Brett, M. J.; Lakhtakia, A. *Nature* 1996, *384*, 616.

(194) Muller, B. *Surface Review and Letters* 2001, *8*, 169.

(195) Turner, S.; Kam, L.; Isaacson, M.; Craighead, H. G.; Shain, W.; Turner, J. *Journal of Vacuum Science & Technology B* 1997, *15*, 2848.

(196) Xue, W. C.; Liu, X. Y.; Zheng, X. B.; Ding, C. X. *Biomaterials* 2005, *26*, 3029.

(197) Variola, F.; Yi, J.-H.; Richert, L.; Wuest, J. D.; Rosei, F.; Nanci, A. *Biomaterials* 2008, *29*, 1285.

(198) Vetrone, F.; Variola, F.; de Oliveira, P. T.; Zalzal, S. F.; Yi, J.-H.; Sam, J.; Bombonato-Prado, K. F.; Sarkissian, A.; Perepichka, D. F.; Wuest, J. D.; Rosei, F.; Nanci, A. *Nano Letters* 2009, *9*, 659.

(199) Gelmi, A.; Higgins, M. J.; Wallace, G. G. *Biochimica Et Biophysica Acta-General Subjects* 2013, *1830*, 4305.

(200) Lamers, E.; te Riet, J.; Domanski, M.; Luttge, R.; Figdor, C. G.; Gardeniers, J. G. E.; Walboomers, X. F.; Jansen, J. A. *European Cells & Materials* 2012, *23*, 182.

(201) Elter, P.; Lange, R.; Beck, U. *Colloids and Surfaces B-Biointerfaces* 2012, *89*, 139.

(202) Dickerson, M. T.; Abney, M. B.; Cameron, C. E.; Knecht, M.; Bachas, L. G.; Anderson, K. W. *Bioconjugate Chemistry* 2012, *23*, 184.

(203) Kuo, C. W.; Chien, F. C.; Shiu, J. Y.; Tsai, S. M.; Chueh, D. Y.; Hsiao, Y. S.; Yang, Z. H.; Chen, P. L. *Nanotechnology* 2011, *22*.

(204) Li, Y. F.; Zhang, J. H.; Liu, W. D.; Li, D. W.; Fang, L. P.; Sun, H. C.; Yang, B. *Acs Applied Materials & Interfaces* 2013, *5*, 2126.

(205) Malmstrom, J.; Christensen, B.; Jakobsen, H. P.; Lovmand, J.; Foldbjerg, R.; Sorensen, E. S.; Sutherland, D. S. *Nano Letters* 2010, *10*, 686.

(206) Kristensen, S. H.; Pedersen, G. A.; Ogaki, R.; Bochenkov, V.; Nejsum, L. N.; Sutherland, D. S. *Acta Biomaterialia* 2013, *9*, 6158.

(207) Fadeev, A. Y.; McCarthy, T. J. *Langmuir* 2000, *16*, 7268.

(208) Chrisey, L. A.; Lee, G. U.; Oferrall, C. E. *Nucleic Acids Research* 1996, *24*, 3031.

(209) Crivat, G., The University of New Orleans, 2007.

(210) Stenger, D. A.; Pike, C. J.; Hickman, J. J.; Cotman, C. W. *Brain Research* 1993, *630*, 136.

(211) Bergkvist, M.; Carlsson, J.; Oscarsson, S. *J. Biomed. Mater. Res. Part A* 2003, *64A*, 349.

(212) Grabar, K. C.; Smith, P. C.; Musick, M. D.; Davis, J. A.; Walter, D. G.; Jackson, M. A.; Guthrie, A. P.; Natan, M. J. *J. Am. Chem. Soc.* 1996, *118,* 1148.

(213) Hull, J. R.; Tamura, G. S.; Castner, D. G. *Biophysical Journal* 2007, *93*, 2852.

(214) Mrksich, M.; Whitesides, G. M. *Annual Review of Biophysics and Biomolecular Structure* 1996, *25*, 55.

(215) Lehnert, M.; Gorbahn, M.; Rosin, C.; Klein, M.; Koeper, I.; Al-Nawas, B.; Knoll, W.; Veith, M. *Langmuir* 2011, *27*, 7743.

(216) Malmsten, M. *Abstracts of Papers of the American Chemical Society* 1994, *207*, 71.

(217) Erickson, H. P. *Journal of Muscle Research and Cell Motility* 2002, *23*, 575.

(218) Koteliansky, V. E.; Glukhova, M. A.; Bejanian, M. V.; Smirnov, V. N.; Filimonov, V. V.; Zalite, O. M.; Venyaminov, S. Y. *Eur. J. Biochem.* 1981, *119*, 619.

(219) Price, T. M.; Rudee, M. L.; Pierschbacher, M.; Ruoslahti, E. *Eur. J. Biochem.* 1982, *129*, 359.

(220) Slater, J. H.; Frey, W. *J. Biomed. Mater. Res. Part A* 2008, *87A*, 176.

(221) Erickson, H. P.; Carrell, N.; McDonagh, J. *Journal of Cell Biology* 1981, *91*, 673.

(222) Williams, E. C.; Janmey, P. A.; Ferry, J. D.; Mosher, D. F. *Journal of Biological Chemistry* 1982, *257*, 4973.

(223) Keselowsky, B. G.; Collard, D. M.; Garcia, A. J. *Journal of Biomedical Materials Research Part A* 2003, *66A*, 247.

(224) Lyles, V.; Serem, W.; Yu, J.-J.; Garno, J. In *Surface Science Techniques*; Bracco, G., Holst, B., Eds.; Springer Berlin Heidelberg: 2013; Vol. 51, p 599.

APPENDIX A: LETTER OF PERMISSION

Chamarra Saner <csaner1@tigers.lsu.edu>

Permission Request Form Contracts-Copyright: ChaMarra Saner
2 messages

Chamarra Saner <csaner1@tigers.lsu.edu> Tue, May 14, 2013 at 5:37 PM
To: Thomas.Schimmel@bjnano.org

To whom it may concern:

I would very much appreciate your permission to use the following material: **Self-assembly of octadecyltrichlorosilane: Surface structures formed using different protocols of particle lithography** (manuscript ID: 1864544, doi: 10.3762/bjnano.3.12, Year Published: 2012, Volume: 3, Pages: 114-122) as part of my Ph.D. Dissertation at Louisiana State University. On the website I have read that of the authors of *Beilstein Journal of Nanotechnology* retain copyright of their articles which are distributed under the terms of the Creative Commons Attribution License, and hence no permissions from the journal are required for me to do so. I also wanted to ensure that the aforementioned manuscript text and figures were free for me to use at my, the first author's, disposal according to Beilstein-Institut zur Förderung der Chemischen Wissenschaften Hessen, Germany as long as proper citations are charged to the appropriate place. If there is additional information that I should fill out that I have overlooked on the website, I would appreciate some direction in this matter. If there are any question in this matter, please feel free to contact me.

Regards,

ChaMarra
--
ChaMarra K. Saner
PhD Candidate
Garno Research Group
Louisiana State University
Office: Choppin Hall-348
Office Phone: (225) 578-3019
Email: csaner1@tigers.lsu.edu

---

bjnano-editorial-office@beilstein-institut.de <bjnano-editorial-office@beilstein-institut.de> Wed, May 15, 2013 at 9:06 AM
To: Chamarra Saner <csaner1@tigers.lsu.edu>

Dear ChaMarra Saner,

Thank you for your email regarding use of the text and Figures from the mentioned manuscript.

I can happily confirm that your interpretation of the copyright agreement is correct, that is, the rights belong to you and your coauthors – no permissions are required. Thus, please feel free to use the text and Figures in your own future work. We only request that the original article is properly cited and, if appropriate, that permission from your coauthors is obtained. Other than this, there are no other formal requirements.

Likewise, if you have any further questions please do not hesitate to contact us.

Kind regards,

Dr. Neil Bennett

Beilstein Journals Editorial Office

Von: Chamarra Saner [mailto:csaner1@tigers.lsu.edu]
Gesendet: Mittwoch, 15. Mai 2013 00:38
An: Thomas.Schimmel@bjnano.org
Betreff: Permission Request Form Contracts-Copyright: ChaMarra Saner

[Quoted text hidden]

APPENDIX B: SUPPLEMENTAL FIGURES FOR SELF ASSEMBLY OF OTS SURFACE STRUCTURES FORMED USING DIFFERENT PROTOCOLS OF PARTICLE LITHOGRAPHY

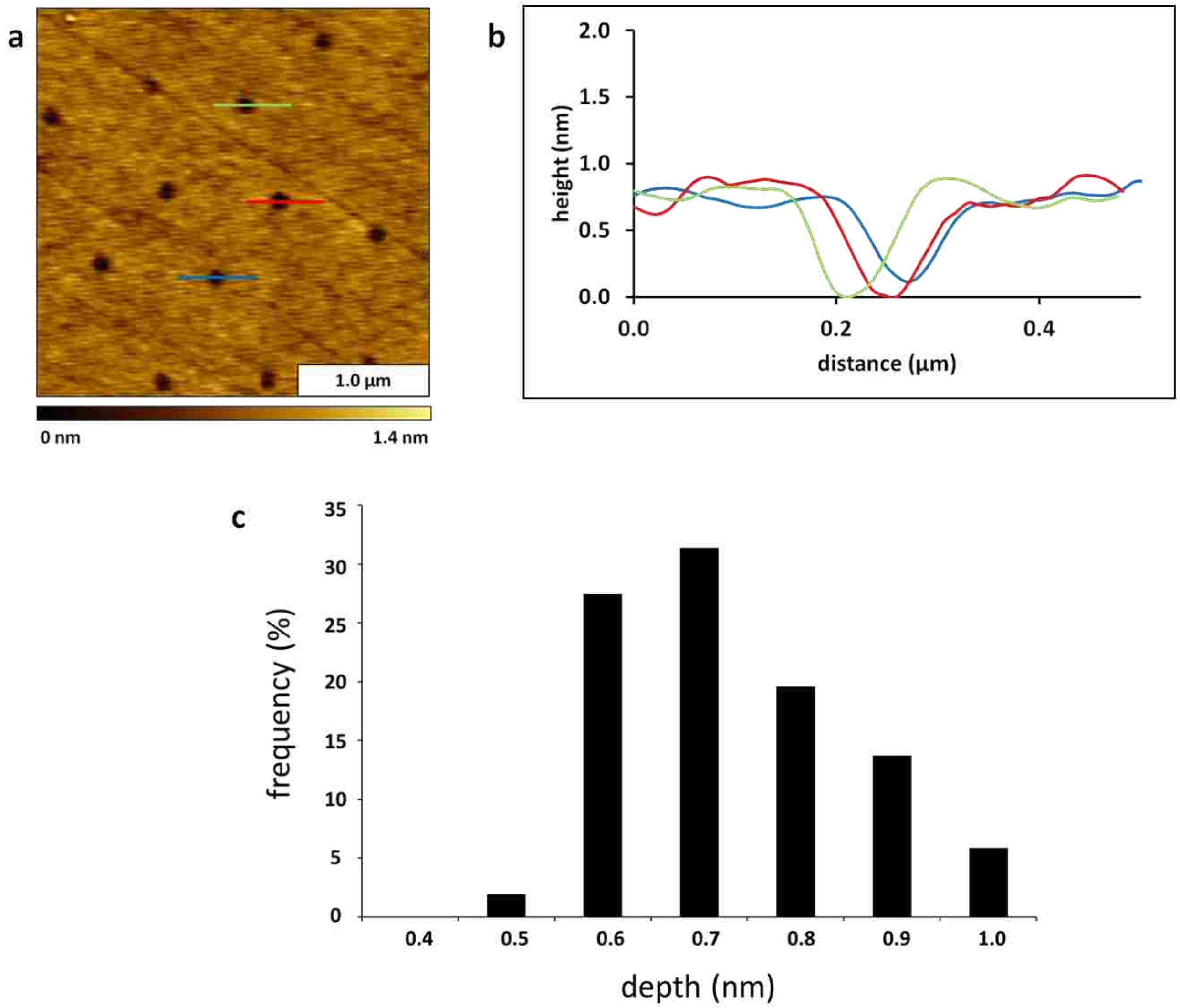

Figure B.1 Representative AFM topograph selected for measuring the thickness of the OTS film. The sample was prepared using immersion particle lithography with an annealed silica mask of 500 nm periodicity. (a) Individual line profiles were used to measure the depth of nanopores, topography frame (3 × 3 μm^2) acquired with contact mode AFM. (b) Example profiles for the cursor lines drawn across the center of the pores in ***a***. (c) Histogram of the measurements of the depth of OTS nanopores ($n = 50$).

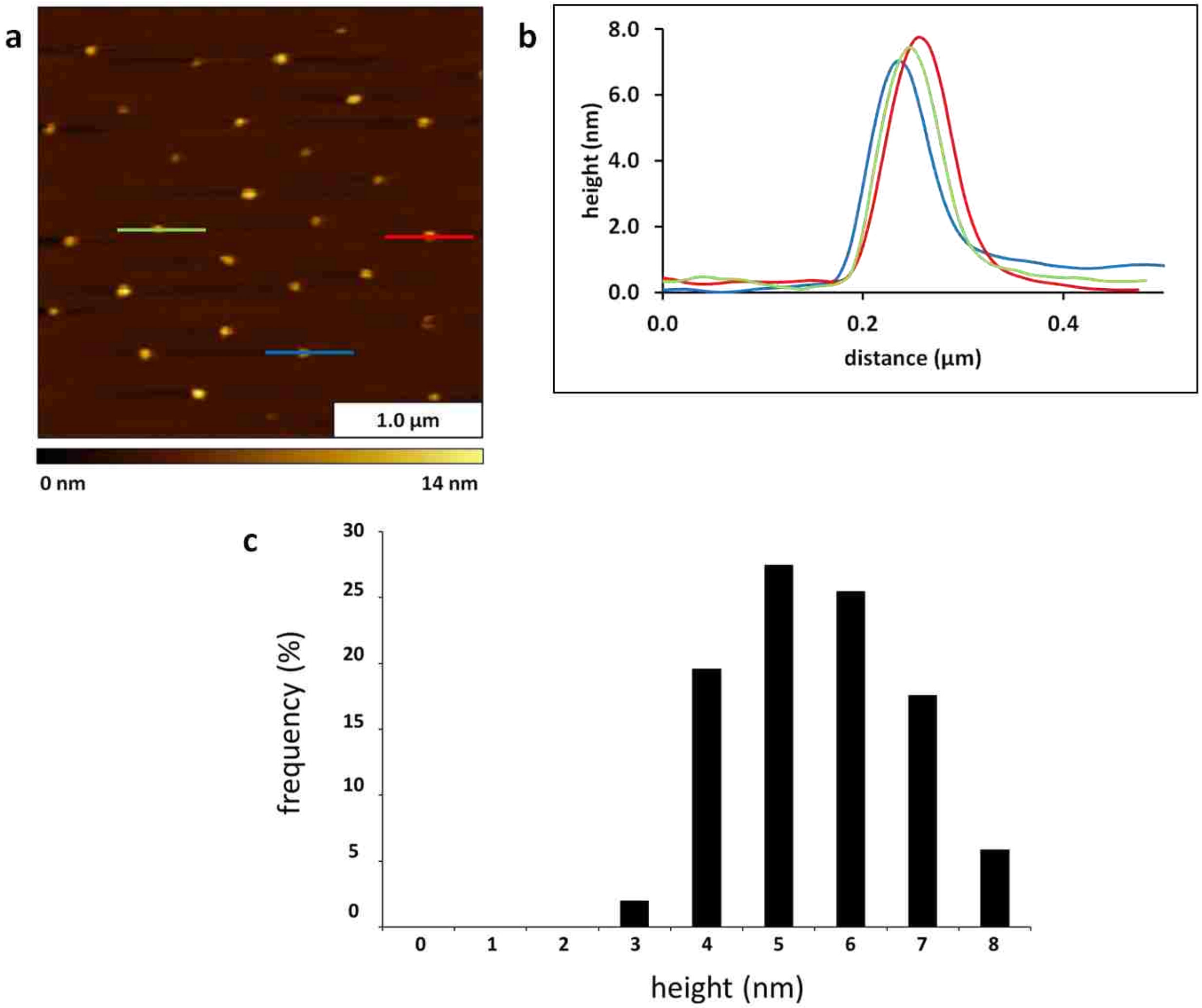

Figure B.2 An increase in height was observed after inserting a heterobifuntional crosslinker, (3-trimethoxysilylpropyl)diethylenetriamine (DETA) into the exposed sites of nanopores within OTS/Si(111). (a) Representative topography image (3 × 3 μm^2) of the nanopores backfilled with DETA, acquired with contact mode AFM. (b) Example height profiles for the lines drawn across the center of the nanodots in *a*. (c) Distribution of thicknesses measured above the OTS after backfilling with DETA referencing the baseline of the OTS matrix (*n* = 50).

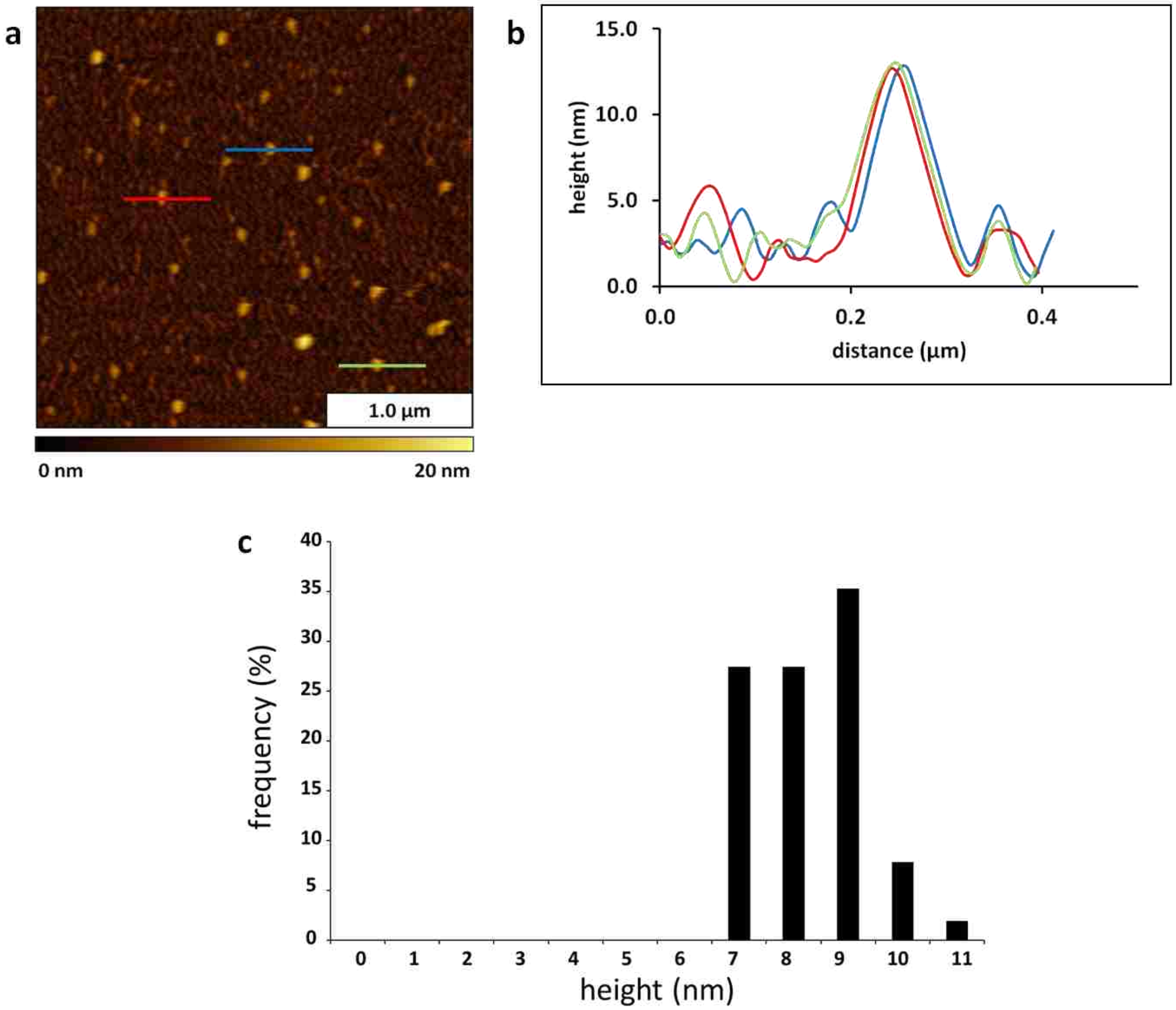

Figure B.3 An increase in heights was detected after binding fibronectin to DETA nanostructures. (a) Surface changes viewed with tapping-mode AFM (3 × 3 μm^2). (b) Example height profiles for the lines in ***a***. (c) Histogram of height measurements after binding fibronectin referencing the surrounding matrix as a baseline ($n = 50$).

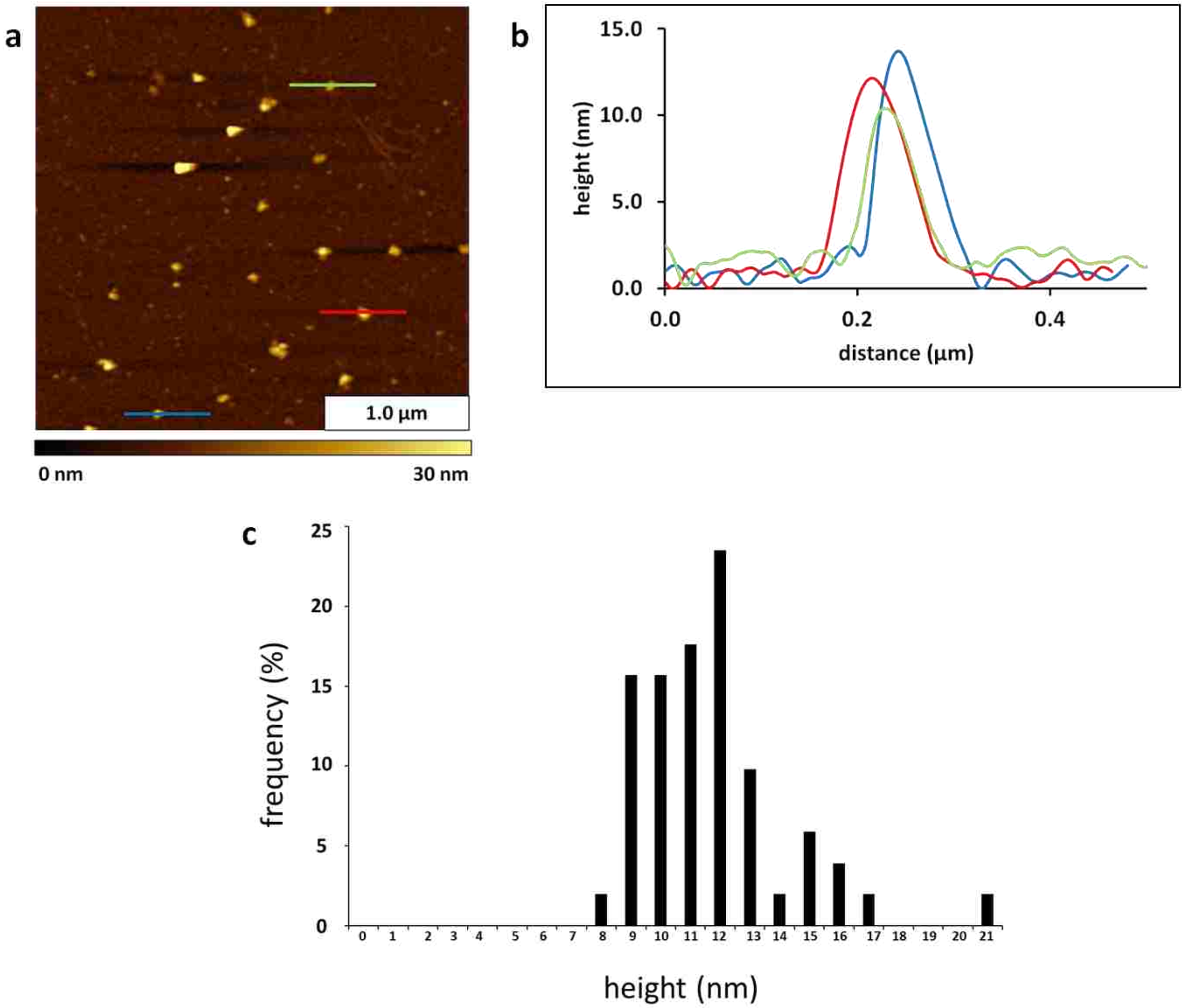

Figure B.4 Surface morphology after binding anti-fibronectin to the nanopatterns of fibronectin. (a) Example AFM topography image (3 × 3 µm^2) acquired with tapping-mode in air. (b) Height profiles for the lines shown in ***a***. (c) Histogram of height measurements after binding IgG, referencing the surrounding matrix areas as the baseline (n = 50).

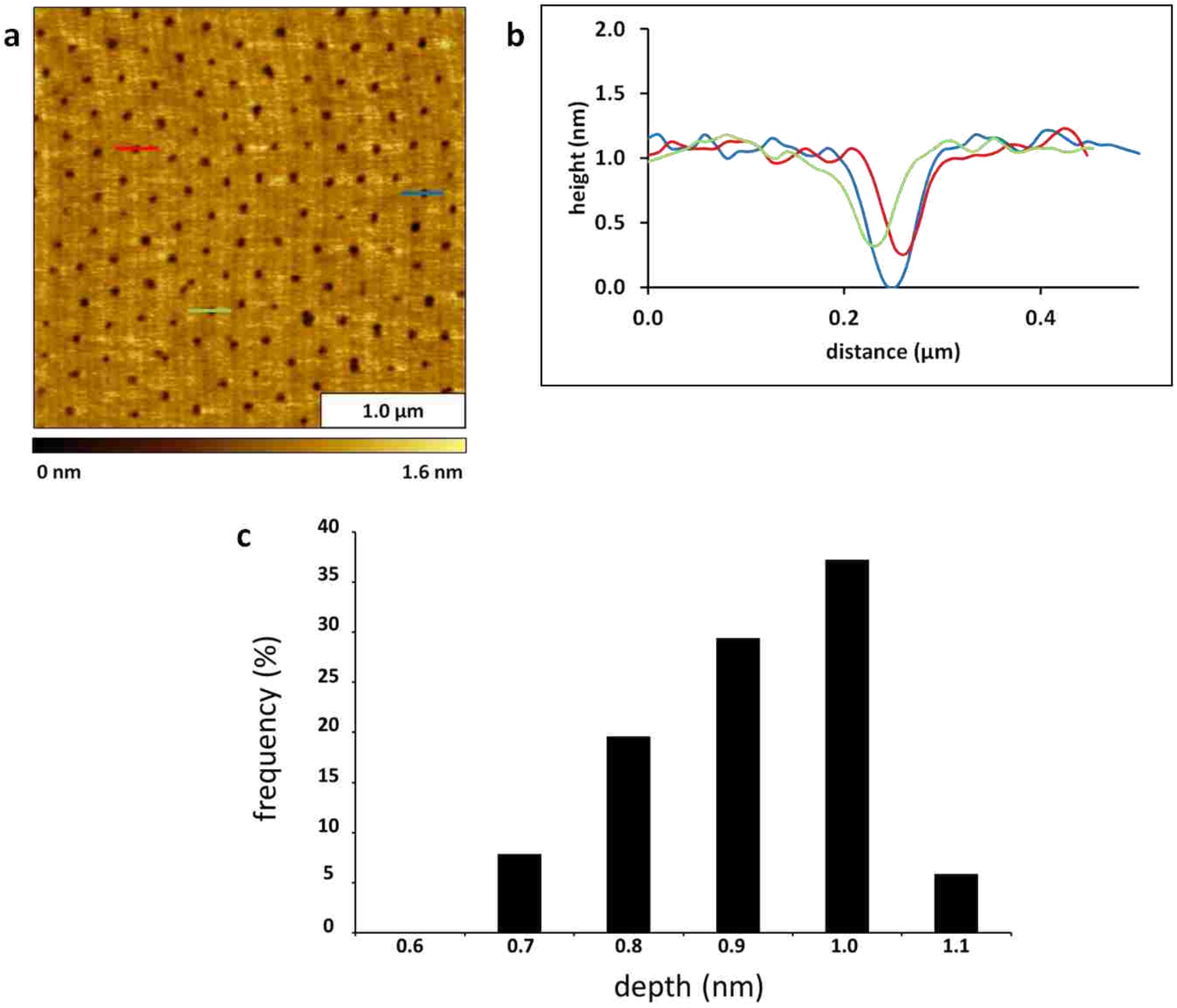

Figure B.5 Nanopores of OTS prepared using a silica mask with 250 nm periodicity. (a) Representative topography image (3 × 3 µm^2) of OTS nanopores acquired with contact mode AFM. (b) Example height profiles for the lines drawn across the center areas of the nanopores shown in ***a***. (c) Distribution of measurements of the depth of OTS nanopores (n = 50).

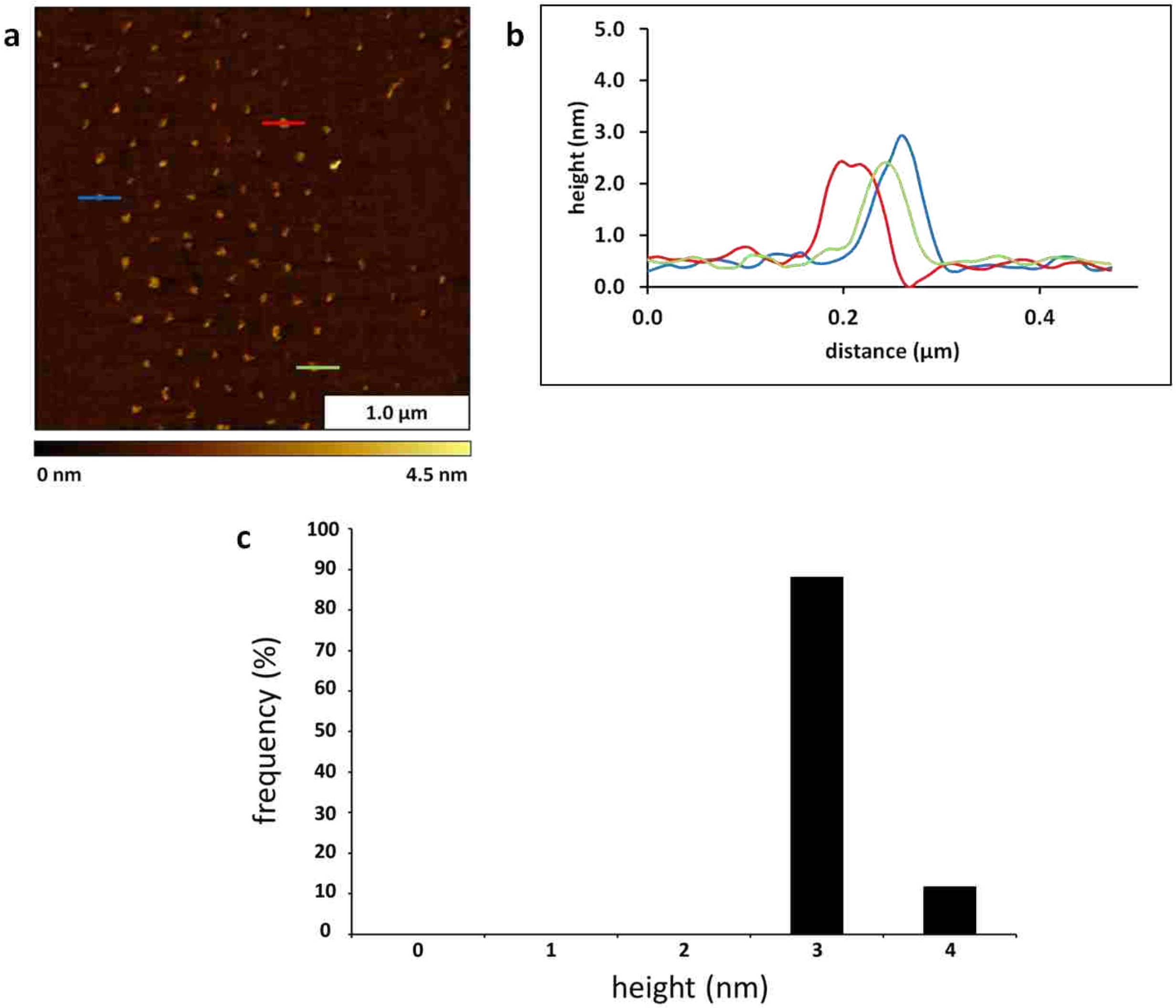

Figure B.6 Nanodot patterns were formed by filling the nanopores with DETA. (a) Representative topography view (3 × 3 µm^2) of nanodots, acquired with contact mode AFM in air. (b) Example height profile for the lines drawn across the center of the nanodots in ***a***. (c) A relatively narrow distribution of heights was observed for nanodots of DETA (*n* = 50), indicating uniform and regular nanostructures were formed using immersion particle lithography.

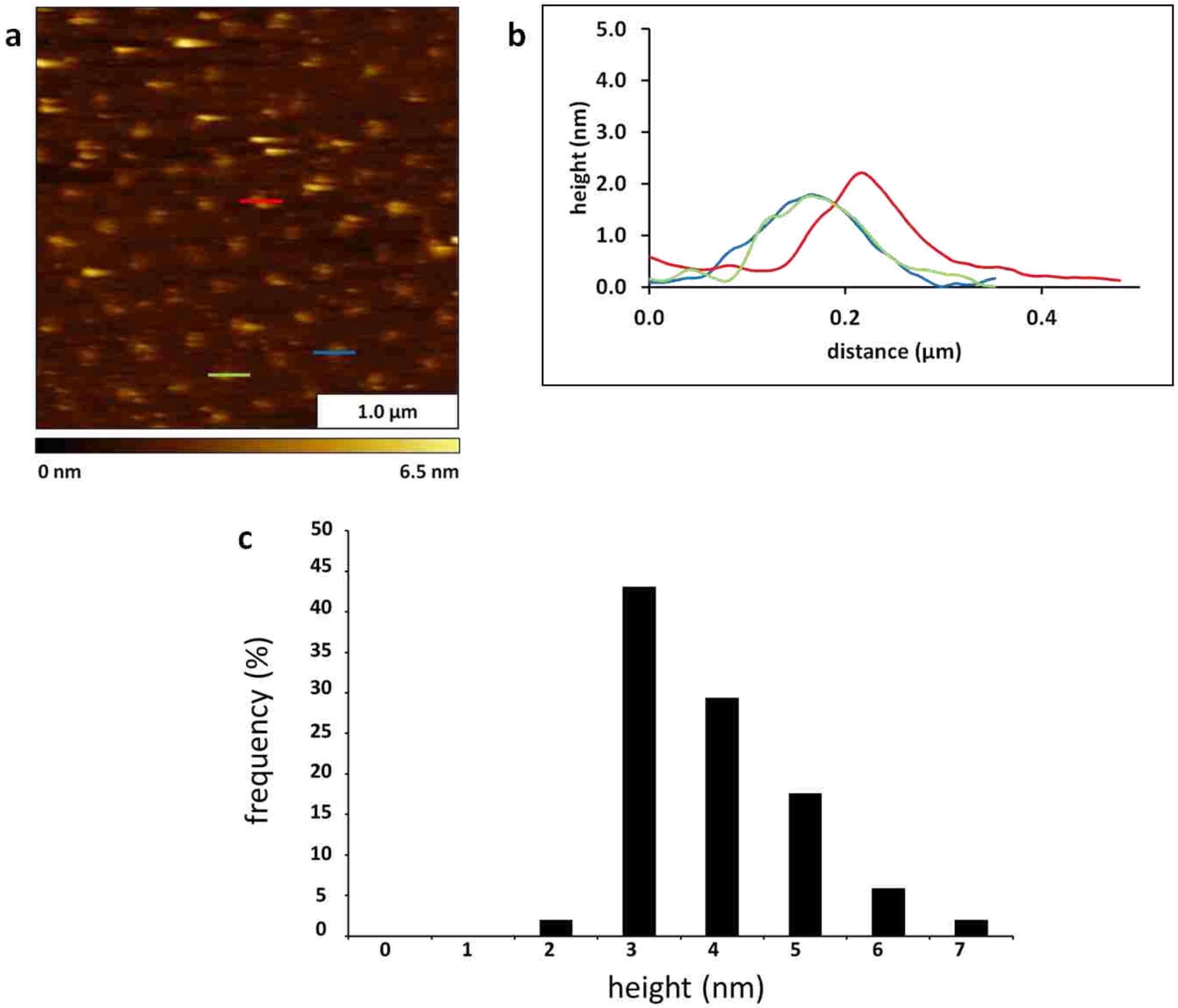

Figure B.7 After binding fibronectin to sites of DETA nanodots, an increase in the heights of the nanopatterns was apparent. The sample was prepared using a surface mask with 205 nm periodicity. (a) Example AFM image (3 × 3 μm^2) of nanopores obtained with contact mode AFM in air. (b) Representative height profile of the lines drawn across the nanodots in ***a***. (c) Histogram of height measurements of fibronectin nanodots ($n = 50$).

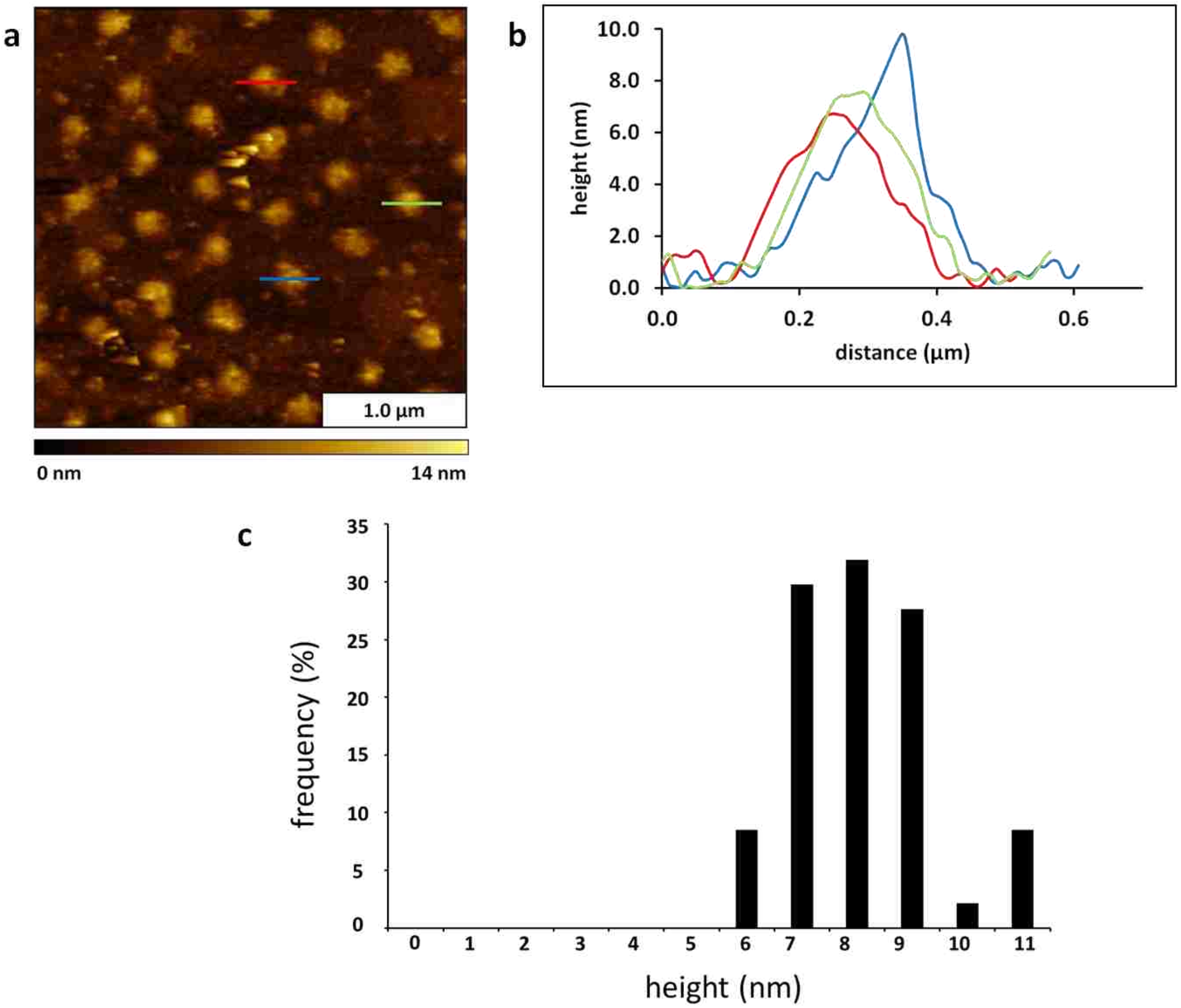

Figure B.8 After binding IgG to fibronectin nanopatterns, further increases in height were observed. (a) Representative topograph (3×3 µm^2) acquired with tapping-mode AFM after binding IgG. (b) Example height profile for the lines drawn across the nanostructures in ***a***. (c) Range of heights measured after binding IgG ($n = 50$).

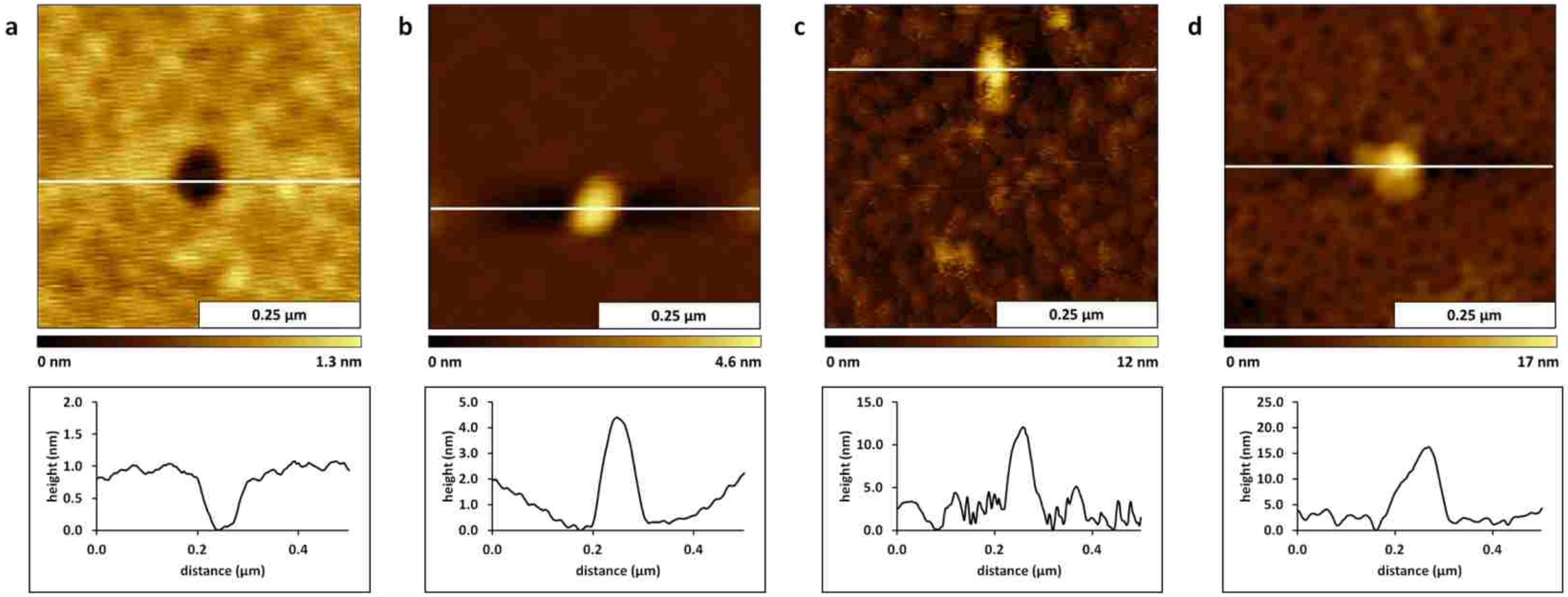

Figure B.9 High resolution views of surface changes after steps for lithography, binding protein and antibody. Topography views (0.5 x 0.5 µm^2) acquired in air for samples prepared with a surface mask of 500 nm silica mesospheres. The AFM images represent different locations of the sample acquired *ex situ*. (a) A single nanopore and height profile indicates a depth of 1 ± 0.1 nm, referencing the bottom of the hole as the baseline. (b) A nanopore backfilled with DETA, with a height measuring 4 ±1.3 nm, referencing the surrounding areas of the matrix of OTS as the baseline. (c) After binding fibronectin to a DETA nanodots, the height measures 12 ± 1 nm. (d) After binding of IgG to the fibronectin the height measured 16 ± 2.5 nm.

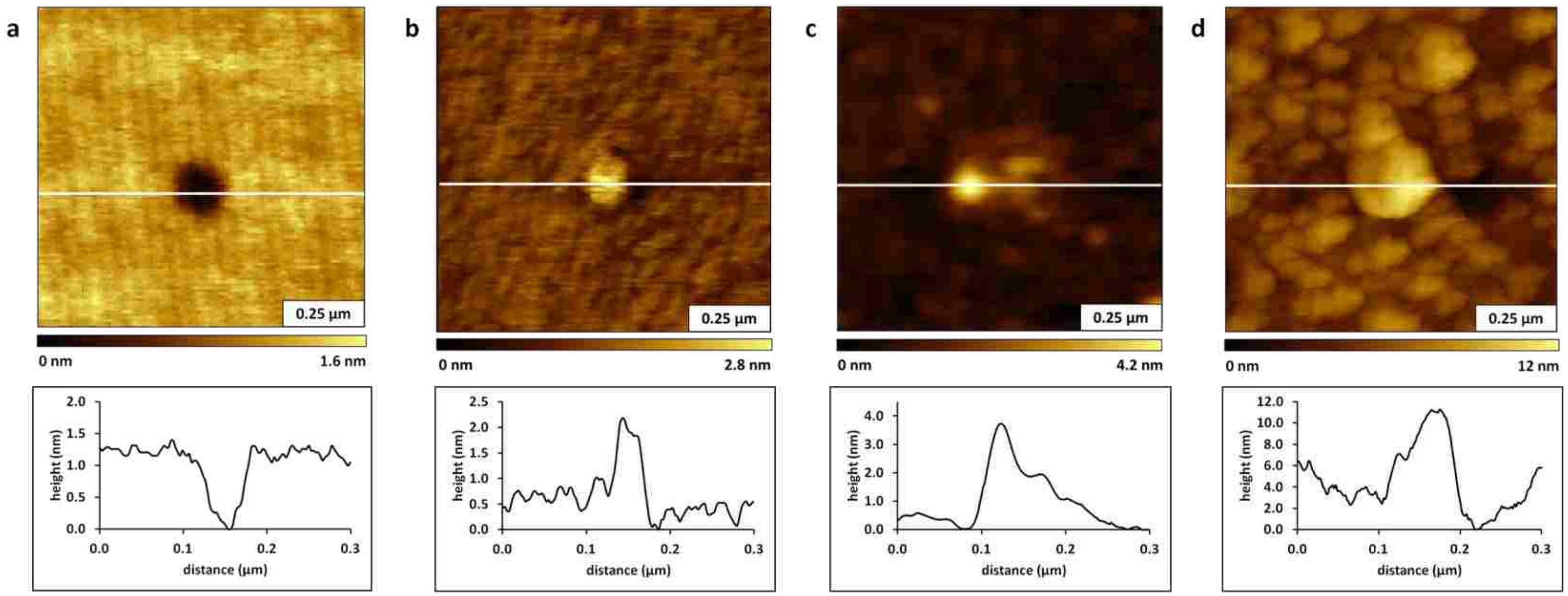

Figure B.10 Magnified views of the surface changes after steps of the protein binding procedure. The sample was prepared with a surface mask of 250 nm silica mesospheres. The AFM topographs(0.5 x 0.5 µm^2) were acquired *ex situ* in air, and represent different locations of the sample. (a) Nanopore with corresponding height profile indicates a depth of 1.3 ± 0.1 nm, referencing the bottom of the hole as the baseline. (b) After the nanopore was filled with DETA the height of the nanostructure measures 2 ± 0.3 nm. (c) After binding fibronectin to a DETA nanodot the height measures 3.5 ± 1 nm, referencing the surrounding areas of the matrix of OTS as the baseline. (d) After binding IgG to the bound protein, the heigh measured 12 ± 1.2 nm.

THE VITA

ChaMarra Karmelia Saner is a native of Taylorsville, North Carolina. She received a Bachelor of Science degree in Chemistry from the University of North Carolina at Pembroke (2004) and a Master of Science degree, with an organic chemistry concentration, from North Carolina Agriculture and Technical State University (2007). She is currently a PhD candidate at Louisiana State University and has successfully defended her dissertation. Ms. Saner is lead author of three journal articles and participated as co-author of two additional articles. ChaMarra is an active participant of organizations such as the local chapters of the American Chemical Society, Iota Sigma Pi, NOBCChE and the chemistry graduate student council where she has held several leadership roles with the latter two. In her research, she has developed new techniques for nanoscale patterning using organosilane chemistry, and then used surface nanostructures as test platforms to investigate protein binding and immunoassays at the molecular level. ChaMarra is a highly cross-functional scientist and has experience leading, integrating and coordinating in both team and individual settings through current and past industry experiences. Ms. Saner has made remarkable progress throughout her graduate career and this is a preface for further accomplishments.